



**HAL**  
open science

# Design, Synthesis and Characterization of Ferrous Complexes Displaying Electroneutrality

Jinping Wang

► **To cite this version:**

Jinping Wang. Design, Synthesis and Characterization of Ferrous Complexes Displaying Electroneutrality. Organic chemistry. Ecole normale supérieure de lyon - ENS LYON; East China normal university (Shanghai), 2015. English. NNT: 2015ENSL0989 . tel-01162983

**HAL Id: tel-01162983**

**<https://theses.hal.science/tel-01162983>**

Submitted on 11 Jun 2015

**HAL** is a multi-disciplinary open access archive for the deposit and dissemination of scientific research documents, whether they are published or not. The documents may come from teaching and research institutions in France or abroad, or from public or private research centers.

L'archive ouverte pluridisciplinaire **HAL**, est destinée au dépôt et à la diffusion de documents scientifiques de niveau recherche, publiés ou non, émanant des établissements d'enseignement et de recherche français ou étrangers, des laboratoires publics ou privés.

# THÈSE

en vue de l'obtention du grade de

**Docteur de l'Université de Lyon, délivré par l'École Normale Supérieure de Lyon**

**En cotutelle avec l' East China Normal University**

**Discipline : Chimie**

**Laboratoire de Chimie, UMR 5182**

**École Doctorale de Chimie de Lyon, ED 206**

présentée et soutenue publiquement le 30/04/2015

par **Mme. Jinping WANG**

---

## **Design, Synthesis and Characterization of Ferrous Complexes Displaying Electroneutrality**

---

Directeur de thèse : M. Jens HASSERODT

Co-tuteur de thèse : Mme. Fan YANG

Devant la commission d'examen formée de :

M. Pierre AUDEBERT, Professeur à École Normale Supérieure de Cachan, Rapporteur

M. Jens HASSERODT, Professeur à École Normale Supérieure de Lyon, Directeur de thèse

Mme. Fan YANG, Professeur à East China Normal University, Co-tuteur de thèse

M. Wanbin ZHANG, Professeur à Shanghai Jiao Tong University, Examineur

M. Xiaobing ZHANG, Professeur à Hunan University, Rapporteur

2015 届研究生博士学位论文

学校代码：10269

学 号：52110606022

# 華東師範大學

## 电中性亚铁配合物的设计、合成及其初步性质研究

院 系： 化学与分子工程学院

专 业： 有机化学

研究 方向： 功能有机分子合成与应用

指导 教师： Jens HASSERODT 教授

杨 帆 教授

博士研究生： 王 晋萍

2015 年 3 月完成

2015 Dissertation for Doctor's Degree

University Code: 10269

Student ID: 52110606022

East China Normal University  
Ecole Normale Supérieure de Lyon

**Design, Synthesis and characterization of Ferrous  
Complexes Displaying Electroneutrality**

Academy: School of Chemistry and Molecular  
engineering at ECNU

Laboratoire de Chimie at ENS-Lyon

Major: Organic Chemistry

Research Field: Synthesis and application of organic  
functional molecules

Supervisor: Prof. Jens HASSERODT

Prof. Fan YANG

Candidate: Jinping WANG

2015, Shanghai

## 华东师范大学学位论文原创性声明

郑重声明：本人呈交的学位论文《\_\_\_\_\_》，是在华东师范大学攻读硕士/博士（请勾选）学位期间，在导师的指导下进行的研究工作及取得的研究成果。除文中已经注明引用的内容外，本论文不包含其他个人已经发表或撰写过的研究成果。对本文的研究做出重要贡献的个人和集体，均已在文中作了明确说明并表示谢意。

作者签名：\_\_\_\_\_

日期： 年 月 日

## 华东师范大学学位论文著作权使用声明

《\_\_\_\_\_》系本人在华东师范大学攻读学位期间在导师指导下完成的硕士/博士（请勾选）学位论文，本论文的著作权归本人所有。本人同意华东师范大学根据相关规定保留和使用此学位论文，并向主管部门和学校指定的相关机构送交学位论文的印刷版和电子版；允许学位论文进入华东师范大学图书馆及数据库被查阅、借阅；同意学校将学位论文加入全国博士、硕士学位论文共建单位数据库进行检索，将学位论文的标题和摘要汇编出版，采用影印、缩印或者其它方式合理复制学位论文。

本学位论文属于（请勾选）

1. 经华东师范大学相关部门审查核定的“内部”或“涉密”学位论文\*，于\_\_\_\_\_年\_\_\_\_\_月\_\_\_\_\_日解密，解密后适用上述授权。

2. 不保密，适用上述授权。

导师签名\_\_\_\_\_ 本人签名\_\_\_\_\_

年 月 日

\* “涉密”学位论文应是已经华东师范大学学位评定委员会办公室或保密委员会审定过的学位论文（需附获批的《华东师范大学研究生申请学位论文“涉密”审批表》方为有效），未经上述部门审定的学位论文均为公开学位论文。此声明栏不填写的，默认为公开学位论文，均适用上述授权）。



# Table of Contents

Abbreviations.....	I
Abstract.....	IV
Résumé.....	VI
摘要.....	VIII
Part I Introduction.....	1
Chapter 1 Introduction about magnetism of matter.....	1
1.1 Magnetism character of matter.....	1
1.1.1 Diamagnetism.....	1
1.1.2 Paramagnetism.....	2
1.1.3 Ferromagnetism.....	2
1.1.4 Antiferromagnetism.....	3
1.1.5 Ferrimagnetism.....	4
1.2 Magnetic moment of an atom or a molecule.....	4
1.2.1 Composition of magnetic moment of an atom or a molecule.....	4
1.2.2 Diamagnetic property.....	5
1.2.3 Paramagnetic property.....	5
1.2.4 Detection of magnetism.....	7
1.3 References.....	9
Chapter 2 MRI as a method to detect magnetism.....	12
2.1 Introduction of MRI.....	12
2.2.1 MRI principle <sup>[4]</sup> .....	13
2.2.2 MRI contrast agents.....	16
2.2.3 ParaCEST contrast agents for MRI.....	25
2.2.4 Design of contrast agents.....	27
2.2.5 MRI probes.....	29
2.3 References.....	35
Part II Thesis work.....	41
Chapter 3 Overall project of which this thesis is part.....	41
3.1 Materials possessing switchable spin states.....	41
3.1.1 Crystal field theory.....	41
3.1.2 Influencing factors on the splitting energy.....	43
3.1.3 Physical stimulus inducing spin transition.....	44
3.1.4 Chemical stimulus inducing spin transition.....	46
3.2 Proposal of the project.....	49
3.2.1 Choice of iron(II).....	50
3.2.2 Design of ligands.....	51
3.3 Previous work in the group.....	52
3.3.1 First example of complexes based on iron(II).....	52
3.3.2 Design of activatable MRI probes.....	53
3.4 Proposal of electroneutrality.....	55
3.5 Thesis project.....	60
3.6 References.....	60

Chapter 4 THESIS PROJECT: Achievement of electroneutrality of complexes based on pyridylcarboxylate .....	66
4.1 Introduction of the project.....	66
4.2 Synthesis of the designed complexes .....	68
4.2.1 Retrosynthetic analysis.....	69
4.2.2 Synthesis of benzyl chloromethylenepyridyl carboxylate.....	69
Scheme 4.1 .....	72
4.2.3 Synthesis of the macrocycle TACN .....	72
4.2.4 Synthesis of the target ligands by alkylation of amines .....	74
4.2.5 Synthesis of the target complexes .....	79
4.2.6 Synthesis of the ligands by reductive amination .....	80
4.2.7 Synthesis of the ligands bearing weinreb amide groups .....	83
4.3 Results and discussion .....	84
4.3.1 Magnetic moment measurements.....	84
4.3.2 Relaxivity measurements .....	87
4.4 Cytotoxicity tests.....	91
4.5 UV-vis spectrum analysis.....	92
4.5.1 UV-vis absorptions .....	92
4.5.2 UV-vis spectra for determination of pKa values .....	93
4.6 Cyclic voltammograms .....	98
4.7 Summary and perspective .....	100
4.8 References.....	101
Chapter 5 Achievement of electroneutrality of complexes based on pyrimidinediol.....	106
5.1 Introduction of the project and design of the target complexes .....	106
5.2 Synthesis of the target ligands bearing pyrimidinediol .....	107
5.2.1 Synthesis of the synthon bromomethylenepyrimidine .....	107
5.2.2 Synthesis of the target ligands.....	110
5.2.3 Synthesis of the complexes bearing protecting groups .....	111
5.2.4 Synthesis of the ligands without protecting groups.....	112
5.3 Results and discussion .....	116
5.4 Summary and Perspectives .....	117
5.5 References.....	117
Part III Experimental section .....	121
General Introductions.....	121
Synthesis I.....	123
Synthesis II.....	142
Synthesis III .....	147
The structures of the complexes.....	151
Acknowledgements.....	153
Compound table.....	155

## Abbreviations

AIBN	azodiisobutyronitrile
Boc/Boc <sub>2</sub> O	butyloxycarbonyl /Di- <i>tert</i> -butyl pyrocarbonate
BPO	benzoyl peroxide
CA (CAs)	contrast agent (or contrast agents)
CFT	crystal field theory
CV	cyclic voltammetry
DCM	dichloromethane
DCE	dichloroethane
DHP	dihydroxypyrimidine
DHMP	2-methyl-4,6-dihydroxypyrimidine
DIPEA	( <i>N</i> , <i>N</i> -diisopropyl- <i>N</i> -ethylamine
4-DMAP	4-dimethylaminopyridine
DMF	dimethylformamide
DMSO	dimethylsulfoxide
DPTACN	1,4-dipicolyl-1,4,7-triazacyclononane
EA	ethyl acetate
ESR	electron spin resonance
EPR	electron paramagnetic resonance
FISP	fast imaging with steady-state precession
HRMS	high resolution mass spectrum
HS	high spin
HSA	human serum albumin
HSAB	hard soft acid base
iPrOH	isopropanol (propan-2-ol)
LD-LISC	ligand driven light-induced spin change
LFT	ligand field theory

LS	low spin
MLCT	metal-ligand charge transfer band
MOMCl	Chloromethyl methyl ether
MOT	molecular orbital theory
MRI	magnetic resonance imaging
MRS	magnetic resonance spectroscopy
MT	magnetization transfer
NBS	<i>N</i> -bromosuccinimide
NMR	nuclear magnetic resonance
NSF	nephrogenic systemic fibrosis
paraCEST	paramagnetic chemical exchange saturation transfer
PBS	phosphate buffer / phosphate buffer saline
PE	petroleum ether
PET	Positron Emission Tomography
RARE	rapid acquisition relaxation enhancement
RF	radiofrequency impulse
RIME	receptor-induced magnetization enhancement
RT	room temperature
SBM	Solomon-Bloembergen-Morgan theory
SCO	spin crossover
SCE	saturated calomel electrode
SNR	signal-noise ratio
SPECT	single photon emission computed tomography
SQUID	superconducting quantum interference device
TACN	1,4,7-triazacyclononane
TFA	trifluoroacetic acid / trifluoroacetate
THF	tetrahydrofuran
TLC	thin layer chromatography
TMSI/TMSCl	Iodotrimethylsilane/ chlorotrimethylsilane

Ts	para-toluenesulfonyl; thus TsOH: para-toluenesulfonic acid
UV-Vis	ultraviolet-visible light spectroscopy
ZFS	zero field splitting

## Abstract

Magnetism is an intrinsic physical property of matter, the paramagnetic materials can be used for chemical and biological research. The magnetism change of a molecule which can be detected by NMR, MRI or ESR stands for a change of environmental conditions caused by some analytes. Thus it is an alternative readout besides the typical methods based on optical properties and it attracts our great interest for research.

The first part introduced the magnetism of matter and MRI as an indispensable tool in modern diagnostics due to their accurate and specific information and moreover the advantages of low toxicity and high spatial resolution. The MRI principle and the influencing factors of relaxation time of water protons were also explained, followed by the elaboration of strategies to design MRI probes then the presentation of advantages of iron(II) and TACN which led to the introduction of the previous work in our group. Afterwards the advantages of the low osmolarity and fast clearance of electroneutral MRI CAs reported in the literatures were presented then the PhD project was proposed.

The second part introduced two strategies to achieve electroneutrality according to pKa values of pyridylcarboxylic acid and pyrimidinediol, which was followed by design, synthesis and studies on basic properties of the target complexes.

The macrocycle TACN was synthesized in large scale which requires much experimental skills, then the monoalkylated TACN was prepared in excellent purity due to the explored methods to form their hydrochlorides.

Four groups (COOBn, COOEt, CONH<sub>2</sub>, CON(Me)(OMe)) for providing carboxyl group on the pyridine ring and three ways (two alkylations and one reductive amination) for its combination with TACN were tried. The ligands bearing the ethyl ester groups were successfully obtained, which were subsequently hydrolyzed under

acidic condition for complexation with iron(II) salt, and the obtained complexes were characterized by HRMS and the low-spin one has its  $^1\text{H}$  NMR and X-Ray Diffraction. Then both of two complexes were used for measurements of their properties such as relaxivities, magnetic moment, UV-vis absorptions, pH titration, cytotoxicity, and cyclic voltammogram. The results showed that they have their own reasonable relaxivities, relatively low cytotoxicity and high stability in physiological media, which implies their potential application in design of MRI probes.

The N6 and N5O1 type complexes bearing four methoxyl groups based on pyrimidine were also successfully synthesized and the former showed high-spin state by its XRD analysis. The deprotection of the N6 ligand was successful after many methods were tried, but the condition should be controlled strictly and its complexation in the presence of some base is suggested for improving the solubility of the ligand in MeOH, EtOH and acetonitrile.

The third part is the experimental section which described all the conditions and results of the successful reactions, and synthesis of the intermediates of some unsuccessful strategies.

In conclusion, the high-spin and low-spin, electroneutral, ferrous and binary complexes based on pyridylcarboxylic acid have been synthesized and characterized. To our knowledge, this is the first instance of an electroneutral version of a low-spin ferrous complex. Their properties pave a promising way for designing MRI probes based on them. The totally novel N6 type complex bearing four methyl groups based on pyrimidinediol has been synthesized and it is worth studying magnetism of the deprotected form compared to its high-spin property. At present a better method of deprotection and complexation is being explored.

**Key words:** magnetism, MRI, TACN, ligands, pyridylcarboxylic acid, pyrimidinediol, electroneutral complexes, high-spin, low-spin

## Résumé

Le magnétisme est une propriété physique et intrinsèque de la matière, les matériaux paramagnétiques peut être utilisé pour la recherche chimique et biologique. Le changement du magnétisme d'une molécule qui peut être détectée par RMN ou ESR IRM représente un changement des conditions environnementales causées par certains analytes. Ainsi, elle est une alternative de méthodes typiques basées sur les propriétés optiques et elle attire les grands intérêts pour la recherche.

La première partie introduit le magnétisme de la matière et l'IRM comme un outil indispensable dans le diagnostic modernes grâce à leur information claire et précise et les avantages de toxicité faible et de haute résolution spatiale. Le principe d'IRM et les facteurs influençant le temps de relaxation des protons de l'eau ont également été expliquées, suivie par l'élaboration de stratégies pour concevoir des sondes IRM puis la présentation des avantages de fer (II) et TACN qui a conduit à l'introduction de l'œuvre précédente dans notre groupe. Ensuite, les avantages de la faible osmolarité et le dédouanement rapide de CAs électroneutre d'IRM rapporté dans les littératures ont été présentés alors le projet de doctorat a été proposé.

La deuxième partie introduit deux stratégies pour atteindre l'électroneutralité selon les valeurs de pKa de l'acide pyridylcarboxylique et pyrimidinedione, qui a été suivie par le design, la synthèse et les études sur les propriétés basique de complexes cibles.

Le TACN macrocyclique a été synthétisé à grande échelle qui nécessite beaucoup des compétences expérimentales, puis l'TACN monoalkylé a été préparé en une excellente pureté grâce aux méthodes explorées pour former leurs chlorhydrates.

Quatre groupes (COOBn, COOEt, CONH<sub>2</sub>, CON(Me)(OMe)) pour fournir l'acide carboxylique sur le cycle pyridine et trois voies (deux alkylations et une amination réductrice) pour sa combinaison avec TACN sont essayés. Les ligands portant les groupes ester d'éthyle sont obtenus qui ont été ensuite hydrolysé dans des conditions

acides pour la complexation avec le fer (II), et les complexes obtenus ont été caractérisés par HRMS et celui-ci avec bas spin a ses  $^1\text{H}$  RMN et diffraction des rayons X. Tous deux ont été utilisés pour la mesure de leurs propriétés telles que relaxivités, moment magnétique, UV-vis absorptions, pH titration, la cytotoxicité, et voltammogramme cyclique. Les résultats ont montré qu'ils ont leurs propres relaxivités raisonnables, relativement faible cytotoxicité et une grande stabilité dans les milieux physiologiques, ce qui implique leur application potentielle dans le design de sondes d'IRM.

Les complexes de type N6 et N5O1 portant quatre groupes méthoxyles basés sur la pyrimidine sont synthétisés et celui de type N6 a montré l'état de haut spin selon son analyse DRX. La déprotection du ligand N6 a réussi après de nombreuses méthodes essayées, mais la condition doit être contrôlée strictement et sa complexation est suggérée dans la présence d'une base pour améliorer la solubilité du ligand dans du MeOH, EtOH et de l'acétonitrile.

La troisième partie est la section expérimentale qui décrit toutes les conditions et les résultats des réactions réussies, et la synthèse des intermédiaires de certaines stratégies efficaces.

En conclusion, deux complexes électroneutres, ferreux et binaires à base d'acide pyridylcarboxylique ont été synthétisés et caractérisés. A notre connaissance, c'est le premier exemple d'un complexe ferreux avec bas spin en version électroneutre. Leurs propriétés ouvrent une voie prometteuse pour le design de sondes d'IRM basés sur eux. Le totalement nouveau N6 complexe protégé par quatre méthyle basé sur pyrimidinedione a été synthétisé et il est intéressant d'étudier le magnétisme de sa forme déprotégée par rapport à sa propriété haut-spin. À l'heure actuelle une meilleure méthode de déprotection et de complexation est à l'étude.

**Mots clés:** magnétisme, IRM, TACN, ligands, l'acide pyridylcarboxylique, pyrimidinediol, complexes électroneutres, haut-spin, bas-spin

## 摘要

磁性是物质本身具有的一种物理性质，而且顺磁性物质在化学和生物领域有着广泛的应用。分子磁性的变化可以由核磁共振、核磁共振成像或电子共振方法来表征，而这种磁性的变化可以反应出其所处环境由于外界分析物所引起的变化。由此可见，化学中除了典型的光学方法可以作为探针设计的原理，磁性也是一种重要的读出方法，从而吸引了我们极大的研究兴趣。

论文中第一部分对物质的磁性、核磁共振成像技术的基本原理和优点进行阐述，指出其因能够提供准确而独特的信息，且具有低毒性与高空间分辨率而成为医学诊断中不可或缺的工具；对水质子弛豫时间的影响因素进行分析，指出核磁共振成像造影剂的设计与工作原理；对核磁共振成像造影剂探针的设计原理进行研究，并对亚铁离子与大环 TACN 衍生物的选择进行介绍，进而引入课题组对造影剂探针的设计理念及应用实例；对电中性核磁共振成像造影剂的优点（低渗透压及快速代谢与清除）进行探索并立题，提出电中性亚铁配合物作为造影剂探针的潜在优势。

论文中第二部分分别对吡啶羧酸与嘧啶二醇的配位作用及羧基的酸性进行研究，设计了新型的高自旋与低自旋的亚铁配合物；克服了反应条件苛刻而难以控制的困难，达到了对实验技能的要求，大量合成了化合物 TACN；同时，成功合成了单取代的 TACN 化合物，并发展了其成盐的方法，保证了化合物的高纯度。

通过对吡啶基羧酸尝试四种羧基保护基（苄基酯，乙基酯，酰胺，weinreb 酰胺）和三种与 TACN 结合的方法（两种取代和一种还原胺化方法），成功合成了带有乙酯基的配体，其经酸性水解、与亚铁离子配位得到相应的配合物，并用高分辨质谱表征，其中，低自旋的配合物还给予氢谱与单晶衍射结构表征；对合成的高自旋与低自旋的配合物均进行了弛豫性能、磁矩、紫外吸收、pH 滴定、细胞毒性与循环伏安图的测定。测试结果表明，其具有相应的合理的弛豫性能，并在生理 pH 下具有较好的稳定性和较小的细胞毒性，为发展新型核磁共振成像

造影剂探针提供了新的途径。

为避免活泼羟基引发副反应以及改善化合物的溶解性,采用甲基对嘧啶二醇的羟基保护,成功合成了带有甲基保护基的 N6 与 N5O1 型配体及其相应的配合物;对 N6 型基于嘧啶二醇的、带有甲基保护基的亚铁配合物进行磁矩测定,结果表明,其具有高自旋状态;对脱甲基的多种方法进行了尝试,最终成功合成了其相应的配体,并给予  $^1\text{H}$ 、 $^{13}\text{C}$  NMR 与 HRMS 表征。但其反应条件较苛刻,需严格控制,而且其在甲醇、乙醇或乙腈中的溶解性很差,配合物的合成受到限制,希望碱的加入能够将其改善并使配位顺利进行,该工作正在尝试中。

第三部分是实验部分,描述了所有成功反应与条件,以及化合物的表征;对在探索合成方法的过程中成功得到的一些中间体进行了相应的合成描述,为后续工作提供借鉴。

总之,基于吡啶基羧酸成功合成、表征了首例低自旋电中性亚铁配合物及相应的高自旋配合物,其性质研究结果为核磁共振成像探针的设计奠定了基础。同时,成功合成了具有高自旋性的、基于嘧啶二醇的 N6 型、带甲基保护基的配合物,其相应的电中性配合物的自旋性值得探究。目前,更好的脱保护与配位的方法正在探索中。

**关键词:** 核磁共振成像, TACN, 配体, 吡啶基羧酸, 嘧啶二醇, 电中性配合物, 高自旋, 低自旋

## Part I Introduction

### Chapter 1 Introduction about magnetism of matter<sup>[1]</sup>

#### 1.1 Magnetism character of matter

Magnetism is an intrinsic physical property which exists in all matter. Matter would be affected to some extent if it is placed in an inhomogeneous magnetic field generated by another magnet like the compass. (Fig. 1.1). This magnetic behavior is dependent on its structure, in other words, it originates from the magnetic moments of elementary particles such as nuclei and electrons (which will be presented afterwards.), and their sum divided by magnetic flux density is referred to as "magnetic susceptibility" or "magnetizability". Typically it is divided into five classes: diamagnetism, paramagnetism, ferromagnetism, antiferromagnetism, ferrimagnetism.

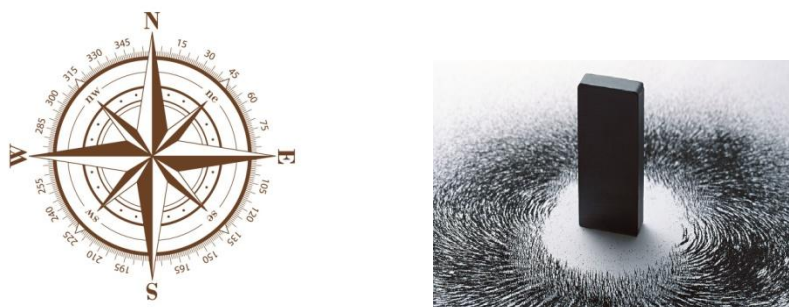


Fig. 1.1 Left, the compass works based on the large magnetic field from the earth; right, the schematic of magnetic matter affected by the field from a bar magnet

##### 1.1.1 Diamagnetism<sup>[2]</sup>

If the magnetic field is induced in the opposite direction to the applied magnetic field, and they would be repelled by each other. The magnetic susceptibility is negative and quite small, only about  $-10^{-6}$ , even it does not change up to the temperature. This

effect exists in all materials but can be obviously observed only in an exact diamagnetic matter such as inert gas elements and some metals which are resistant to corrosion. In most materials diamagnetism is very weak, compared to the magnetism of paramagnetic materials, it is dimensionless. However, as a diamagnetic representative, superconductors can cause magnetic levitation because of enormous repulsive interaction with all fields.

### **1.1.2 Paramagnetism<sup>[3]</sup>**

In a pure paramagnetic material, its paramagnetism is much bigger than its diamagnetism so that its diamagnetism is totally covered.

In contrast, the magnetic field caused by paramagnetic materials is in the same direction with the applied magnetic field and they are attracted by each other. The magnetic susceptibility is positive and it is linear that the total of magnetic moment of atoms or molecules which consist of the material. Actually they have their own permanent magnetic moments (named dipoles) even without the applied field, which roots in the spin of unpaired electrons in atomic or molecular electron orbits. In that case, all the dipoles do not interact with each other and they prefer align randomly to make the net magnetic moment of material zero. Thus the Paramagnetic materials do not retain the magnetic properties any more in the absence of an applied magnetic field, because induced magnetization derives from the ordered alignment of spins caused by the applied field. When it is removed, thermal motion can randomize all the spin orientations and the disorder comes back so that the total magnetization drops to zero. The magnetic susceptibility decreases with the increasing of temperature. Generally two nearby magnetic dipoles prefer align in two opposite directions thus their magnetic fields offset one another, and the alignment of dipoles resulting from the external field is very easily destroyed by thermal fluctuations.

### **1.1.3 Ferromagnetism<sup>[4]</sup>**

Materials possessing ferromagnetism like paramagnetic ones have also unpaired electrons. At the beginning, the magnetization is also zero in the absence of the external magnetic field, then it would increase to a maximum value with increasing of the applied magnetic field strength. But afterwards when the applied magnetic field is decreased gradually it would not get back to the same value at the same magnetic field strength, that is, it is bigger than that shown during the magnetization process which is called hysteresis.

In a few substances there exists spontaneous magnetization. That is, the intrinsic magnetic moments of electrons tend to align parallel to each other for stabilization with lower energy. Because the strong electrostatic repulsion forces the neighboring electrons to keep a certain distance so that it benefits their great exchange interaction which produces some energy to make them stand up in the same direction then further forms a magnetic domain. Different domains in a material have different magnetic moments and magnetizations, thus the total one is still zero. That is why some unmagnetized ferromagnets such as iron, nickel, cobalt and their alloys still have an "unmagnetized" state. Furthermore, like paramagnetic materials, once they are put in a magnetic field, they will reorient the domains so that more spins of electrons align in the direction of the field. What is the different, they will keep those domains even though the external field is removed, which creates a permanent magnet extending into the space around it after very long time sometimes even hundrands of years.

Nevertheless, when the temperature reaches to a certain point which is called Curie temperature<sup>[5-6]</sup>, ferromagnetic materials can lose their spontaneous magnetization properties due to the thermal motions. So when the temperature is above this point, they are just paramagnetic materials. Below it, they just have very small induced magnetization and it does not change proportionally to temperature. Every ferromagnetic substance has its own Curie temperature.

#### **1.1.4 Antiferromagnetism<sup>[7]</sup>**

In antiferromagnetic materials there exist electrons which spin in parallel in the opposite directions and those materials can never show the spontaneous magnetization in a lattice because the electrons from one sublattice spin in the opposite direction with those from another sublattice. The formed magnetic domains have no any magnetic moment or magnetization, naturally the total magnetization is always zero. But the macroscopical property is paramagnetic and its magnetic susceptibility is positive but quite small. It increases with decrease of temperature. This kind of matter also has their critical temperatures, which are called Neel temperature.

### **1.1.5 Ferrimagnetism<sup>[7-8]</sup>**

Ferrimagnetism is not relative to ferromagnetism, but similar to antiferromagnetism. Because ferrimagnetic materials have opposing spins of neighboring electrons but their magnetic moments are not equal. Consequently they still keep some spontaneous magnetization and they also have their own Curie temperatures. In addition, when temperature goes down to some point (magnetization compensation point) below the Curie temperature, the two magnetic moments in opposing directions are equal and the net magnetic moment gets zero.

In addition, ferrimagnetic materials are insulators due to their high resistivity. They can also be used as isolators, circulators or gyrators because interaction between the anisotropic property and the applied field makes microwave signals can pass through the material. Generally ferrites and magnetic garnets exhibit ferrimagnetism.

## **1.2 Magnetic moment of an atom or a molecule**

### **1.2.1 Composition of magnetic moment of an atom or a molecule<sup>[9-11]</sup>**

Fundamentally, there are two kinds of sources for magnetic moment of any system: motion of charges and the intrinsic magnetism of elementary particles.

As we have known, an atom consists of its nucleus and electrons, so its magnetic

moment is naturally the sum of orbital ones caused by motion of electrons around its nucleus and those caused by spins of all particles. Similarly, molecular magnetic moment results from two contributions: orbital ones caused by motion of electrons around molecule and all spins of electrons and nuclei.

What I want to point out is, considering that two electron spins in opposite directions can cancel each other out, so herein the electron spins are referred to as unpaired electron ones. The total magnetic moment caused by orbital motions is expressed by angular momentum. And the net value of the nuclear spin(s) which consists of those of protons and neutrons is much smaller than that of electron spins by three orders of magnitude. Consequently, it is negligible to the overall magnetic moment and thus the observed magnetic moment of an atom or a molecule is principally caused by electronic contributions. Nevertheless, Nuclear Magnetic Resonance (NMR) basing on nuclear magnetic moment is a still useful tool to analyze the structure of a compound.

### **1.2.2 Diamagnetic property**

In view of the presentation above, we focus on the electron spins of the atom or molecule. According to Pauli's exclusion principle, two electrons occupying the same orbital will align in pairs and spin in opposite directions so that their magnetic moments cancel each other out. However, their orbital magnetic moments are slightly different because of the slight different distance between the electrons and the nucleus. Consequently the magnetic moment of spins in opposite direction to the applied magnetic field is slightly bigger than the one parallel to it, and the direction of the net magnetic moment is opposite to the one of the external magnetic field which are repelled by each other. This effect is referred to as diamagnetic contribution, which is extremely small.

### **1.2.3 Paramagnetic property**

Besides of the property possessed by diamagnetic atoms or molecules, paramagnetic ones have unpaired electrons which lead to the major contribution to the overall magnetic moment in the direction of the applied field. This effect is obvious enough that can cancel the diamagnetic effect out. The microscopic magnetic moment of the electrons is quantized and they do Larmor procession in the external magnetic field which results from their motion affected by the external field as well as their spin around its own axis. Consequently, the final angular momentum is represented by  $J$ , which is equal to the sum of orbital angular momenta ( $L$ ) and the spin ones ( $S$ ). Then the effective magnetic moment ( $\mu_{\text{eff}}$ ) can be given by a formula (Russell-Saunders coupling, Fig. 1.2):

$$\mu_{\text{eff}} = g_J \mu_B [j(j+1)]^{1/2} \quad J = L + S$$

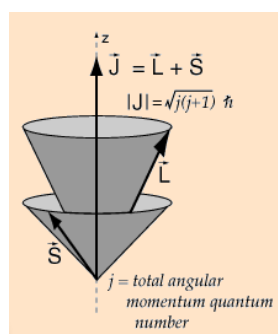


Fig. 1.2 The illustration about angular momentum of an atom doing Larmor procession

Here,  $j$  is the total angular momentum quantum number which is related to  $J$ ,  $g_J$  is the Landé  $g$ -factor (a kind of a  $g$ -factor, and Alfred Landé first described it in 1921. It is used for describing the total angular momentum quantum.), and  $\mu_B$  is the Bohr magneton.

Seeing from the formula, we can see the importance of unpaired electrons whose number determines the value of the total spin quantum number ( $S$ ).

Normally those unpaired electrons move between some electron orbits of the nucleus which possess not only the same energy but also the symmetry, even available vacancies for electrons. In addition, the moving electrons cannot keep the completely

same state because of Pauli's exclusion principle, thus they either keep the spin or the orbital directions different. However, when other atoms approach to form some compounds, for example, ligands approach to form complexes, the initial degeneracy of multiple orbits disappears so that the orbital contribution to paramagnetism is quenched.

However, the Russell-Saunders equation is just suitable for the lighter atom. The reason can be explained by the term spin-orbit interaction which describes the coupling of the electron spin with its motion. This electromagnetic interaction can cause shifts of atomic energy levels because of the interaction between spin of electrons and the magnetic field generated by the movement of electrons around the nucleus. The longer distance between nucleus and electrons, the more freely the electrons move which is typically expressed with electronic velocity, the more pronounced the magnetic field generated by their movements so that the spin-orbit interaction becomes stronger. Thus the bigger the atomic number  $Z$ , the more the orbital contribution. In the consequence, for heavier elements this interaction determines the overall magnetic moment and it is calculated by  $j - j$  coupling. While for the lighter elements such as the first row transition metals, their spin and orbital contributions are just simply added together.

#### **1.2.4 Detection of magnetism<sup>[12]</sup>**

The volume magnetic susceptibility ( $\chi_v$ ) can be used to describe the magnetism of a material, which is measured at the earliest by Gouy<sup>[13]</sup>. This method is based on a apparent mass change of a substance before and after the effect of a magnetic field. There is an alternative named Faraday balance whose principle is almost the same. Afterwards there is another method called Evans balance which is more convenient and is suitable to all forms of samples such as solids, liquids, and gases. This method is not expensive, neither requires a precision of the weighting device. Then some techniques such as SQUID (superconducting quantum interference device)<sup>[14]</sup> and

Hall-sensors<sup>[15]</sup> based on it are developed.

In electromagnetism, there is a parameter closely related to volume magnetic susceptibility. It is the term permeability ( $\mu$ ) which expresses the degree of total magnetization of material under the influence of the external field. The term was coined by Oliver Heaviside in 1885. Its reciprocal is magnetic reluctivity. The relationship between  $\chi_v$  (the volume magnetic susceptibility) and  $\mu$  (the magnetic permeability) can be described by the formula ( $\mu_0$  is the magnetic constant.):

$$\mu = \mu_0(1 + \chi_v)$$

In general, both volume magnetic susceptibility and permeability are not constants, and they vary with some factors such as the frequency of the external field, the position in the medium, humidity, temperature and so on.

Even though the three balance methods have to use radiofrequencies to make the sample excited, they are environmental harmless. As the times progress, some strategies based on magnetic resonance such as EPR (direct detection) and NMR (indirect detection) are commonly used and developing.

Electron paramagnetic resonance (EPR)<sup>[16]</sup> was first observed by Yevgeny Zavoisky in 1944. It is a technique for direct detection of unpaired electrons and its basic principle is similar to that of nuclear magnetic resonance (NMR), thus it is also called electron spin resonance (ESR).

Because of the mass difference of electron and nucleus, the magnetic moment of an electron is obviously larger than that of a nucleus. Consequently an electron requires a higher electromagnetic frequency in order to generate spin resonance. In addition, electrons are normally associated with one or more atoms, thus they are definitely affected by the magnetic moment of the associated nucleus as long as this nuclear spin is not zero. This is so called hyperfine coupling which can split the EPR resonance signals.

Because EPR can provide some information about rates of chemical reactions by

spectral line, also about electronic structure or in other words the atomic or molecular orbital of the atom or molecule containing the unpaired electron by  $g$ -factor and hyperfine coupling, its spectroscopy is quite useful for studying some organic radicals or metal complexes, especially for providing evidence of the radicals produced in chemical reactions or the reactions themselves. This technique is also useful in biological models to tag biological systems by spin label, then monitor the protein interactions.

Nuclear Magnetic Resonance (NMR) is an indirect way<sup>[17]</sup> to measure the magnetism of a compound in question which can influence the magnetic field further both the chemical shifts and relaxation times of the detected nucleus. For example, Evans' method, it measures the magnetic moment of the studied compound based on the chemical shift of protons from *t*BuOH. Magnetic Resonance Spectroscopy (MRS) is very useful in medicinal field by detecting signals from the specific compound according to the chemical shifts. Paramagnetic chemical exchange saturation transfer (paraCEST) works on the principle that the chemical shift of water protons in the presence of paramagnetic compound differs from that without it. Magnetic Resonance Imaging (MRI) reflects the magnetism of the compound by different relaxation times of water protons in different environments. Some of them will be presented in detail afterwards in this thesis.

Even though the disadvantages of low sensitivity and high costs, the techniques based on NMR are being improved by variable strategies to enhance signals and construction of inexpensive devices, and already have practical application in clinical diagnosis.

### **1.3 References**

- [1] Helmut K. Handbook of Magnetism and Advanced Magnetic Materials. 2007, 5. Set. John Wiley & Sons. ISBN 978-0-470-02217-7.

- [2] Roland J. John Tyndall and the Early History of Diamagnetism, *Annals of Science*. 2014, 4.
- [3] Miessler G. L., Tarr D. A. *Inorganic Chemistry* (3rd Ed). 2003, Pearson/Prentice Hall publisher. ISBN 0-13-035471-6.
- [4] Chikazumi S. *Physics of Ferromagnetism*. 1997, Clarendon Press. ISBN 9780198517764.
- [5] Charles K. *Introduction to Solid State Physics* (6th ed.). 1986, John Wiley and Sons. ISBN 0-471-87474-4.
- [6] Skomski R., Sellmyer D. J. Curie Temperature of Multiphase Nanostructures. *J. Appl. Phys.* 2000, 87, 4756.
- [7] Néel L. Propriétés Magnétiques Des Ferrites, Férrimagnétisme et Antiferromagnétisme. *Annales de Physique*, 1948, 3, 137.
- [8] Spaldin N. A. *Ferrimagnetism. Magnetic Materials: Fundamentals and Applications* (2nd ed.). 2010, Cambridge University Press. ISBN 9780521886697.
- [9] Tilley R. J. D. *Understanding Solids*. 2004, John Wiley and Sons. ISBN 0-470-85275-5.
- [10] Tipler P. A., Llewellyn R. A. *Modern Physics* (4th ed.). 2002, Macmillan. ISBN 0-7167-4345-0.
- [11] Crowther J. A. *Ions, Electrons and Ionizing Radiations*. 2007, Rene Press. ISBN 1-4067-2039-9.
- [12] O'Connor C. J., Lippard S. J. Magnetic Susceptibility Measurements. *Prog. Inorg. Chem.* 1982, 29, 203.
- [13] Aime S., Botta M., Gianolio E., Terreno E. A p(O<sub>2</sub>)-Responsive MRI Contrast Agent Based on the Redox Switch of Manganese(II/III)-Porphyrin Complexes. *Angew. Chem. Int. Ed.* 2000, 39, 747.
- [14] a) Chen J. W., Sans M. Q., Bogdanov A., Weissleder R. Imaging of Myeloperoxidase in Mice by Using Novel Amplifiable Paramagnetic Substrates. *Radiology* 2006, 240, 473; b) Li Y., Sheth V. R., Liu G., Pagel M. D. A Self-calibrating PARACEST MRI Contrast Agent That Detects Esterase Enzyme Activity. *Contrast Media & Molecular Imaging* 2011, 6, 219.
- [15] a) Jasanoff A. MRI Contrast Agents for Functional Molecular Imaging of Brain Activity. *Curr.*

- Opin. Neurobiol.* 2007, 17, 593; b) Major J. L., Parigi G., Luchinat C., Meade T. J. Physical Sciences-Chemistry. The Synthesis and In Vitro Testing of a Zinc-Activated MRI Contrast Agent. *Proc. Natl. Acad. Sci. U. S. A.* 2007, 104, 13881; c) Que E. L., Chang C. J. Responsive Magnetic Resonance Imaging Contrast Agents as Chemical Sensors for Metals in Biology and Medicine. *Chem. Soc. Rev.* 2010, 39, 51.
- [16] Schweiger A., Jeschke G. Principles of Pulse Electron Paramagnetic Resonance. 2001, Oxford University Press. ISBN 978-0-19-850634-8.
- [17] Frei K. and Bernstein H. J. Method for Determining Magnetic Susceptibilities by NMR. *J. Chem. Phys.* 1962, 37 (8), 1891–1892.

## **Chapter 2 MRI as a method to detect magnetism**

### **2.1 Introduction of MRI**

Developing a suitable and powerful method to detect some biochemical processes or monitor some kinetic changes in an organism is so important that more and more readout techniques emerged by detecting physical and chemical signals. Nowadays It is the possibility of repeatable and non-invasive assessment, and quantification of gene and protein function, interactions between two proteins, signal transduction and so on that makes molecular imaging particularly attractive in biomedical applications. Molecular Imaging techniques such as Single photon emission computed tomography (SPECT), Optical imaging, Magnetic resonance imaging (MRI), Positron emission tomography (PET) and so on have become indispensable tools in modern medical diagnostics due to their accurate and specific information<sup>[1]</sup>. While all of those modalities are applied for early disease detection, real-time monitoring of therapeutic responses and investigating drug efficacy, we think of MRI because of its absence of ionizing radiation and the advantages of low toxicity and high spatial resolution (50  $\mu\text{m}$ ) (Fig. 2.1).

MRI was developed based on the nuclear magnetic resonance (NMR) for detecting magnetism of a sample. In 2003 P. Mansfield and P. C. Lauterbur were awarded the Noble Prize in Physiology or Medicine for their discoveries that human body can be transformed to images by MRI to achieve spatial resolution.

After that it was extensively applied in medicinal field because it creates images with high anatomical resolution in a applied field and RF which contributes to the harmlessness and non-penetration limit. Until now there have been a number of examples of its application to detect some diseases. Here I just give one to show its power in this field. For example, MRI was used to detect the human epidermal growth

factor receptor-2 (Her-2 receptor) which can be observed in approximate 30 % of breast cancer tumors regardless of its low density<sup>[2]</sup>. Moreover, people are interested not only in  $^1\text{H}$  MRI, the common one, but also in  $^{19}\text{F}$  MRI<sup>[3]</sup>, the special one. Even though the sensitivity of  $^{19}\text{F}$  MRI is limited by its trace amounts of  $^{19}\text{F}$  ( $<10^{-6}$  M) in the human body, the fluorinated tracers are developed to overcome it.

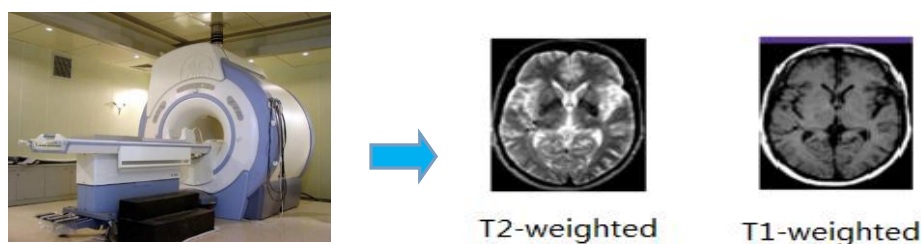


Fig. 2.1 Left, MRI instrument used in a hospital; right,  $T_2$ -weighted and  $T_1$ -weighted images generated by MRI. From the website.

## 2.2.1 MRI principle<sup>[4]</sup>

MRI is based on the principle of NMR spectroscopy, whose signals come from the detected paramagnetic nucleus (i.e. protons) present in the object. After the linear and time-varying magnetic field gradients are applied, those nuclear signals are spatially encoded so that MRI images are generated. Normally the MRI used in the clinic is based on signals of water protons from different tissues in the human body. Because about two-thirds of its weight is water, which makes MRI image more intensive.

### 2.2.1.1 NMR principle<sup>[5]</sup>

In thermodynamic state, all the non-zero nuclear spin dipoles are randomly oriented and the net magnetic moment is equal to zero. When placed in an external magnetic field  $B_0$ , the spins rearrange their directions responding to the field. As far as the protons ( $S = 1/2$ ) are concerned, they align only in two separate, quantized energy states in two directions, parallel (lower energy) and anti-parallel (higher energy) to  $B_0$  (Fig. 2.2). The difference of energy between two states is represented by  $\Delta E = \gamma\hbar B_0$ .

In each direction protons precess at their own Larmor frequencies which are also related to the strength of the magnetic field ( $\nu_0 = (\gamma/2\pi)B_0$ ). So the overall net magnetization of all the protons is the combination of those in two directions, and the overall energy is calculated in the same way. Actually there exist only a small excess of the nuclei in the direction parallel to  $B_0$  which can change their directions in the presence of the radiofrequency wavelengths (RF). When the frequency of RF is equal to that of Larmor precession, the proton jumps from the lower energy state to the higher one. That is so called nuclear resonance.

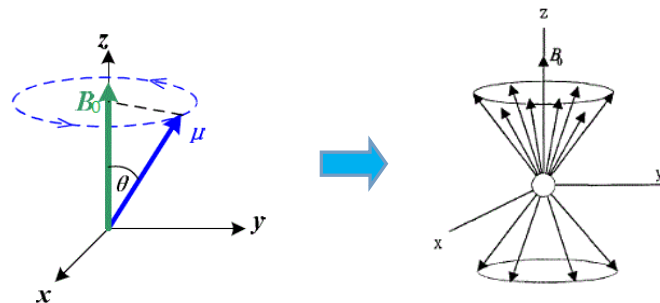


Fig. 2.2 Left, one proton's Larmor precession; right, the macroscopic magnetization. From the website.

### 2.2.1.2 Relaxation time of protons in MRI<sup>[6]</sup>

MRI images are generated by detection of relaxation times  $T_1$  or  $T_2$  of water protons based on NMR. The explanation is given as following.

As the description above, when the protons in an external magnetic field are submitted to pulses of radio waves, their magnetic moments realign thus the initial magnetic alignment is disrupted. That causes nuclear resonant excitation into the perpendicular plane. After the radio frequency (RF) pulses are removed, they relax back to their previous states to keep a thermodynamic equilibrium. While the magnetization vector also returns to the same direction with the field. The relaxation process normally is described in longitudinal and transverse directions. The former,

termed as spin-lattice interaction, is caused by release of energy to its surroundings from the excited state and measured by  $T_1$ ; the latter, termed as spin-spin interaction, is caused by neighboring spins dephasing vector in the plane which is perpendicular to the external magnetic field and measured by  $T_2$ .  $T_1$  represents the time that the z component of the nuclear spin magnetization vector recovers to 63% of its thermal equilibrium value, and  $T_2$  represents the time that transverse magnetization vector decreases to 37% of its original magnitude (Fig. 2.3). Generally the rate of  $T_1$  relaxation ( $1/T_1$ ,  $r_1$ ) is strongly dependent on the NMR frequency so that it significantly varies with strength of the magnetic field ( $B$ ). Moreover, only small amount of paramagnetic substances in a sample can speed up relaxation quite much; while  $1/T_2$  or  $r_2$  is generally much less dependent on  $B$ .  $T_2$  is always equal to or shorter than  $T_1$ .

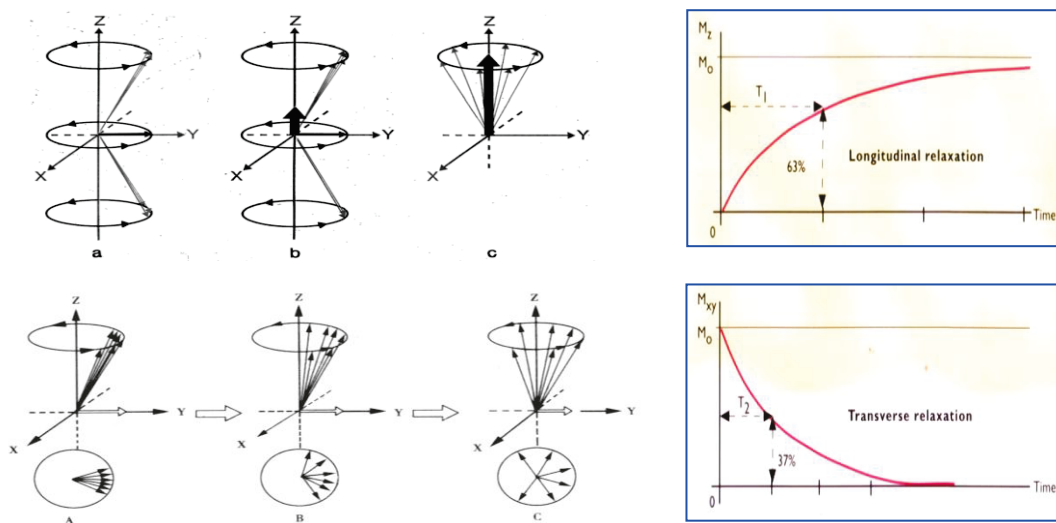


Fig. 2.3 The illustration about the relaxation,  $T_1$  and  $T_2$  of water protons, from the website.

MRI signals tend to increase with increasing relaxivity  $r_1$  and decrease with increasing relaxivity  $r_2$ . The images obtained by using pulse sequences that emphasize changes in  $r_1$  are referred to as  $T_1$ -weighted ones and the more intense the signals are, the more bright the regions are; while those  $T_2$ -weighted ones are obtained by using pulse sequences that emphasize changes in  $r_2$ , and they are associated with darker

regions.

## 2.2.2 MRI contrast agents

The intensity of MRI signals depends on that of protons in the region of research and the polarization degree of nuclear spin states. The endogenous MR differences among different tissues are weak, thus in MRI tests a contrast agent (CA) is often required to provide additional contrast to distinguish a target tissue from others. Ample evidences have shown that CAs are paving the way for MRI to become a true contender in molecular imaging era. CAs can be various kinds of chemicals such as chelates, nanoparticles, polymers and so on ( Fig 2.4).

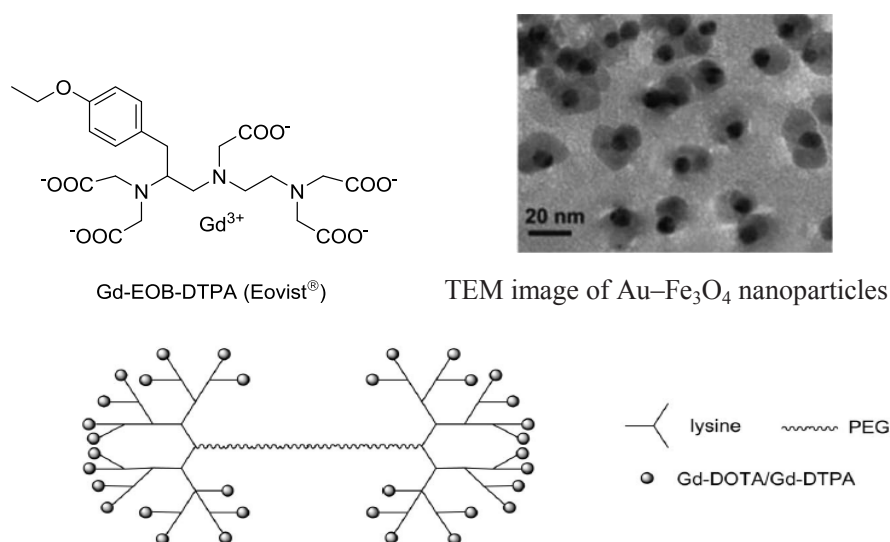


Fig. 2.4 Three representatives of CAs. Chelating agent and the polymer come from the *Chem. Rev.* 2010, 110, 2921; Nanoparticles comes from *Adv. Mater.* 2009, 21, 2133.

### 2.2.2.1 Relaxation time of water protons in the presence of CAs<sup>[6-7]</sup>

CAs themselves do not directly give signals nor are visualized but affect their surrounding water molecules by catalyzing the relaxation process of their protons to decrease  $T_1$  and  $T_2$ . The difference of accumulation of a CA in different soft tissues enhances the contrast.

Herein  $Gd^{3+}$  contrast agents are taken as a sample to explain the principle that CAs enhance the relaxation and then some influencing factors of relaxation time. In general the observed relaxation,  $(1/T_i)_{obs}$ , is the sum of the intrinsic relaxation rate of water protons in the absence of the paramagnetic species,  $(1/T_i)_w$ , and the additional relaxation rate attributed to paramagnetic substance,  $(1/T_i)_p$ .

$$\frac{1}{(T_i)_{obs}} = \frac{1}{(T_i)_w} + \frac{1}{(T_i)_p} \quad i = 1, 2 \quad (1)$$

CAs affect either  $T_1$ ,  $T_2$  or both at the same time. Two types of the relaxation catalysts are generally used, and they increase both  $r_1$  and  $r_2$  to varying degrees which depend on their natural properties as well as the applied magnetic field. Generally when CAs lead to a much larger increase in  $r_1$  (or  $r_2$ ) than in  $r_2$  (or  $r_1$ ), the images should be obtained by  $T_1$ -weighted (or  $T_2$ -weighted) scans so that the contrast between different tissues is more obvious. If they increase  $r_1$  and  $r_2$  by roughly similar amounts, it should be better use  $T_1$ -weighted scans since the percentage change in  $r_1$  in tissue is much greater than that in  $r_2$ . Typically the values of  $r_1$  and  $r_2$  refer to the amounts of increase respectively in  $1/T_1$  and  $1/T_2$  per millimolar agent, thus they are defined in units of  $mM^{-1} s^{-1}$ .  $T_1$  agents, also named positive CAs, usually have  $r_2/r_1$  ratios of 1-2, while the value of  $T_2$  agents named negative CAs such as iron oxide particles is about 10 or even more.

By far reduction of  $T_1$  is more attractive, thus 90% of all CAs-assisted MRI examinations in clinic belong to the family of paramagnetic metal complexes and most of them target  $T_1$ . It is attributed to that  $T_1$  is significantly longer than  $T_2$  thus its shortening can be more pronounced, and that it allows for increasing signal intensity with increasing the number of scans in the same time period.

Relaxivity enhancement induced by CAs is more unambiguously associated with the contrast agent activity. Usually this enhancement originates from the dipole-dipole interactions between the nuclear magnetic moments of protons and the fluctuating local magnetic field caused by the unpaired electron spins of the paramagnetic substance. So the activity of a CA depends on the distance between the ion and the diffusion of water molecules. Usually we classify interactions between water and the metal ion into three types: (1) the first coordination sphere which is direct coordination of water to the ion, (2) the secondary coordination sphere whose coordination is caused by hydrogen-bond between water and the ligand of the ion, (3) bulk water that diffuses translationally past the metal (Fig. 2.5). Typically the relaxation in the first coordination sphere is referred to as inner-sphere one and the outer-sphere consists of the second coordination sphere and bulk water.

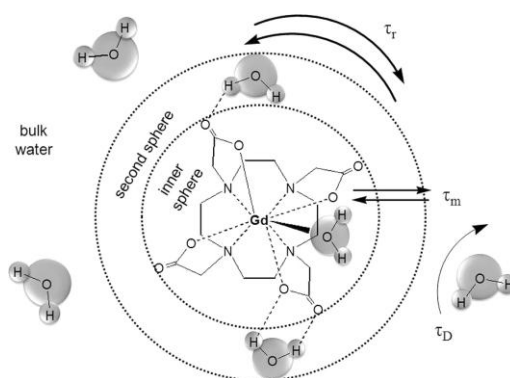


Fig. 2.5 Relaxation coordination spheres of water: inner-sphere, secondary-sphere, and bulk water, from *Chem. Rev.* 2010, 110, 2921.

Therefore Paramagnetic relaxation is the sum of that in inner-sphere and outer-sphere.

$$\frac{1}{(T_i)_p} = \frac{1}{(T_i)_{\text{inner-sphere}}} + \frac{1}{(T_i)_{\text{outer-sphere}}} \quad i = 1, 2 \quad (2)$$

It is directly proportional to the concentration of the paramagnetic compound,  $C_{\text{agent}}$  (in units of mmol/L), by the relaxivity  $(r_i)_{\text{agent}}$  (in the units of  $\text{mM}^{-1}\text{s}^{-1}$ ) which is a function of its paramagnetism and its interaction with water protons.

$$\frac{1}{(T_i)_p} = (r_i)_{\text{agent}} C_{\text{agent}} \quad i = 1, 2 \quad (3)$$

In view of the above, the measured relaxation rate  $r_i^{obs}$  is described as following. It consists of three parts, the intrinsic relaxation rate of water protons without presence of magnetic substances  $r_i^W$ , the contribution of inner-sphere  $r_i^{IS}$  and that of outer-sphere  $r_i^{OS}$ .

$$r_i^{obs} = r_i^{IS} + r_i^{OS} + r_i^W \quad i = 1, 2 \quad (4)$$

### 2.2.2.2 Inner-sphere enhancement of relaxivity

The inner-sphere relaxation is usually described by Solomon-Bloembergen-Morgan (SBM) Equations.

The subscript ‘‘m’’ refers to the solvent molecule in the inner-sphere.  $P_m$  is the mole fraction of solvent molecule nuclei,  $q$  is the number of bound water per metal ion (or the hydration number),  $\tau_m$  is the average residence time of water molecule in the complex (it is equal to the reciprocal of the solvent exchange rate,  $k_{ex}$ ).  $\Delta\omega$  refers to the difference between Larmor frequency of the inner coordination sphere and that of bulk water.

$$\frac{1}{(T_1)_{\text{inner-sphere}}} = \frac{qp_m}{T_{1m} + \tau_m} \quad (5)$$

$$\frac{1}{(T_2)_{\text{inner-sphere}}} = q P_m \frac{1}{\tau_m} \left[ \frac{T_{2m}^{-1} (\tau_m^{-1} + T_{2m}^{-1}) + \Delta\omega_m^2}{(\tau_m^{-1} + T_{2m}^{-1})^2 + \Delta\omega_m^2} \right] \quad (6)$$

Relaxation of water protons bound to a paramagnetic center happens principally via the dipole-dipole interactions (DD) and scalar coupling (SC) as following equation,

$$\frac{1}{(T_i)_m} = \frac{1}{T_i^{DD}} + \frac{1}{T_i^{SC}} \quad i = 1, 2 \quad (7)$$

Therein when  $i$  is equal to 1,  $T_1^{DD}$  and  $T_1^{SC}$  are described like this,

$$\frac{1}{T_1^{DD}} = \frac{2}{15} \frac{\gamma_1^2 g^2 \mu_B^2 S(S+1)}{r^6} \left[ \frac{3\tau_{c1}}{1+\omega_1^2 \tau_{c1}^2} + \frac{7\tau_{c2}}{1+\omega_s^2 \tau_{c2}^2} \right] \quad (8)$$

$$\frac{1}{T_1^{SC}} = \frac{2}{3} S(S+1) \left( \frac{A}{\hbar} \right)^2 \left[ \frac{\tau_{e2}}{1+\omega_s^2 \tau_{e2}^2} \right] \quad (9)$$

$$\omega = \gamma B \quad (10)$$

Here,  $\gamma_1$  is the nuclear gyromagnetic ratio,  $g$  stands for the electronic  $g$ -factor,  $\mu_B$  is the Bohr magneton, the letter  $r$  stands for the distance between the proton and the electron spin,  $\omega_1$  and  $\omega_s$  respectively are the Larmor precession frequencies of proton and electron which are directly related to  $\gamma$ ,  $\tau_c$  and  $\tau_e$  are the dipole-dipole and scalar correlation times,  $S$  represents the total electron spin of the metal ion.

As far as  $1/(T_2)_m$  is concerned,  $T_2^{DD}$  and  $T_2^{SC}$  are depicted as following, the  $A/\hbar$  means the electron-nuclear hyperfine coupling constant,

$$\frac{1}{T_2^{DD}} = \frac{1}{15} \frac{\gamma_1^2 g^2 \mu_B^2 S(S+1)}{r^6} \times \left[ \frac{3\tau_{c1}}{1+\omega_1^2 \tau_{c1}^2} + \frac{13\tau_{c2}}{1+\omega_s^2 \tau_{c2}^2} + 4\tau_{c1} \right] \quad (11)$$

$$\frac{1}{T_2^{SC}} = \frac{1}{3} S(S+1) \left( \frac{A}{\hbar} \right)^2 \left[ \frac{\tau_{e2}}{1+\omega_s^2 \tau_{e2}^2} + \tau_{e1} \right] \quad (12)$$

The correlation times  $\tau_c$  and  $\tau_e$  mentioned above are characterized with the equations,

$$\frac{1}{\tau_{ci}} = \frac{1}{T_{ie}} + \frac{1}{\tau_m} + \frac{1}{\tau_R} \quad i = 1, 2 \quad (13)$$

$$\frac{1}{\tau_{ei}} = \frac{1}{T_{ie}} + \frac{1}{\tau_m} \quad i = 1, 2 \quad (14)$$

$\tau_R$  is the rotational correlation time of the entire metal-water complex,  $T_{1e}$  and  $T_{2e}$  are the electronic longitudinal and transverse relaxation times of the metal ion and they are described by those equations:

$$\frac{1}{T_{1e}} = B \left[ \frac{1}{1+\omega_S^2\tau_V^2} + \frac{4}{1+4\omega_S^2\tau_V^2} \right] \quad (15)$$

$$\frac{1}{T_{2e}} = \frac{B}{2} \left[ \frac{5}{1+\omega_S^2\tau_V^2} + \frac{2}{1+4\omega_S^2\tau_V^2} + 3 \right] \quad (16)$$

$$B = \frac{1}{5\tau_{S0}} = \frac{\tau_V}{25} \Delta^2 [4S(S+1) - 3] \quad (17)$$

$\tau_{S0}$  stands for the electronic relaxation time at zero field,  $\tau_V$  is a correlation time caused by the transient zero field splitting (ZFS), then  $\Delta$  means the trace of the ZFS tensor.

Seen from the above, all the equations demonstrate us that the relaxation is a function of magnetic field and it is also true for the electronic relaxation of those ions whose electronic spin  $S$  is bigger than 1/2.

### 2.2.2.3 Outer-sphere relaxation enhancement

Theoretically the SBM equations can also describe the relaxation enhancement from the second coordination sphere. In that case it refers to the protons which are hydrogen-bonded to the contrast agent and they relax by the dipole-dipole interaction with the paramagnetic species. However,  $\tau_m$  is quite short and it is not easy to know the number of water molecules from the second coordination sphere and the ion-H distances so that quantification of the second coordination relaxation  $T_{1m}$  is limited to some extent. In view of that, a rigid-sphere model (Hwang and Freed model) is proposed, which describes the outer-sphere relaxation by translational diffusion of water molecules in this sphere past the metal complex. Its hard sphere consists of the water molecules and metal complex.

The following equations come from the model.

$$\frac{1}{(T_1)_{\text{outer-sphere}}} = C[3j(\omega_I) + 7j(\omega_S)] \quad (18)$$

$$\frac{1}{(T_2)_{\text{outer-sphere}}} = C[2 + 1.5j(\omega_I) + 6.5j(\omega_S)] \quad (19)$$

$$C = \left(\frac{32\pi}{405}\right) \gamma_I^2 \gamma_S^2 \hbar^2 S(S+1) \frac{N_A M}{1000 a D} \quad (20)$$

$$j(\omega) = \text{Re} \left\{ \frac{1 + \frac{1}{4} \left( i\omega\tau_D + \frac{\tau_D}{T_{ie}} \right)^{1/2}}{1 + \left( i\omega\tau_D + \frac{\tau_D}{T_{ie}} \right)^{1/2} + \frac{4}{9} \left( i\omega\tau_D + \frac{\tau_D}{T_{ie}} \right) + \frac{1}{9} \left( i\omega\tau_D + \frac{\tau_D}{T_{ie}} \right)^{3/2}} \right\} \quad i = 1, 2 \quad (21)$$

$$\tau_D = \frac{a^2}{D} \quad (22)$$

$I$  and  $S$  subscripts represent respectively proton and electron. Obviously  $\omega_I$  and  $\omega_S$  are respectively the Larmor angular velocities of proton and electron,  $C$  is related to  $D$  (the sum of the diffusion constants of the complex and water molecules),  $\gamma$  ( $\gamma_I$  and  $\gamma_S$ , the nuclear and electronic gyromagnetic ratios),  $S$  (the electronic spin),  $M$  (the concentration of the metal ion) and  $a$  (the closest distance between a proton and the paramagnetic complex),  $j(\omega)$  stands for the spectral intensity function, and it is the real part of that from the brace, which is what  $\text{Re}$  means,  $\tau_D$  (the diffusional correlation time) is pretty important to  $j(\omega)$ .

#### 2.2.2.4 Influencing factors of relaxation time $T_1$ <sup>[8-9]</sup>

Suffice it to say that the outer-sphere relaxivity is too complex to estimate. Generally the researchers focus on designing and developing  $\text{Gd}^{3+}$ -based MR contrast agents with considering the influencing factors of the inner-sphere relaxation. Basically  $\text{Gd}^{3+}$ -based MR agents have the character of the ionic bonding, so the hyperfine

coupling constant,  $A/\hbar$ , is very small so that the inefficient scalar relaxation ( $T^{\text{SC}}$ ) can be ignored. Afterwards the inner-sphere relaxation is dependent on dipole-dipole relaxation ( $T^{\text{DD}}$ ).

In view of that, we can say the major factors influencing the relaxation rate are  $S$ ,  $q$ ,  $\tau_m$ ,  $\tau_R$ ,  $r$ ,  $T_{1e}$ , and  $T_{2e}$  besides of the external field and temperature (Fig. 2.6).

The value of  $S$  (the electronic spin of the metal ion) is calculated from the number of unpaired electrons, and it dominantly determines the magnetic moment of metal complexes. It goes without saying that it is the crucial parameter. Seen from the Equations 7-9 and Equations 11-12 in SBM theory, relaxation rate  $1/T_{1m}$  and  $1/T_{2m}$  is proportional to  $S(S+1)$ . So the metal ions like Fe(III) and Mn(II) with 5 unpaired electrons have lower relaxivities than that of the Ln<sup>3+</sup> ions (like Gd<sup>3+</sup>) with 7 unpaired, so does the Fe(II) with 4 unpaired electrons when it is high-spin<sup>[10-11]</sup>.

By the way, the relative numerical comparison of  $1/T_{1m}$  and  $1/T_{2m}$  for the same metal ion is dependent on the electronic relaxation rate (or electronic relaxation time), which determines that the complex is  $T_1$  or  $T_2$  agent. For example, the unpaired electrons of lanthanide ions except Gd<sup>3+</sup> are placed in their f orbits anisotropically, which results in the lower energy excited state, and thus leads to strong magnetic anisotropy and their short electronic relaxation time ( $10^{-13}$  s)<sup>[12-13]</sup>. While the ground state of Gd<sup>3+</sup> with seven electrons is symmetric and thus its electronic relaxation rate is slower than them by 6 orders of magnitude<sup>[14-17]</sup>. Consequently the formers are suitable to used as  $T_2$  agents, on the contrary, the latter as  $T_1$  agents.

The bigger the hydration number ( $q$ ), the better the inner sphere relaxivity. But consequently the complex which contains more water molecules has lower thermodynamic stability. Once it is decomposed both its ligand and Gd<sup>3+</sup> generally have some inevitable toxicity.

$\tau_m$  represents the residence time to describe the exchange speed between water molecules coordinated to metal center and those in the bulk solvent. The fast

exchange leads to decrease of relaxation time.  $\tau_R$  is rotational correlation time that stands for rotation of the complex. Typically the larger molecules have some difficulty in tumbling. Thus the big steric hindrance as well as the hydrodynamic size generally slows the rotation velocity and increases  $\tau_R$  so that the relaxivity is improved. The optimal values of these  $Gd^{3+}$ -based CAs at 1.5 T should be approximately 10 ns for  $\tau_m$  and at least 10 ns for  $\tau_R$  according to SBM theory.

The letter  $r$  means the distance between the water proton and the unpaired electron spin, which significantly affect the relaxivity because it exists in the form of  $1/r^6$  in the formula. For example, the  $r$  of  $Gd^{3+}$ -based complexes is normally around 3.1 Å. According to the SBM theory, if it is shortened by 0.1 Å,  $r_1^{IS}$  will increase by 20 %, while lengthening it by 0.2 Å can reduce  $r_1^{IS}$  by 50 %.

$T_{1e}$ , and  $T_{2e}$  are electronic parameters related to the magnetic field. All these variables can be considered to make an increase in the relaxivity that results in a decrease in the application dose in MRI.

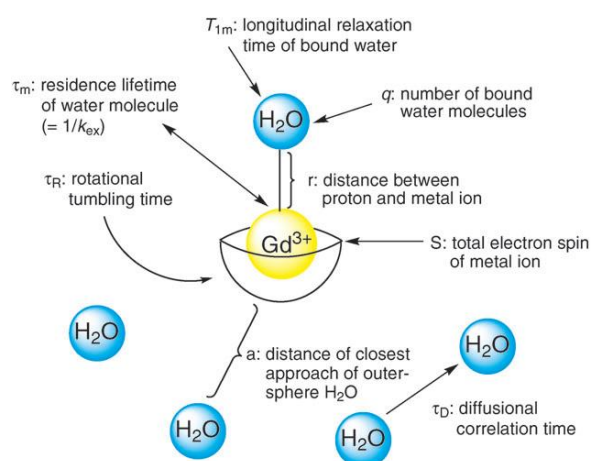


Fig. 2.6 Variables contributing to contrast agent relaxivity, from *Chem. Soc. Rev.* 2010, 39, 51.

Obviously it is not very easy to find a perfect method for ameliorating relaxivity. One method is to increase molecular rigidity to increase its weight meanwhile optimize the  $\tau_R$ . Others can be considered from the variables  $\tau_m$  and  $q$ . The measurement of proton relaxivity as a function of pH at low temperatures ( $\tau_R$  is long) can make us observe the phenomenon that acid or base can catalyze the proton exchange then aid in optimizing

$\tau_m$ . Even though it is a great challenge that the requirement of increasing the hydration number  $q$ , maintaining thermodynamic stability/kinetic inertness and preventing formation of ternary complexes with some endogenous ligands in the body such as carbonate and phosphate, it is still an important concern.

In theory a CA can increase the relaxivity of water protons in different normal and healthy tissues at the same time. How can we enhance the contrast between different tissues? That is derived from the accumulation of the agent in them due to the different permeability of different vasculatures, especially hyperpermeability of tumor one. Moreover, tumor cells proliferate quite rapidly so that the density of vasculature for transporting nutrients is high, which is another reason for higher accumulation of CAs in tumors. Usually people increase molecular weight of a CA to prolong  $\tau_R$  as well as plasma circulation which cause a preferentially accumulation in tumors.

### **2.2.3 ParaCEST contrast agents for MRI<sup>[18-21]</sup>**

Normally the MRI CAs we talk about are positive which can make the bright part brighter. However there is another kind of CAs are also familiar to us, those are paraCEST contrast agents, which belong to negative CAs for MRI. Those agents darkening the MRI images to give contrast enhancement are usually based on lanthanide(III) ions.

In fact paraCEST is a technique based on the chemical shifts of water protons rather than the relaxation time. During NMR process, the different protons in different electronic environment feel different effective magnetic fields, thus their resonance frequencies vary upon the electron density which shields the proton from the applied field by their generating local one. As a result, the NMR signals dependent on fields can provide some useful information about the molecular structure. However, the frequency differences are too small to show us clearly, thus usually they are transformed into the chemical shifts. The proton with high electronic density should be shown in the up-field and the corresponding chemical shift should be low.

As the presentation in Chapter 1, paramagnetic sample can generate its local magnetic field and thus significantly modify the effective one to the protons so that the change of chemical shifts can reflect the magnetism of the sample. That is the basic principle of paraCEST contrast agents for MRI (Fig. 2.7).

This kind of contrast is upon dynamic chemical exchange saturation transfer (CEST) mechanism. It is found that some paramagnetic lanthanide ions experience slow exchange of bound and bulk water and this process transfers labile protons saturated by pre-saturation pulse into the bulk water which results in a decrease of net magnetization and a reduction of signal intensity of the bulk water pool.

But this technique is bound by the  $k_{\text{ex}} \leq \Delta\omega \leq R_1$  condition, where  $k_{\text{ex}}$  represents exchange rate,  $\Delta\omega$  stands for the frequency (chemical shift) difference between two exchanging pools and  $R_1$  is longitudinal relaxation rate. However, usually the  $\Delta\omega$  is so small (less than 6 ppm) that a high enough field is required which is difficult to meet. And another intrinsic problem is that it is not easy to distinguish the CEST effects of the agent *in vivo* imaging from the inherent tissue magnetization transfer (MT) effects which was first demonstrated for by Balaban<sup>[22-23]</sup>. Nevertheless, this technique still garnered significant attention due to some  $\text{Ln}^{3+}$  which can induce considerable NMR hyperfine shifts (up to several hundred ppm) in nearby NMR nuclei. It can easily facilitate saturation of one exchangeable spin pool, while the other one (bulk water pool) cannot get any partial saturation. Another advantage is that the exchangeable sites are not limited to protons of N-H or O-H groups but those of bound and bulk water exchange can also be considered.

Therefore, paraCEST agents are an alternative of  $T_1$  or  $T_2$  agents from conceptual difference even though both paraCEST and  $T_2$  agents are negative for MRI.

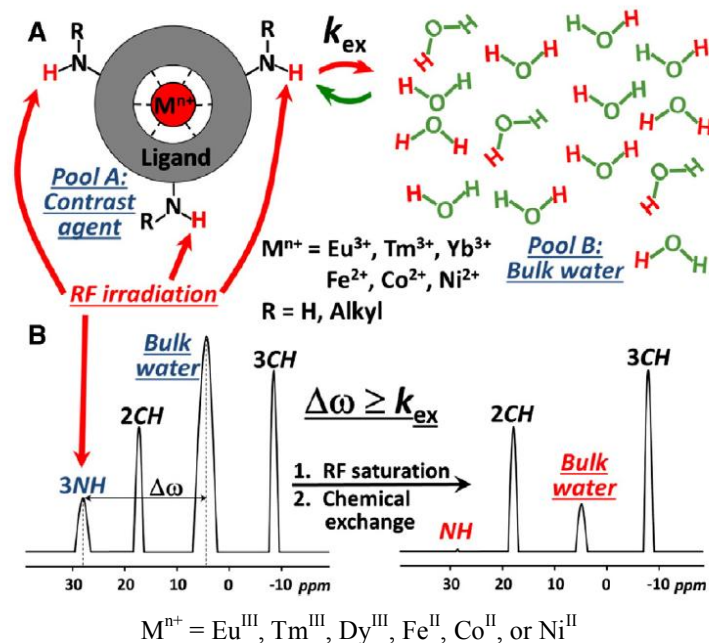


Fig. 2.7 (A) Schematic of a paraCEST contrast agent based on metal ions with C3-symmetry containing three exchangeable NH proton groups. (B) Schematic of corresponding  $^1H$  NMR spectrum of a CEST agent. From *J. Inorg. Biochem.* 2014, 133, 143.

Meanwhile what has to be mentioned is that paraCEST agents also show great promise to create new opportunities for designing and developing responsive MRI probes (which will be explained later). Water exchange is significantly sensitive to all varieties of environmental or structural changes, which allows for signal changes in physiological or biological processes by MRI. Nevertheless, herein I do not talk about them too much considering that they are not very important to my project.

## 2.2.4 Design of contrast agents<sup>[17]</sup>

It has to meet the requirements to design a practical and general MRI CA. Herein it can be summarized from three points as following: 1) High relaxivity. The relaxivity of a paramagnetic complex is its intrinsic property that can symbolize its ability to increase the relaxation rate of water protons. The most important variables that affect it have been introduced previously. 2) High stability. Contrast agents should have high thermodynamic stability after they are administrated in human body in order to improve their cytotoxicity. Thus transmetalation kinetics and dissociation play a

important role in determining the fate of a complex *in vivo*. Metal complexes with acyclic ligands usually have fast kinetics character, while macrocyclic complexes tend to be significantly more inert. It is reported that the chain ligands cannot make the corresponding complexes much stable. For example, in 2013 S. Aime group<sup>[24]</sup> reported the degradation speeds of some commercial MRI Gd-Based CAs in Cells fibroblasts and macrophages. They found that the acyclic series of Gd<sup>3+</sup> MRI CAs degraded more rapidly than their macrocyclic analogues. The acquired information about their cellular fate in the case of nephrogenic systemic fibrosis (NSF) provides useful insights to the understanding of their cytotoxicity and even estimation of their analogues.

Thus the CAs are designed from two aspects, one of which is ligands and the other is metal ions. we should make endeavor in exploring a cage in suitable size which is fit to the metal ion (i.e. Gd<sup>3+</sup>). We also give a prior consideration of nontoxic metal ions on the premise that they are paramagnetic. In case they are dissociated *in vivo* leading to the release of the toxic metal ion and ligand which tend to be harm to people. For example, the metal Gd<sup>3+</sup> can target the binding sites of Ca<sup>2+</sup> to make them blocked so that it deposits in skeletal tissue (Gd<sup>3+</sup> radius is about 1.05-1.11 Å, Ca<sup>2+</sup> radius is 1.00-1.06 Å)<sup>[6]</sup>. This irreversible process inevitably triggers healthy lesion. Of course, free Gd<sup>3+</sup> also has other potential possibilities that it interacts with various serum proteins. Thus LD<sub>50</sub> is 0.2 mmol kg<sup>-1</sup> in mice of free Gd<sup>3+</sup>, and it is kind of importance to keep the chelate staying intact in the body after MRI session. 3) Good solubility and low osmolality. Development of a good CA focuses on not only the increase of relaxivity of water protons and its low toxicity, but also other factors such as route of excretion and clearance rate that determine the efficacy *in vivo* in obtaining high quality images. As what is predicted previously, even though macromolecular agents can meet the requirements of high relaxivity and high stability, they are hardly used in clinical applications just because of their slow body excretion which is related to their

toxicity. This tolerance is reflected by the value of LD<sub>50</sub>. Then generally clearance is dependent on the properties of the agents such as their size, charge, shape and chemical makeup, and it occurs primarily via renal filtrate. Nowadays more and more biodegradable macromolecular MRI CAs are designed to alleviate this problem. Those agents initially give superior contrast enhancement as macromolecular CAs and after the MRI examinations they are degraded *in vivo* into small molecular chelates that can be rapidly excreted and cleared.

### **2.2.5 MRI probes**

The application of MRI modality is so broad in biomedical field. It is not only the contribution of those conventional CAs, but also the MRI probe which can respond to some chemical or enzyme then meet the need of some more complex and kinetic diagnosis. Thus an exciting frontier for MRI is the development of responsive contrast agents as probes which possess special binding ability toward some biological targets to report chemical species and reactions of interest in living biological systems.

In view of that, In order to meet some special requirements such as kinetic detection, all kinds of truly functional MRI probes should be developed. According to the various factors presented previously that govern the relaxivity of water protons, by modifying them many approaches can be exploited on purpose of designing MRI probes. Most of prevalent reported MRI probes succeed in modifying the numbers of water molecules, and sometimes there are also some examples by modifying the rotational correlation time  $\tau_R$ .

#### **2.2.5.1 MRI probes responsive to enzymes**

Based on this concept above, the pioneer T. J. Meade<sup>[25]</sup> developed a responsive probe to detect  $\beta$ -galactosidase activity. They chose the typical Gd<sup>3+</sup> complex for their research, whose eight coordination sites were occupied by the chelating ligand, and the remaining one was available for water. Then they attempted to block this site by

steric hindrance of galactopyranose residue so that the effect of the complex on  $T_1$  was diminished, and remove this blocking group by cleavage of the bond which was accomplished by the specific enzyme. This achieved an irreversible change from a weak to a strong relaxivity state. This can be explained by the Fig. 2.8.

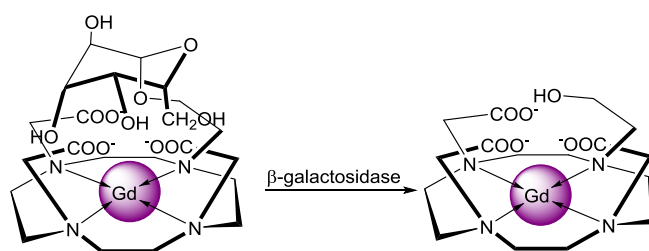


Fig. 2.8 Smart MRI probe responding to  $\beta$ -galactosidase

Then another type of enzyme-activated MRI contrast agents containing self-immolative spacer was developed by them<sup>[26]</sup> (Fig. 2.9). Obviously the cleavage of the  $\beta$ -glucuronic acid moiety by corresponding  $\beta$ -glucuronidase switches coordination state of one arm of the complex then modulates that of water molecule. And the application of the self-immolative linker may construct a new model for future agents, considering that the linker may be used for improving the stability of the complex, or for restricting water access to the complex by connecting the opposite sides of the macrocycle.

At the same time, there were many probes designed based on the similar mechanisms<sup>[27-38]</sup>, but some of them were designed as the responsive MRI paraCEST agents.

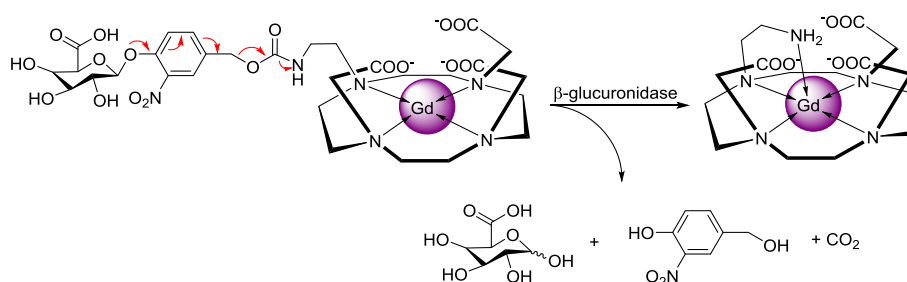


Fig. 2.9  $\beta$ -glucuronidase-activated MRI contrast agents containing self-immolative spacer

### 2.2.5.2 MRI probes responsive to pH

The “smart contrast agents” can also be designed for detection of pH values of the environments by their pH dependence of the relaxivity.

Here only those developed specifically for extracellular pH were focused on. Normally they can be designed by introduction of some acidic groups like phosphate. For example, the first generation of pH-dependent complex<sup>[39]</sup>, GdDOTA-4AmP<sup>5-</sup>, contains phosphonate arms which can reveal pH changes through the protonation or deprotonation to open or close the phosphonate structure thus facilitate or hamper water accessibility to Gd<sup>3+</sup>. It can be used to detect tumors in the light of their acidic extracellular pH (pH<sub>e</sub>) compared to normal tissues and the inverse relationship between pH<sub>e</sub> and tumor perfusion (Fig. 2.10). At the same time, there were also some similar reports on this aspect<sup>[40-41]</sup>.

Either they can be achieved by protonation of some moiety that should have been coordinated to metal ion resulting in its decooordination<sup>[42]</sup>. The Fig. 2.11 shows that the initiate state of the complex prevents water molecule away from it due to its steric hindrance of one moiety, then after decooordination caused by protonation of sulfonamide it can accommodate two water molecules.

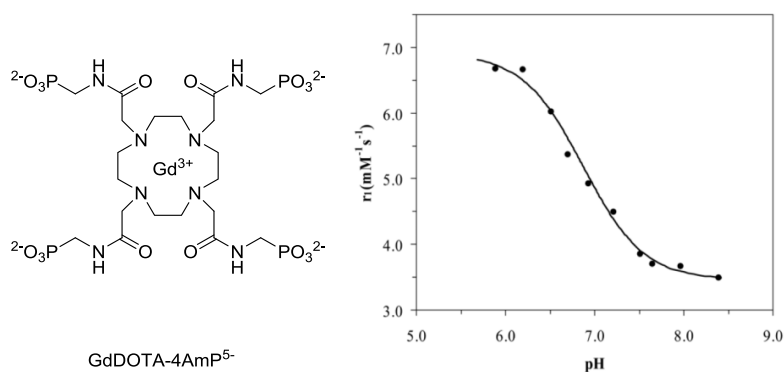


Fig. 2.10 Dependence of GdDOTA-4AmP<sup>5-</sup> T<sub>1</sub> relaxivity on pH (37°C, 4.7 T). The dots represent experimental data and the solid line the best fit to the Hill-modified Henderson Hasselbach equation:  $\text{pH} = 6.87 + \log \left( \frac{(6.91 - r_1)}{(r_1 - 3.45)} \right) / 1.28$ .

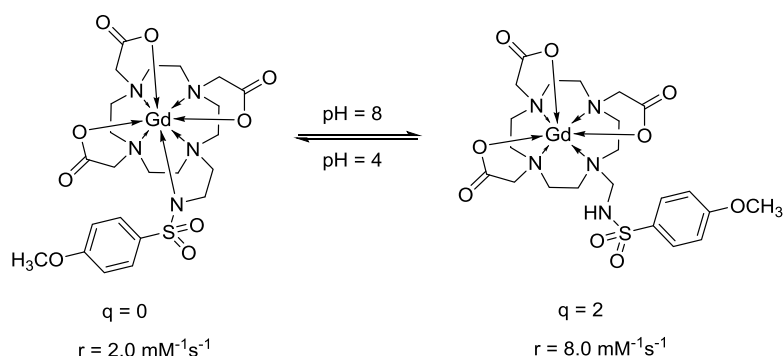


Fig. 2.11 pH responsive probe based on switching coordination by protonation

### 2.2.5.3 MRI probes responsive to metal ions

If a MRI contrast agent can selectively respond to some specific metal ion, it can be an excellent candidate for sensors in biological application.

The sensitive CAs to s-block (potassium, calcium and magnesium) or d-block (zinc, iron and copper) metal ions have been designed with different strategies which are depicted by Fig. 2.12. For example, a) The initial  $\text{Gd}^{3+}$  complex bearing two units (i.e. typical ligands or crown ether) that are sensitive to a specific ion ( $\text{M}^{n+}$ ) has strong relaxivity, then the relaxivity would decrease as the addition of  $\text{M}^{n+}$  because the coordination of the two units and  $\text{M}^{n+}$  together blocks the ninth coordination site (i.e.  $\text{K}^+$ ,  $\text{Mg}^{2+}$ )<sup>[43]</sup>. b) The steric hindrance of a big unit blocks the site, and its coordination to  $\text{M}^{n+}$  makes it opened. The relaxivity switches from weak to strong (i.e.  $\text{Cu}^{2+}$ )<sup>[44]</sup>. c) At the beginning the structure of the  $\text{Gd}^{3+}$  complex is flexible, however, the coordination of some parts to  $\text{M}^{n+}$  induces rigidification so that water approaches  $\text{Gd}^{3+}$  easily (i.e.  $\text{Zn}^{2+}$ )<sup>[45]</sup>.

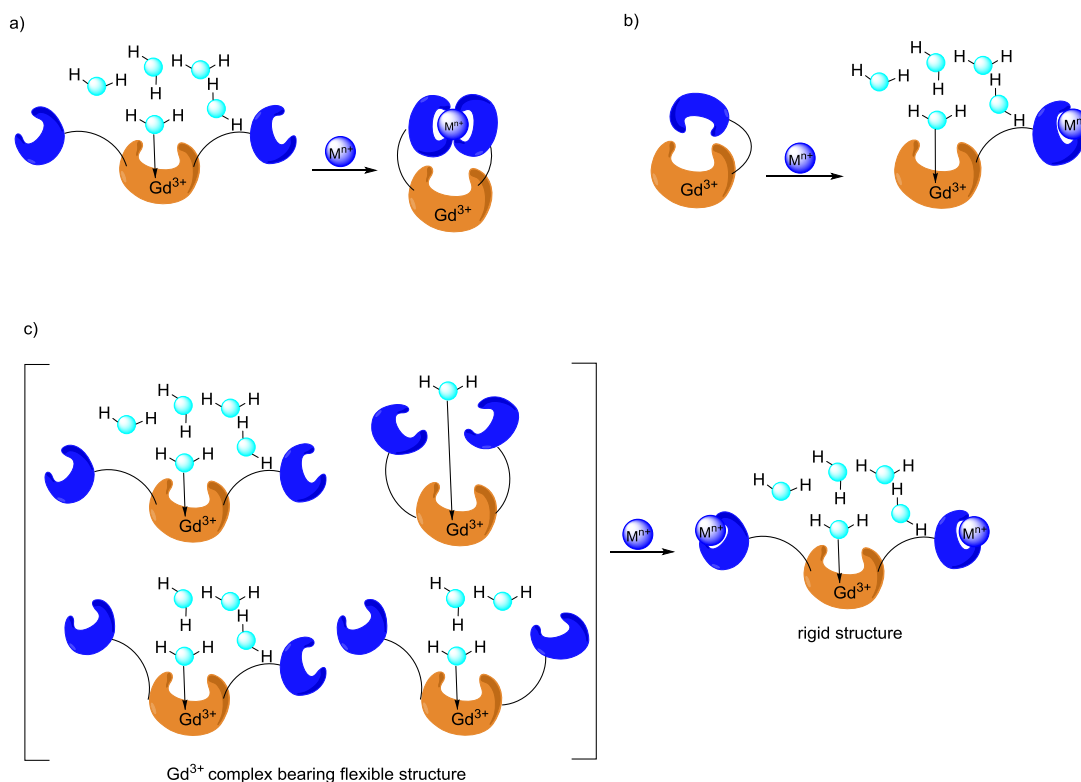


Fig. 2.12 Three kinds of mechanisms for probes sensitive to metal ions

### 2.2.5.3 MRI probes responsive to proteins

Besides of the responses to those factors mentioned above, there were other CAs which can detect glucose<sup>[46]</sup>, lactate<sup>[47]</sup>, nitric oxide<sup>[48]</sup> and so on. What is more important, the CAs that can detect some proteins attract much interest due to the biological applications.

It has been previously mentioned several times that the rapid speed of molecular rotation limits its relaxivity. So some people focus on improving the relaxivity by binding a MRI contrast agent to a target protein to slow its rotation which is called receptor-induced magnetization enhancement (RIME) mechanism.

Based on the mechanism, MS-325 (Ablavar) targeting the vasculature as the first representative member of this type of agents was coupled to human serum albumin (HSA) (Fig. 2.13), resulting in an increase of its relaxivity from 5.5 to 25 mM<sup>-1</sup> s<sup>-1</sup> (at 37°C, 60 MHz) ( $\tau_R$  was prolonged from 115 ps to 10 ns)<sup>[49-50]</sup>.

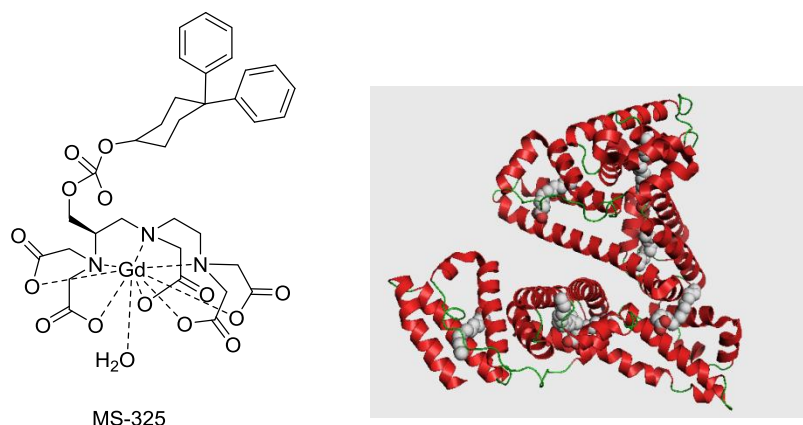


Fig. 2.13 Left, the structure of MS-325; right, the structure of HSA.

The great success of MS-325 prompted further investigation and research on developing other Albumin-Affinity agents<sup>[51-53]</sup> and other Protein-Binding agents<sup>[54-57]</sup>. For example, the typical example is the contrasts binding to Halo Tag protein reported in 2011 (Fig. 2.14). The specificity and the covalent interaction between the protein of Halo Tag and the substrate can make imaging opportunities increased and  $\tau_R$  prolonged thus cause a higher relaxivity<sup>[58]</sup> (up to 6-fold increase in  $r_1$ , from 3.8 to 22  $\text{mM}^{-1} \text{ s}^{-1}$ ). This class of contrast agents containing its substrate moiety normally can be designed by conjugating some functional groups onto the terminal of the haloalkane targeting one. One more example also can prove the RIME concept. The density of the metabotropic glutamate receptors mGluR<sub>5</sub> is related to several diseases such as Alzheimer's and Parkinson's diseases, anxiety, depression neuropathic pain. Fortunately, the relaxivity of contrast agents binding to it can reveal its density, thus prompt studies on the nervous system<sup>[59]</sup>.

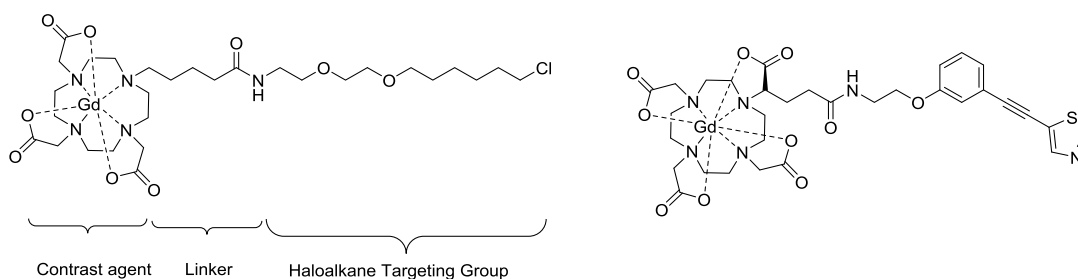


Fig. 2.14 Left, HaloTag-targeted contrast agents. A macrocyclic Gd(III) chelator is connected to a

haloalkane group via a flexible linker to generate a HaloTag-targeted contrast agent. right, representative probe responsive to mGluR<sub>5</sub>.

## 2.3 References

- [1] Bellin M.-F. MR Contrast Agents, the Old and the New. *European Journal of Radiology* 2006, 60314.
- [2] Bartusik D., Aebischer D., Tomanek B. A review of new approaches in Her-2 targeting and <sup>1</sup>H MRI application. *Med. Chem. Res.* 2014.
- [3] Tirotta I., Dichiarante V., Pigliacelli C., Cavallo G., Terraneo G., Bombelli F. B., Metrangolo P., Resnati G. <sup>19</sup>F Magnetic Resonance Imaging (MRI): From Design of Materials to Clinical Applications. *Chem. Rev.* 2015, 115, 1106.
- [4] Bottomley P. A., Foster T. H., Argersinger R. E., Pfeifer L. M. A Review of Normal Tissue Hydrogen NMR Relaxation Times and Relaxation Mechanisms from 1–100 MHz: Dependence on Tissue Type, NMR Frequency, Temperature, Species, Excision, and Age. *Med. Phys.* 1984,11, 425.
- [5] Tu C., Osborn E. A., Louie A. Y. Activatable T<sub>1</sub> and T<sub>2</sub> Magnetic Resonance Imaging Contrast Agents. *Annals of Biomedical Engineering*, 2011, 39, 1335.
- [6] Villaraza A. J. L., Bumb A., Brechbiel M. W. Macromolecules, Dendrimers, and Nanomaterials in Magnetic Resonance Imaging: The Interplay between Size, Function, and Pharmacokinetics. *Chem. Rev.* 2010, 110, 2921.
- [7] Werner E. J., Datta A., Jocher C. J., Raymond K. N. High-Relaxivity MRI Contrast Agents: Where Coordination Chemistry Meets Medical Imaging. *Angew. Chem. Int. Ed.* 2008, 47, 8568.
- [8] Caravan P. Strategies for Increasing the Sensitivity of Gadolinium Based MRI Contrast Agents. *Chem. Soc. Rev.* 2006, 35, 512.
- [9] Que E. L., Chang C. J. Responsive Magnetic Resonance Imaging Contrast Agents as Chemical Sensors for Metals in Biology and Medicine. *Chem. Soc. Rev.*, 2010, 39, 51.

- [10] Tóth é., Helm L., Merbach A. in *The Chemistry of Contrast Agents in Medical Magnetic Resonance Imaging*, John Wiley & Sons, Ltd, 2013, 25-81.
- [11] Kowalewski J., Kruk D., Parigi G. in *Adv. Inorg. Chem., Vol. Volume 57*, Academic Press, 2005, 41-104.
- [12] Pintacuda G., John M., Su X.-C., Otting, G. NMR Structure Determination of Protein-Ligand Complexes by Lanthanide Labeling. *Acc. Chem. Res.* 2007, 40, 206.
- [13] Helm L., Toth E., Merbach A. E. In *Lanthanides and Their Interrelations with Biosystems*; Sigel A., Sigel H., Eds. *Metal Ions in Biological Systems*. Marcel Dekker Inc.: New York, 2003, 40, 589.
- [14] Geraldes, C. F. G. C.; Luchinat, C. In *Lanthanides and Their Interrelations with Biosystems*; Sigel, A., Sigel, H., Eds. *Metal Ions in Biological Systems*. Marcel Dekker Inc.: New York. 2003, 40, 513.
- [15] Otting G. Prospects for Lanthanides in Structural Biology by NMR. *J. Biomol. NMR* 2008, 42, 1.
- [16] Peters J. A., Huskens J., Raber D. J. Lanthanide Induced Shifts and Relaxation Rate Enhancements. *Prog. Nucl. Magn. Reson. Spectrosc.* 1996, 28, 283.
- [17] Caravan P., Ellison J. J., McMurry T. J. Lauffer R. B. Gadolinium(III) Chelates as MRI Contrast Agents: Structure, Dynamics, and Applications. *Chem. Rev.* 1999, 99, 2293.
- [18] Tsitovich P. B., Burns P. J., McKay A. M., Morrow J. R. Redox-activated MRI Contrast Agents Based on Lanthanide and Transition Metal Ions. *J. Inorg. Biochem.* 2014, 133, 143.
- [19] Adair C., Woods M., Zhao P., Pasha A., Winter P. M., Lanza G. M., Athey P., Dean-Sherry A., Kiefer G. E. Spectral Properties of a Bifunctional PARACEST Europium Chelate: an Intermediate for Targeted Imaging Applications. *Contrast Media Mol. Imaging* 2007, 2, 55.
- [20] Viswanathan S., Kovacs Z., Green K. N., James-Ratnakar S. J., Dean-Sherry A. Alternatives to Gadolinium-Based Metal Chelates for Magnetic Resonance Imaging. *Chem. Rev.* 2010, 110, 2960.
- [21] Terreno E., Delli-Castelli D., Viale A., Aime S. Challenges for Molecular Magnetic

- Resonance Imaging. *Chem. Rev.* 2010, 110, 3019.
- [22] Dagher A. P., Aletras A. H., Choyke P., Balaban R. S. Imaging of Urea Using Chemical Exchange-Dependent Saturation Transfer at 1.5T. *J. MRI* 2000, 12, 745.
- [23] Ward K. M., Aletras A. H., Balaban R. S. A New Class of Contrast Agents for MRI Based on Proton Chemical Exchange Dependent Saturation Transfer (CEST). *J. Magn. Res.* 2000, 143, 79.
- [24] Gregorio E. D., Gianolio E., Stefania R., Barutello G., Digilio G., Aime S. On the Fate of MRI Gd-Based Contrast Agents in Cells. Evidence for Extensive Degradation of Linear Complexes upon Endosomal Internalization. *Anal. Chem.* 2013, 85, 5627.
- [25] Moats R. A., Fraser S. E., Meade T. J. A “Smart” Magnetic Resonance Imaging Agent That Reports on Specific Enzymatic Activity. *Angew. Chem. Int. Ed. Engl.* 1997, 36, 725.
- [26] Duimstra, J. A.; Femia, F. J.; Meade, T. J. A Gadolinium Chelate for Detection of  $\beta$ -Glucuronidase: A Self-Immolative Approach. *J. Am. Chem. Soc.* 2005, 127, 12847.
- [27] Louie A. Y., Huber M. M., Ahrens E. T., Rothbacher U., Moats R., Jacobs R. E., Fraser S. E., Meade T. J. In Vivo Visualization of Gene Expression Using Magnetic Resonance Imaging. *Nat. Biotechnol.* 2000, 18, 321.
- [28] Nivorozhkin A. L., Kolodziej A. F., Caravan P., Greenfield M. T., Lauffer R. B., McMurry T. J. Enzyme-Activated  $Gd^{3+}$  Magnetic Resonance Imaging Contrast Agents with a Prominent Receptor-Induced Magnetization Enhancement. *Angew. Chem., Int. Ed.* 2001, 40, 2903.
- [29] Zhao M., Josephson L., Tang Y., Weissleder R. Magnetic Sensors for Protease Assays. *Angew. Chem., Int. Ed.* 2003, 42, 1375.
- [30] Querol M., Chen J. W., Weissleder R., Bogdanov A. DTPA-bisamide-Based MR Sensor Agents for Peroxidase Imaging. *Org. Lett.* 2005, 7, 1719.
- [31] Wei Q., Seward G. K., Hill P. A., Patton B., Dimitrov I. E., Kuzma N. N., Dmochowski I. J. Designing  $^{129}Xe$  NMR Biosensors for Matrix Metalloproteinase Detection. *J. Am. Chem. Soc.* 2006, 128, 13274.
- [32] Yoo B., Pagel M. D. A PARACEST MRI Contrast Agent To Detect Enzyme Activity. *J. Am.*

- Chem. Soc.* 2006, 128, 14032.
- [33] Giardiello M., Lowe M. P., Botta M. An Esterase-activated Magnetic Resonance Contrast Agent. *Chem. Commun.* 2007, 4044.
- [34] Yoo B., Raam M. S., Rosenblum R. M., Pagel D. Enzyme-Responsive PARACEST MRI Contrast Agents: a New Biomedical Imaging Approach for Studies of the Proteasome. *Contrast Media Mol. Imaging* 2007, 2, 189.
- [35] Breckwoldt M. O., Chen J. W., Stangenberg L., Aikawa E., Rodriguez E., Qiu S., Moskowitz M. A., Weissleder R. Tracking the Inflammatory Response in Stroke In Vivo by Sensing the Enzyme Myeloperoxidase. *Proc. Natl. Acad. Sci. U.S.A.* 2008, 105, 18584.
- [36] Chauvin T., Durand P., Bernier M., Meudal H., Doan B.-T., Noury F., Badet B., Beloeil J.-C., Toth E. Detection of Enzymatic Activity by PARACEST MRI: A General Approach to Target a Large Variety of Enzymes. *Angew. Chem., Int. Ed.* 2008, 47, 4370.
- [37] Mizukami S., Takikawa R., Sugihara F., Hori Y., Tochio H., Walchli M., Shirakawa M., Kikuchi K. Paramagnetic Relaxation-Based  $^{19}\text{F}$  MRI Probe To Detect Protease Activity. *J. Am. Chem. Soc.* 2008, 130, 794.
- [38] Chauvin T., Torres S., Rosseto R., Kotek J., Badet B., Durand P., Toth E. Lanthanide (III) Complexes That Contain a Self-Immolative Arm: Potential Enzyme Responsive Contrast Agents for Magnetic Resonance Imaging. *Chem. Eur. J.* 2012, 18, 1408.
- [39] Garcia-Martin M. L., Martinez G. V., Raghunand N., Dean-Sherry A., Zhang S., Gillies R. J. High Resolution pH Imaging of Rat Glioma Using pH-Dependent Relaxivity. *Magn. Reson. Med.* 2006, 55, 309.
- [40] Raghunand N., Zhang S., Sherry A. D., Gillies R. J. In vivo Magnetic Resonance Imaging of Tissue pH Using a Novel pH-Sensitive Contrast Agent, GdDOTA-4AmP. *Academic Radiology* 2002, 9, 481.
- [41] Raghunand N., Howison C., Sherry A. D., Zhang S., Gillies R. J. Renal and Systemic pH Imaging by Contrast-Enhanced MRI. *Magn. Reson. Med.* 2003, 49, 249.
- [42] Bonnet C. S., Tei L., Botta M., Tóthé. in *The Chemistry of Contrast Agents in Medical*

*Magnetic Resonance Imaging*, John Wiley & Sons, Ltd, 2013, 343.

- [43] Hifumi H., Tanimoto A., Citterio D., Komatsua H., Suzuki K. Novel 15-crown-5 ether or b-diketone incorporated gadolinium complexes for the detection of potassium ions or magnesium and calcium ions. *Analyst*, 2007, 132, 1153.
- [44] Que E. L., Gianolio E., Baker S. L., Wong A. P., S. Aime, Chang C. J. Copper-Responsive Magnetic Resonance Imaging Contrast Agents. *J. Am. Chem. Soc.* 2009, 131, 8527.
- [45] Hanaoka K., Kikuchi K., Urano Y., Narazaki M., Yokawa T., Sakamoto S., Yamaguchi K., Nagano T. Design and Synthesis of a Novel Magnetic Resonance Imaging Contrast Agent for Selective Sensing of Zinc Ion. *Chemistry & Biology* 2002, 9, 1027.
- [46] Zhang S., Trokowski R., Sherry A. D. A Paramagnetic CEST Agent for Imaging Glucose by MRI. *J. Am. Chem. Soc.* 2003, 125, 15288.
- [47] Aime S., Delli Castelli D., Fedeli F., Terreno E. A Paramagnetic MRI-CEST Agent Responsive to Lactate Concentration. *J. Am. Chem. Soc.* 2002, 124, 9364.
- [48] Liu G., Li Y., Pagel M. D. Design and Characterization of a New Irreversible Responsive PARACEST MRI Contrast Agent that Detects Nitric Oxide. *Magn. Reson. Med.* 2007, 58, 1249.
- [49] Lauffer R. B., Parmelee D. J., Dunham S. U., Ouellet H. S., Dolan R. P., Witte S., McMurry T. J., Walovitch R. C. MS-325: Albumin-Targeted Contrast Agent for MR Angiography. *Radiology* 1998, 207, 529.
- [50] Caravan P., Cloutier N. J., Greenfield M. T., McDermid S. A., Dunham S. U., Bulte J. W., Amedio J. C. Jr., Looby R. J., Supkowski R. M., Horrocks W. D. Jr., McMurry T. J., Lauffer R. B. The Interaction of MS-325 with Human Serum Albumin and Its Effect on Proton Relaxation Rates. *J. Am. Chem. Soc.* 2002, 124, 3152.
- [51] Aime S., Botta M., Fasano M., Crich S. G., Terreno E. Gd(III) Complexes as Contrast Agents for Magnetic Resonance Imaging: a Proton Relaxation Enhancement Study of the Interaction with Human Serum Albumin. *J. Biol. Inorg. Chem.* 1996, 1, 312.
- [52] Aime S., Chiaussa M., Digilio G., Gianolo E., Terreno E. Contrast Agents for Magnetic

- Resonance Angiographic Applications:  $^1\text{H}$  and  $^{17}\text{O}$  NMR Relaxometric Investigations on Two Gadolinium(III) DTPA-like Chelates Endowed with High Binding Affinity to Human Serum Albumin. *J. Biol. Inorg. Chem.* 1999, 4, 766.
- [53] Prokop M., Schneider G., Vanzulli A., Goyen M., Ruehm S. G., Douek P., Dapra M., Pirovano G., Kirchin M. A., Spinazzi A. Contrast-enhanced MR Angiography of the Renal Arteries: Blinded Multicenter Crossover Comparison of Gadobenate Dimeglumine and Gadopentetate Dimeglumine. *Radiology* 2005, 234, 399.
- [54] Gustafsson B., Youens S., Louie A. Y. Development of Contrast Agents Targeted to Macrophage Scavenger Receptors for MRI of Vascular Inflammation. *Bioconjugate Chem.* 2006, 17, 538.
- [55] Langereis S., Kooistra H.-A. T., Genderen M. H. P. v., Meijer E. W. Probing the Interaction of the Biotin–Avidin Complex with the Relaxivity of Biotinylated Gd-DTPA. *Org. Biomol. Chem.* 2004, 2, 1271.
- [56] Karfeld L. S., Bull S. R., Davis N. E., Meade T. J., Barron A. E. Use of a Genetically Engineered Protein for the Design of a Multivalent MRI Contrast Agent. *Bioconjugate Chem.* 2007, 18, 1697.
- [57] Aime S., Frullano L., Crich S. G. Compartmentalization of a Gadolinium Complex in the Apoferritin Cavity: A Route To Obtain High Relaxivity Contrast Agents for Magnetic Resonance Imaging. *Angew. Chem., Int. Ed.* 2002, 41, 1017.
- [58] Strauch R. C., Mastarone D. J., Sukerkar P. A., Song Y., Ipsaro J. J., Meade T. J. Reporter Protein-Targeted Probes for Magnetic Resonance Imaging. *J. Am. Chem. Soc.* 2011, 133, 16346.
- [59] Mishra A., Gottschalk S., Engelmann J., and Parker D. Responsive Imaging Probes for Metabotropic Glutamate Receptors. *Chem. Sci.*, 2012, 3, 131.

## Part II Thesis work

### Chapter 3 Overall project of which this thesis is part

#### 3.1 Materials possessing switchable spin states

The spin state of various molecules and materials based on transition metal ions with  $d^4$ - $d^7$  electron configuration can be switched depending on the strength of their ligand-field which is related to the enthalpy of the  $M \rightarrow L$  bonds of the low-spin state and the configurational and vibrational entropy of the high-spin state<sup>[1]</sup>. Normally when the latter overcomes the former by the stimulus such as heat, light, pressure and so on, it occurs from the low-spin to high-spin form. This phenomenon, called spin transition or spin crossover, can be observed commonly in some complexes of iron (II)<sup>[2]</sup>, iron (III)<sup>[3-4]</sup> and cobalt (II)<sup>[5]</sup>, especially in iron(II) complexes with nitrogen-donor ligands which can exhibit the greatest structural differences between two states<sup>[6]</sup>.

##### 3.1.1 Crystal field theory

The spin state of a complex based on a transition metal ion can be explained by the Crystal Field Theory (CFT) or the Ligand Field Theory (LFT). Herein I take iron(II) as an example to show the possibility of two spin states<sup>[1]</sup>.

As we have known, the CFT says that five degenerate d orbitals of a metal ion split in energy into two sets as a ligand approaches it. Because the electrons from the ligand will get close to some of the d-orbitals and far away from the others, which leads to a loss of degeneracy. Thus the former results in a higher energy while the latter causes lower energy. In octahedral symmetric field the energy difference between two d-orbital groups is described by a gap  $\Delta_o$ , splitting energy, and the energy of  $d_{xy}$ ,  $d_{xz}$  and  $d_{yz}$  orbitals is lower than that of  $d_{z^2}$  and  $d_{x^2-y^2}$ , therefore the electrons of the

ligand and the metal ion experience more repulsion in orbitals  $d_{z^2}$  and  $d_{x^2-y^2}$ . On basis of the theory of molecular symmetry, the three orbitals with lower energy are referred to as  $t_{2g}$ , and the other two with higher energy are expressed by  $e_g$ .

The value of  $\Delta_o$  is dependent on the strength of the ligand field. In other words, strong ligand field causes big  $\Delta_o$ , on the contrary,  $\Delta_o$  should be small. This theory is fairly important to the metal ions bearing  $d^4 - d^7$  electrons, which can have different electron configurations according to its ligand. Because two paired electrons in the same orbital repel each other, thus it requires energy, which is referred to as spin-pairing energy,  $P$ ). When it is greater than that cost in placing an electron in an  $e_g$  ( $P > \Delta_o$ ), according to Pauli exclusion principle and Hund's rule the electrons in parallel arrange preferably in  $t_{2g}$  and  $e_g$  orbitals, which leads to high-spin state, conversely, the electrons preferably fill in the  $t_{2g}$  in pair ( $P < \Delta_o$ ), which causes low-spin state. The high-spin and low-spin orbital energy diagrams of Fe(II) are given below (Fig. 3.1):

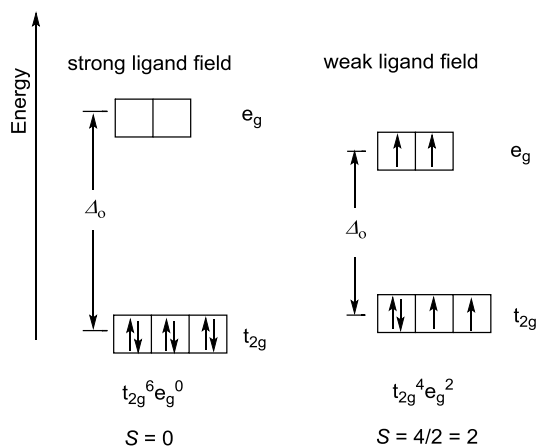


Fig. 3.1 Electronic configuration of iron(II) ion ( $d^6$ ) in the HS and LS state

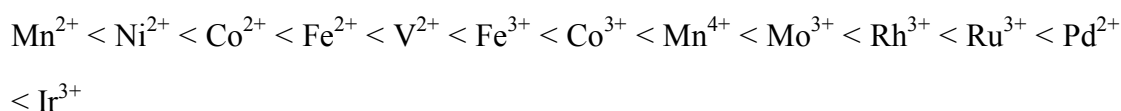
This also can be explained with LFT that combines CFT and Molecular Orbital Theory (MOT). The molecular orbitals, including bonding, non-bonding and anti-bonding ones, are created by linear combination of those of ligand and metal ion. Those orbitals can be filled in two ways: one is that as many electrons as possible are paired and placed in the non-bonding orbitals. The other is that some electrons are placed in the anti-bonding orbitals in parallel. The former case belongs to low-spin,

while the latter is high-spin.

As far as the other metal ions are concerned, their outer electrons should be filled in the corresponding split d orbitals then its spin state can be known.

### 3.1.2 Influencing factors on the splitting energy

In addition, the splitting energy is related to the intrinsic nature of metal ion which here is referred to the charge and radius. The positive charges of the metal ions attract the electrons derived from its ligands, and they increase the distance between ligands and the metal ion so that the overlap of the electrons of ligands with the vacant orbitals of the metal ion is increased. Both two reasons provide the results that the higher the oxidation number, the smaller the pairing energy, which leads to favoring the LS state. The increase of the metal ion radius also results in its favor of LS state due to the bigger overlap causing the drastic increase of the splitting energy. Consequently generally the third-row metal ions lead to higher splitting energy than those in the second-row. So the nature of the metal ions led to the following series of splitting energy:



The splitting energy also depends on the geometry (and symmetry) of ligand's approach, which can make the metal ion stay in the different crystal fields in corresponding shapes, and certainly cause the energetic difference of five d-orbitals of the metal ions. The stronger the overlap of electrons of a ligand with a d-orbital of the metal ion, the higher the energy of the corresponding d-orbital due to their repulsion. Consequently the differences of energetic increases among d-orbitals lead to the energy splitting. That is, the different geometries of the crystal ligands make the different energy splitting. For instance, if four monodentate ligands form a square planar field, the ligands approach the metal ion along the x and y axis. The electrons of the ligands overlap much with the  $d_{x^2-y^2}$  orbital of the metal ion, while overlap a little part in the

XY plane with the  $d_{z^2}$  and  $d_{xy}$  to different extents then almost do not overlap with  $d_{xz}$  and  $d_{yz}$ . That causes the significant energetic differences. However, if the ligands form a tetrahedral field which is less anisotropic than the square planar one, the energy splitting just makes two sets of d-orbitals, like an octahedral field but in a converse way (Fig. 3.2).

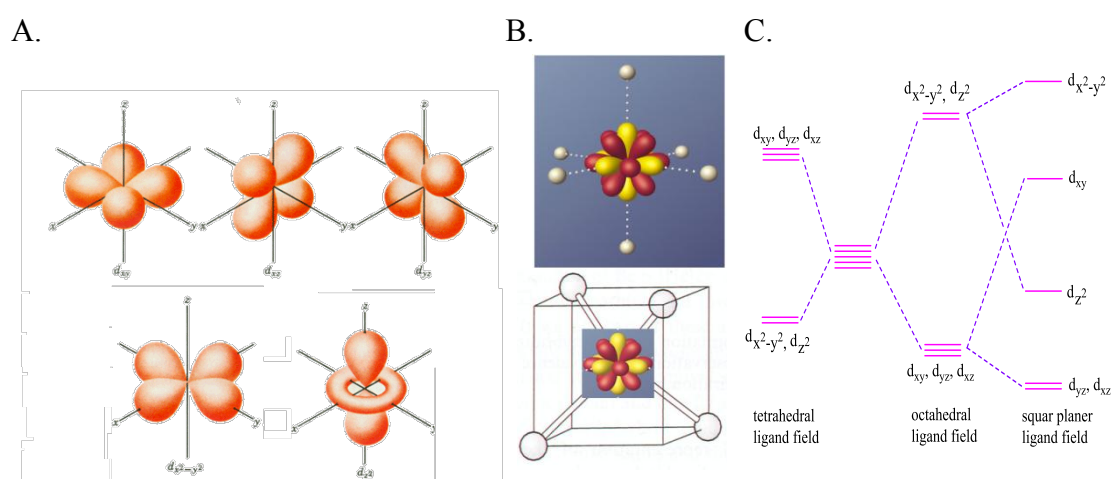
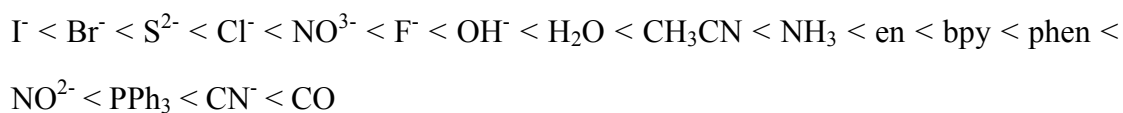


Fig. 3.2 A) d orbitals; B) the relative directions of ligand fields and d orbitals; C) d-orbitals' energy splitting in ligand fields of different geometries.

Seen from the overlap between the electrons of the ligands and metal orbitals, the series of the splitting energy can also be concluded from other aspects such as electronic negativity of coordination atoms, the bond (L→M) length and strength. Usually the splitting energies increase in the following order:



### 3.1.3 Physical stimulus inducing spin transition

Spin-crossover compounds have attracted a great deal of attention for some device and sensor applications, and usually the magnetism change of the complexes is accompanied by the color, dielectric constant and conductivity (electrical resistance).

The spin states of most of spin-crossover compounds are dependent on temperatures

which can cause an electron transition and rearrangement in the ligand field, thus they are called thermal spin-transition. And the pressure can also make spin transition of the complex. Normally the molecule in the HS state is bigger than that in the LS state. Indeed, in 1990 the variable-temperature and variable-pressure Mossbauer experiments on  $[\text{Fe}(\text{2-pic})_3]\text{Cl}_2 \cdot \text{EtOH}$  showed that elevated pressure and temperature increased the distance of ligand-metal<sup>[7]</sup>. The complex  $[\text{Fe}(\text{ptz})_6](\text{BF}_4)_2$  is also a good example because of its magnetic property dependence of the temperature, a change of the Fe-N bond length (0.18 Å) and color (20K, purple; 293K, colorless)<sup>[8-9]</sup>. It can be induced by light, and normally the spin state changes due to the electron transition in the split energy levels but still keeps the same geometry. However, there is a special ion, Ni(II). Even though its electron configuration is  $d^8$ , the spin transition can be caused by the change of the geometry<sup>[10]</sup> (Fig. 3.3).

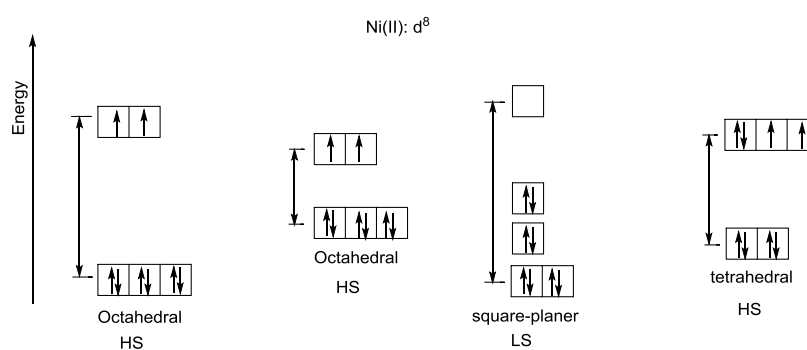


Fig. 3.3 The electron configuration of Ni(II) related to the geometry.

For example, Herges R. and his co-workers<sup>[11]</sup> reported a kind of individual molecules that can switch the spin states in solution by the so-called ligand driven light-induced spin change (LD-LISC) approach. As we have known, Ni(II) is diamagnetic (low-spin,  $S = 0$ ) and paramagnetic (high-spin,  $S = 1$ ), respectively, in square-planar coordination and octahedral one. While in pentacoordinated Ni(II) complexes (square-pyramidal) exist both spin states. In the context of this theory, they found that the electron-withdrawing square-planar ligands and the electron-rich axial ligand can give

preferably high-spin pentacoordinate complexes. They applied Ni(II)-tetrakis(pentafluorophenyl)porphyrin (Ni-TPFPP) as the square-planar platform and azopyridines as the photodissociable axial ligands (Fig. 3.4).

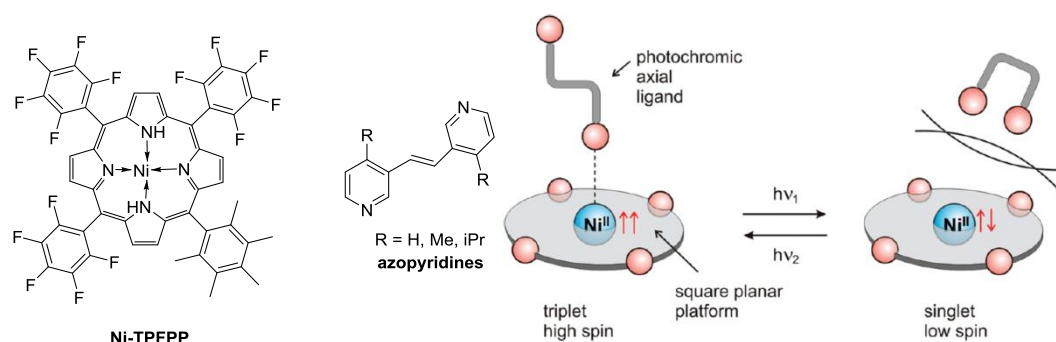


Fig. 3.4 Schematic representation of the spin-state switching of square planar Ni(II) complexes by light-induced association and dissociation of a photochromic axial ligand.

### 3.1.4 Chemical stimulus inducing spin transition

The investigation and research on the spin-crossover compounds mainly focus on the physical stimuli and on the crystalline samples. However, only the molecules changing their magnetic properties in solution upon the chemical stimulus are interesting in biological applications. Typically there are two ways to achieve this goal, either by modifying the electron number of the metal ion to change its oxidation state, or modifying the coordination sphere to change the ligand field. In the former case, a redox-active analyte (a certain redox potential) is necessary and it might be useful for controlling some processes of life, even investigating an evolution of pathologies like cancer<sup>[12-13]</sup>.

The latter case is more practical due to its unique sensitivity of magnetic properties to the environment (non-redox analytes). The interaction between the analyte and the ligand can lead to a change of the coordination bond length and strength or a new coordination bond's formation or cleavage. Some literatures have explained this point<sup>[14-18]</sup>.

### 3.1.4.1 Modification of coordination bond length and strength

The magnetism of a complex is obviously dependent on the  $M \rightarrow L$  bond length and strength. The stronger the bond, the more the  $\sigma$ -bond contribution, the more the complex prefers its low-spin state. Generally it is influenced by the polarity of solvent because of the dipolar interactions and dispersion effects, also by the hydrogen bond, protonation and Lewis acid, all of which affect the electron density of coordinated atoms thus the bond strength. The following two examples (Fig. 3.5) can show us the hydrogen bond draws the electrons away from the coordinated nitrogen atoms<sup>[19]</sup> and protonation makes N-Fe bond length longer because of stronger electron repulsion<sup>[20-21]</sup>, consequently the former decreases the magnetic moment of the complex while the latter increases it.

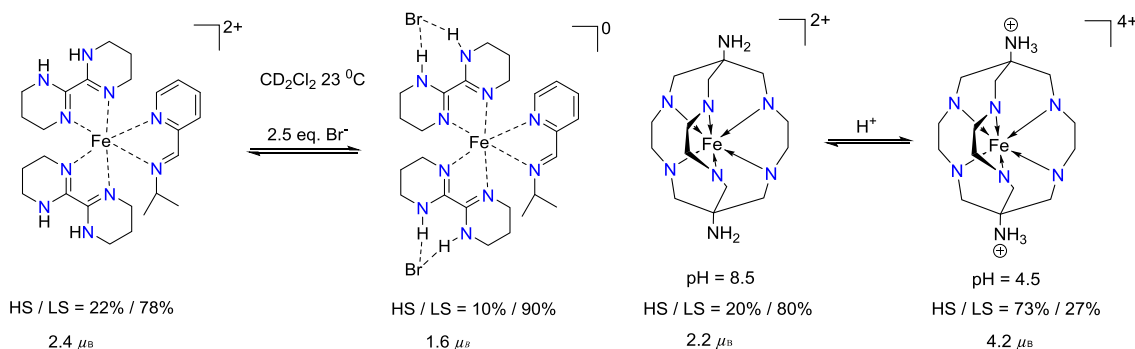


Fig. 3.5 Left, magnetically responsive anion chemosensors based on H-bonding mechanism.

Magnetic response is obtained at RT but only in apolar solvent like DCM. right, magneto-modulation upon protonation of the coordinated nitrogen atoms.

### 3.1.4.2 Modification of coordination bond's formation or cleavage

Most of modifications of the coordination bond length and strength are achieved by the interactions between the analyte and the periphery of the complex. On the contrary, forming or breaking of a coordination bond generally occurs through a stronger stimulus, which may cause a dramatic change of magnetism. Because the

coordination change is inevitably accompanied by the ligand field and further the splitting energy change. Its great potential application for sensing purposes attracts more interest in developing modification methods. In general, replacement of a monodentate ligand is a good scenario to achieve this goal. Normally the exchangeable unit can be replaced by the one providing stronger ligand field if the quantity of two units is equal. However, its reverse also exists when the quantity of the weak ligand is infinitely larger than that of the stronger. This phenomenon can be often observed between two kinds of solvent molecules. For example, the acetonitrile or pyridine molecules coordinated to a metal ion such as iron (II) can be replaced by any alcohol or water molecules (solvent). In that case the replacement renders the complex paramagnetic<sup>[22-23]</sup>. That is why sometimes people choose acetonitrile as solvent to prepare high-spin complex in order to avoid its oxidation. There is also a possibility that a labile exchangeable unit can be replaced by some anions or substrates existing in the system to change the magnetism of the complex<sup>[24]</sup> (Fig 3.6), but two ligands with the similar coordination ability replacing each other cannot change the magnetism. It reminds us that when we want to change the magnetic properties of the complex in solution by decreasing the coordination number, we cannot use acetonitrile or pyridine as the solvent. Usually the way by changing the coordination number occurs on Ni(II) based on the switch among three geometries<sup>[25]</sup>, sometimes it occurs on Fe(III) based on the change from octahedral to distorted one shape<sup>[26]</sup>.

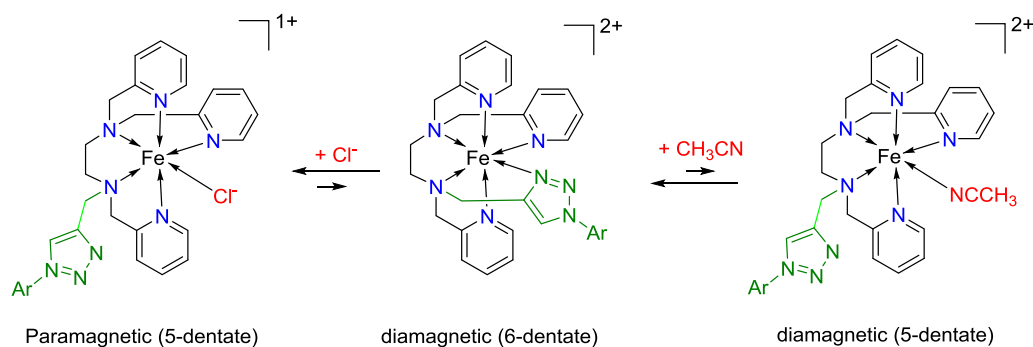


Fig. 3.6 The example that an anion can replace the tethered arm (in green) to change its magnetism. And the solvent molecule ( $\text{CH}_3\text{CN}$ ) is replaced by the this moiety, but cannot change the magnetism.

### 3.2 Proposal of the project

In view of the previous presentation, the magnetic molecular probe can be designed by using the property of switchable spin state based on a transition metal ion. As a probe, it should fulfill some necessary requirements: a) specific (selectively respond to a particular target); b) sensitive (maximal Signal-Noise Ratio); c) rapid (fast response) and d) safe (non-toxic, very important for the applications *in vivo*). We have to consider these conditions when any molecular probe is designed and the detection way is chosen. If all the requirements above can be optimal, this probe and the detection method should be ideal. Herein the probes which can give changes of magnetic properties are attractive because of several reasons:

- 1) Maximal signal gap (true off-on mode). If a molecule (complex based on a transition metal ion) can give zero signal in the initial state (low-spin) then intense signals after its activation (high-spin), the difference between two states should be quite obvious, which generates the maximum SNR. In that case, the difference of magnetic moments in two states is optimal thus it can be observed easily by MRI images.
- 2) Binary response. It means all the probes are supposed to be activated by the target, and there does not exist an equilibrium between the initial and activated form. Consequently an irreversible response to a specific chemical analyte should be optimal.
- 3) Fast response kinetics. the maximum SNR requires as many as possible probes are activated at the same time once they encounter the target so that the most intense signals can be obtained. Moreover, Considering its application *in vivo*, this process

should take as less as possible time in order to limit the diffusion of signals and also minimize the loss of resolution. But as far as a simple detection without requirement of spatial resolution is concerned, the diffusion effect is not so important that the probes do not have to react with the trigger immediately, as long as the net total signal is collected and measured after their response. However in practice, it is a big challenge because the spatial resolution has to be considered and the cleavage of a covalent bond like the enzymatic recognition of its substrate never occurs instantaneously. By the way, the fast detection is also necessary.

4) Robustness. The probes should be inert to anything in the experimental environment except the trigger. It is a very strict requirement because the media in life contains various of chemicals which may compete with the analyte to interact with the probes or destroy the probe molecules. It is noticeable that the strong stability without any degradation or decomposition is required.

In view of that, the project is proposed based on the magnetic probes which are responsive to specific chemical analytes or enzymes in a true off-on mode and the magnetism changes will be detected by MRI whose advantages have been mentioned in Chapter 2.

### **3.2.1 Choice of iron(II)**

Many paramagnetic metal ions can offer contrast enhancement, such as  $\text{Mn}^{2+}$ ,  $\text{Mn}^{3+}$ ,  $\text{Fe}^{3+}$ ,  $\text{Cu}^{2+}$ , and  $\text{Gd}^{3+}$ . Among them  $\text{Gd}^{3+}$  showed better efficacy due to its 7 unpaired electrons ( $S = 7/2$ ), which has long electron spin relaxation time and high magnetic moment, then thus it is playing an important role in the field of MR contrast agents. However, generally the ligand (polyaminopolycarboxylate ligand) is octadentate so that the ninth coordination site of  $\text{Gd}^{3+}$  allows for approach of one water molecule. Subsequently the rapidly exchanging between coordinated water molecule and the bulk water transmits the paramagnetic relaxation effect which cannot be avoided in any  $\text{Gd}^{3+}$ -based CAs. Whereas as we have seen, the design of an imaging probe

requires attention to an essential additional criterion : signal ratio before and after activation to maximize the signal-to-noise ratio *in vivo*. It is better choose a metal ion which can make it possible that its magnetic state changes from diamagnetism to paramagnetism, rather than from weak to strong paramagnetism before and after the response to the targets. It means that the ion should switch states between low-spin (inactive) and high-spin (active) by the action of a specific stimulus.

Fe(II) is a specially attractive ion. Because iron is the most abundant transition metal element not only in the earth's crust but also in any live organism which biochemically recognizes it. What is more important is that it can show different magnetism which is dependent on strength of its ligand in terms of CFT because of its electronic configuration  $3d^6$ , as the previous presentation.

According to Hard-Soft-Acid-Base theory (HSAB), Fe(II) is borderline acid. Thus it can bind well to both oxygen and nitrogen base, including neutral oxygen donors and heterocyclic nitrogen donors. This versatility is useful for realizing the goal of designing responsive contrast agents that can be turned on and off upon the different ligands.

### **3.2.2 Design of ligands**

There are hundreds of options to choose some suitable ligands for formation of complexes. Considering the stability of the required complexes, the macrocyclic ligands are more preferable than the acyclic ones which typically can be dissociate in solution to some extent. Moreover, the acyclic ligands often easily form the binuclear or even multinuclear complexes which are not our interest for magnetism research. The small tridentate macrocycle 1,4,7-triazacyclononane (TACN) and its derivatives ("pendant donor" macrocyclic, the term is first proposed in 1980<sup>[27]</sup> and is used to describe the macrocycle attaching additional donor groups to its periphery.) have been applied to form stable complexes with many metal centers<sup>[28]</sup> in the coordination chemistry, and also stabilize and produce interesting coordination chemistry<sup>[29-31]</sup> in

early period. Usually two TACN molecules form a sandwich complex with the general formula  $[M([9]aneN3)_2]^{n+}$ , and its application is limited by metal ions if we do not make any modification on the cycle. While *N*-functionalized TACN has some difficulty in binding metal ions to form sandwich complexes due to the steric hindrance between the bulky substituents<sup>[28]</sup>. Consequently the pendant donor macrocycles as ligands are more and more popular and are being synthesized in large numbers. The three old reviews in 1984<sup>[32]</sup>, in 1990<sup>[33]</sup> and 1997<sup>[34]</sup> published their basic synthesis, and at the same time their various application such as enzyme simulations<sup>[35]</sup>, carrying a radionuclide to a targeted cell<sup>[36]</sup> and magnetic resonance imaging contrasts<sup>[37]</sup>.

In conclusion, the pendant donor macrocycles of TACN can immobilize transition metal ions to form stable complexes with tunable physicochemical and functional properties, which attracted our attentions for the application in MRI.

### **3.3 Previous work in the group**

In view of that presented above, Prof. Jens Hasserodt proposed to use iron (II) as the metal center ion and the pendant donor macrocycles of TACN to synthesize the corresponding complexes as MRI CAs even to design responsive MRI probes. All the previous work from the proposal of complexes based on iron (II) as MRI CAs to as probes established a strong foundation and paved an extensive way for the coming research.

#### **3.3.1 First example of complexes based on iron(II)**

At the very beginning two simple molecules were designed and synthesized for measurement of their relaxivities and magnetic moments, also for their application in MRI phantom images in 2008<sup>[38]</sup>. The obtained results were very exciting as they both behaved as expected. The N6 type of complex based on iron (II) showed low-spin

state while the one belonging to N5O1 type exhibited its high-spin state. Their MRI phantom images showed us the relaxation time of HS complex changed with increasing its concentration (Fig. 3.7).

The data above proved that the relaxivities of the designed low-spin and high-spin  $\text{Fe}^{2+}$ -complexes are significantly extremely different and their ratio approaches infinity in view of the virtual absence of relaxivity for the low-spin version. This significant gap offers a promising point of departure and a possibility to develop responsive MRI probes.

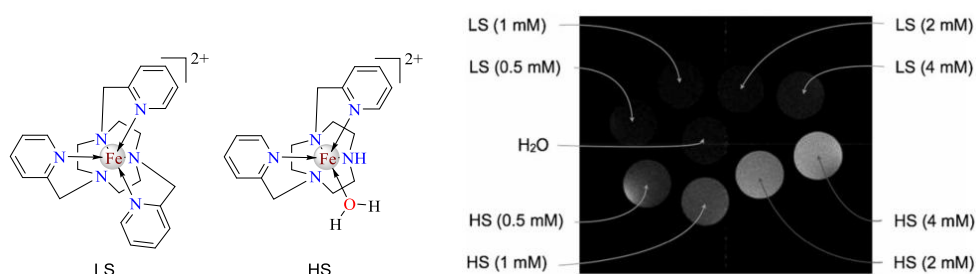


Fig. 3.7  $T_1$ -weighted MR images of tubes containing  $[\text{Fe}(\text{tptacn})][\text{BF}_4]_2$  (LS), and  $[\text{Fe}(\text{dptacn})][\text{BF}_4]_2$  (HS), at a series of concentrations (4.0, 2.0, 1.0, 0.5 mM).

Reference: tube containing pure water.

### 3.3.2 Design of activatable MRI probes

One of the great advantages of  $\text{Fe}^{2+}$ -complexes is their potential to be MRI probes. After the identification of those two complexes, Prof. Hasserodt proposed the first strategy to design MRI contrast agents responding to enzyme given that its attractive perspective in monitoring a number of biological events<sup>[39]</sup>. The designed low-spin candidate should be suitable to most of hydrolytic enzymes depending on the substrates in the auto-immolative pendent arm. Herein the arm bears  $\beta$ -galactose which is susceptible to corresponding enzyme and auto-immolative spacer that was hypothesized to liberate a phenylogous hemiaminal fragment thereby produce a pentacoordinated paramagnetic complex. However, in fact the intermediate could not

fragment, which was attributed to the strong coordination effect (Fig. 3.8).

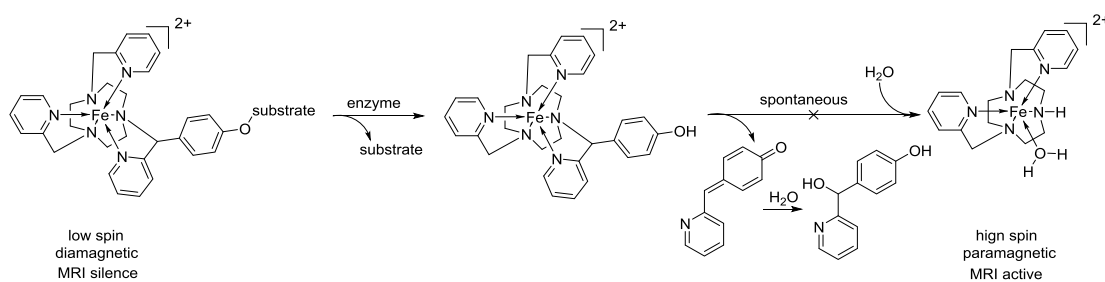


Fig. 3.8 The first unsuccessful strategy to design the responsive MRI probe to  $\beta$ -galactase.

Then the second generation strategy was proposed that a diamagnetic iron (II) complex was irreversibly switched to a paramagnetic one by a chemical stimulus (sodium dithionate) at pH 3.0 in an aqueous solution (Fig. 3.9)<sup>[40]</sup>. The conversion was achieved by protonation of the amidine moiety which competed with coordination to Fe(II) inducing its decoordination and approach of water. The process was monitored by measurement of  $T_1$  and the different UV-vis spectra also showed this change. This work was so satisfactory due to robustness of the diamagnetic iron(II) complex and great signal-to-background ratio.

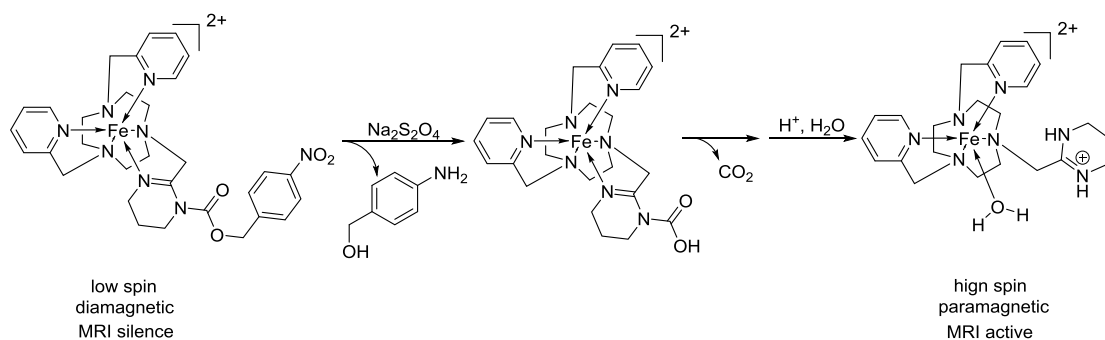


Fig. 3.9 The first successful strategy : a MRI probe responsive to chemical stimulus ( $\text{Na}_2\text{S}_2\text{O}_4$ ).

However, that response occurred only under relatively harsh conditions which brought many constraints on its application especially at physiological pH 7.4. Afterwards new probes were designed which could be triggered by either a chemical reagent ( $\text{H}_2$ , Pd/C) or an enzyme (penicillin amidase)<sup>[41]</sup>. The low-spin complex carries the trigger unit as well as the auto-immolative moiety spacer. Elimination and hydrolysis lead to

departure of the entire pendent arm that is accompanied by the generation of paramagnetic chelate (Fig 3.10).

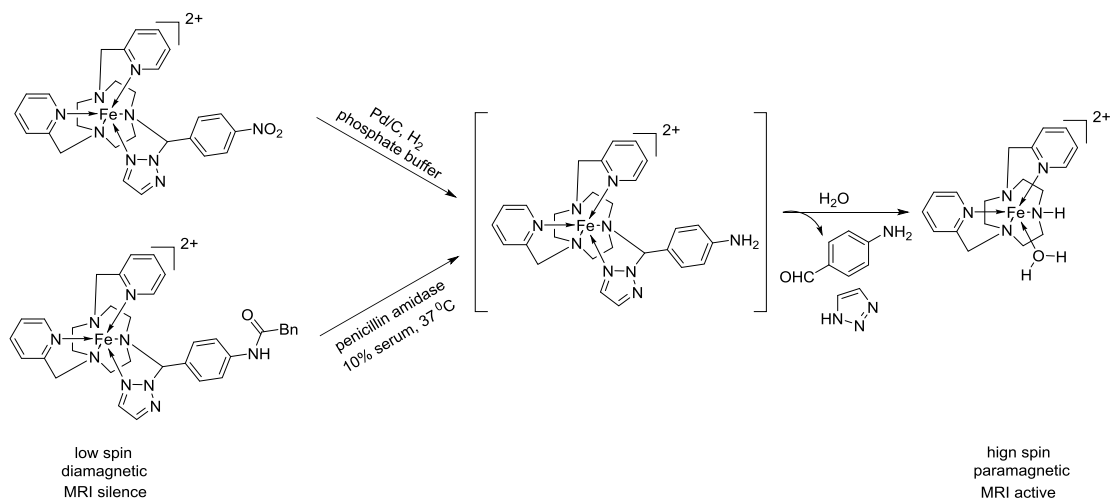


Fig. 3.10 The 2<sup>nd</sup> successful strategy : two MRI probes responsive to chemical stimulus (Pd/C, H<sub>2</sub>) or penicillin amidase.

### 3.4 Proposal of electroneutrality

The contrast agents work for detection of tumors, abscesses and inflammation sites by enhancing the relaxivity of water protons in non-invasive MRI imaging, and most of conventional MRI CAs diffuse from the vascular into interstitial and extracellular space of tissues. However, only 30% of tissue water is extracellular, while 70% is intracellular. A new window for improving access to the unexplored intracellular space needs to be proposed. Positively charged complexes cannot go through the lipid bilayer of cell membrane. While converted into charge-neutral, they can penetrate the cell membrane. Thus MRI images can provide enhanced intracellular signals in cells of healthy and diseased tissues.

Even though the macrocyclic lanthanide complexes as either positive or negative MRI CAs have attracted considerable interest, their potential utility *in vivo* requires good toleration in the body. On this account M. Woods et al.<sup>[42]</sup> examined the effects of the

charge on the fate of those chelates postinjection (dissociation and excretion). At low doses, those complexes (Fig. 3.11) did not tend to dissociate *in vivo* because of high kinetic inertness which indicated irrespective of the charge; while at high doses, all 3 tri-cationic complexes studied were acutely toxic.

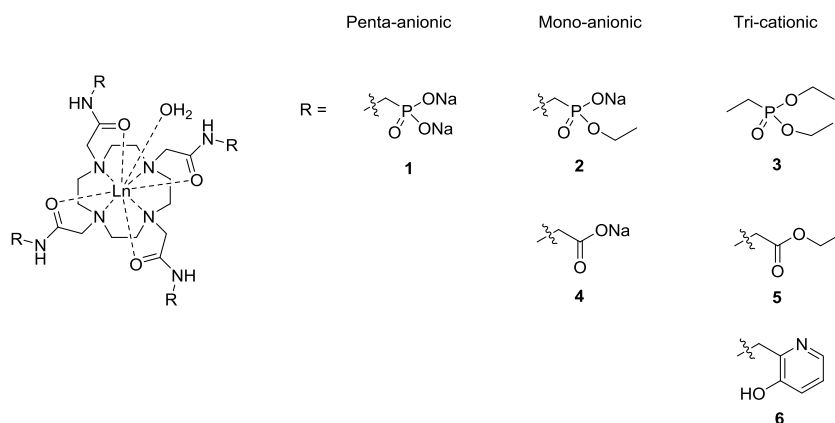


Fig. 3.11 Complexes used for research by M. Woods et al.

As mentioned previously, S. Aime et al.<sup>[43]</sup> took three complexes as examples to investigate their stability in two types of cells (J774A.1 murine macrophages and NIH/3T3 murine fibroblasts). They chose ([Gd-DTPA-BMA] as representative of the electroneutral linear complexes, [Gd-DTPA]<sup>2-</sup> as representative of negatively charged linear complexes and [Gd-HPDO3A] as representative of electroneutral macrocyclic complexes (Fig. 3.12). The results showing only the [Gd-HPDO3A] is robust enough after the administration up to 96 h clearly indicated the potential promising application of macrocyclic complexes in MRI.

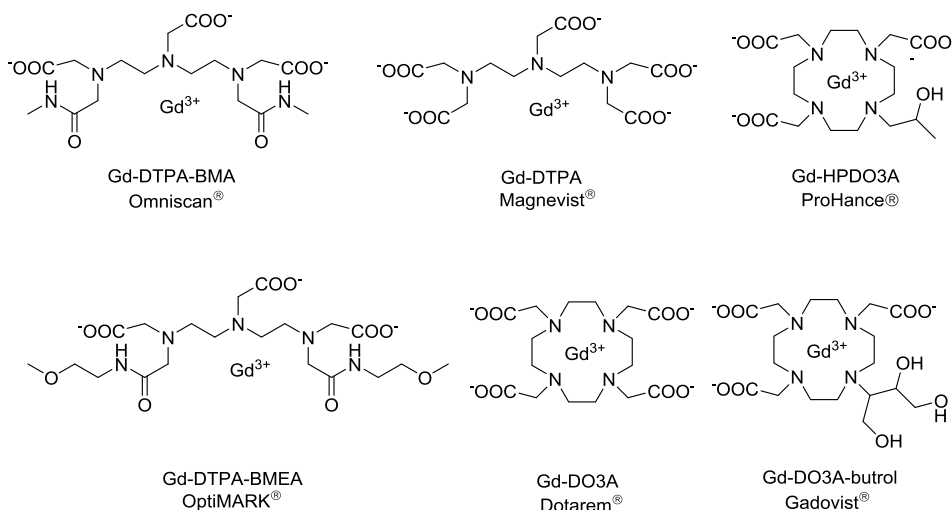


Fig. 3.12 Complexes used for research by S. Aime and T. J. McMurry et al.

T. J. McMurry et al.<sup>[44]</sup> also compared the relaxivity and stability of some commercial lanthanide ion Gd (III) complexes (Fig. 3.12 and Table 3.1) as MRI CAs. Then we can understand why most of commercial MRI CAs are almost electroneutral or negatively charged. For example, Gd-DTPA has been applied as an extracellular CA in diagnostic MRI images in patients.

Table 3.1 Thermodynamic Stabilities and Relaxivities of the Commercial Extracellular Agents

Chemical name	Brand name	Company	1/T <sub>1</sub> (mM <sup>-1</sup> s <sup>-1</sup> )	Log K (therm)
[Gd(DTPA)(H <sub>2</sub> O)] <sup>2-</sup>	Magnevist <sup>®</sup>	Schering (Germany)	4.30 <sup>a,c</sup>	22.46 <sup>h</sup>
[Gd(DOTA)(H <sub>2</sub> O)]	Dotarem <sup>®</sup>	Guerbet (France)	4.20 <sup>a,c</sup>	25.30 <sup>i</sup>
[Gd(DTPA-BMA)(H <sub>2</sub> O)]	Omniscan <sup>®</sup>	Nycomed (Norway)	4.39 <sup>a,d</sup>	16.85 <sup>j</sup>
[Gd(HP-DO3A)(H <sub>2</sub> O)]	ProHance <sup>®</sup>	Bracco (Italy)	3.70 <sup>b,e</sup>	23.80 <sup>i</sup>
[Gd(DO3A-butrol)(H <sub>2</sub> O)]	Gadovist <sup>®</sup>	Schering (Germany)	3.60 <sup>b,f</sup>	21.80 <sup>k</sup>
[Gd(DTPA-BMEA)(H <sub>2</sub> O)]	OptiMARK <sup>®</sup>	Mallinckrodt (U. S.)	4.70 <sup>b,g</sup>	16.84 <sup>i</sup>

a. Relaxivities in water at 20 MHz and 25 °C. b. Relaxivities in water at 20 MHz and 40 °C. c. *Magn. Reson. Chem.* 1991, 29, 923. d. *J. Am. Chem. Soc.* 1996, 118, 9333. e. *Magn. Reson. Chem.* 1996, 35, 928. f. *Eur. J. Radiol.* 1995, 21, 1. g. *Invest Radiol.* 1991, 26, 217. h. Smith *et al.* 1997, *NIST Standard Reference Database* 46, 3.0 ed. i. *Inorg. Chem.* 1994, 33, 3567. j. *Magn. Reson.*

Considering the clearance rate, it is reported that positively charged copper complexes demonstrate slow clearance in the body in comparison to neutral complexes<sup>[45]</sup>.

In addition, since the pharmacokinetic (PK) properties of charged and neutral extracellular agents are similar, neutral agents are promising in MRI application given that they possess high water solubility and potential to lower the osmolality of aqueous solutions (Table 3.2).

Osmolality is a key factor that cannot be ignored for MRI contrast agents. Especially when very large doses of CAs are used, the improvement in tolerability should be seriously treated. It was achieved by switching from charged to neutral molecules as CAs which do not require any counterion. This formulation bears fruits that the solutions of neutral CAs have lower osmolality closer to that of serum as well as lower viscosity, which bodes well for their application with rapid injection<sup>[46]</sup>.

Table 3.2 Some contrast agents with their osmolality and viscosity properties

Chemical name	Concn (M)	osmolality <sup>a</sup> (osmol kg <sup>-1</sup> )	Viscosity <sup>a</sup> (mP s)
[Gd(DTPA)(H <sub>2</sub> O)] <sup>2-</sup>	0.5	1.96	2.9
[Gd(DOTA)(H <sub>2</sub> O)] <sup>-</sup>	0.5	1.35	2.0
[Gd(DTPA-BMA)(H <sub>2</sub> O)]	0.5	0.65	1.4
[Gd(HP-DO3A)(H <sub>2</sub> O)]	0.5	0.63	1.3
[Gd(DO3A-butrol)(H <sub>2</sub> O)]	0.5	0.57	1.43
[Gd(DO3A-butrol)(H <sub>2</sub> O)]	1.0	1.39	3.9
[Gd(BOPTA)(H <sub>2</sub> O)] <sup>2-</sup>	0.5	1.97	5.3
[Gd(EOB-DTPA)(H <sub>2</sub> O)] <sup>2-</sup>	0.25	0.89	1.22

a. Osmolality and viscosity measured at 37 °C.

Fe(II) complexes are in the same situation. The Fe(II) complexes carrying two positive charges generally lack thermodynamic stability due to lack of coulombic charge compensation. Those with (a) free coordination site(s) also likely exercise

non-negligible Lewis acid activity compared with closed-shell Fe(II) complexes, which likely increases toxicity *in vivo*. Typically they also have an unfavorable osmolality. This statement was also accepted by J. R. Morrow in her review<sup>[47]</sup>. What is more, the typical way to design a chelator to make the overall charge of a complex disappear is that the uncomplexed chelator is anionic at physiological pH. Normally the groups containing active proton such as phenolic hydroxy, thiol, phosphate, carboxylate have potential to meet this requirement.

In this context our group hypothesized that rendering the complexes electroneutral may relieve these limitations.

Based on the complex models previously presented, the strategy to satisfy the requirement of electroneutrality was raised. Two identical of the three arms of TACN-based ligands contribute the two necessary properties, one of which is to provide inherent coordination effects by imine-type nitrogen atoms and the other is to exhibit a lower pKa than physiological pH. Considering the attractive aqueous pKa (~5) of tetrazole, F. Touti, PhD student in our group preceding me, introduced two tetrazoles in the form of a protected synthon with benzyl group to TACN to synthesize the corresponding high-spin complex (N3(amine)N2-(tetrazol)O(H<sub>2</sub>O) coordination)<sup>[48]</sup> (Fig. 3.13).

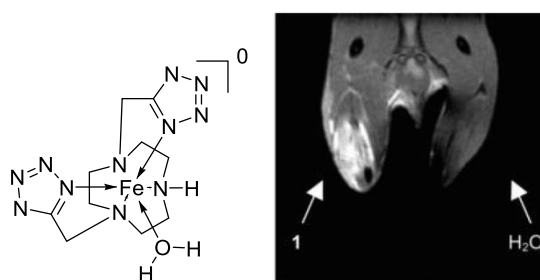


Fig. 3.13  $T_1$ -weighted images 24 h postinjection of mouse that was treated with the complex (the structure shown on the left, 50  $\mu$ L of 50 mM) in the left leg and pure water into the right leg. From *J. Med. Chem.* 2011, 54, 4274.

The MRI image in mouse of this binary and macrocyclic ferrous complex demonstrated its efficiency in raising contrast as predicted and at the same time better

tolerance *in vivo* was observed compared with positively charged complexes.

### 3.5 Thesis project

In view of the advantages that electroneutrality may confer onto ferrous complexes as hypothesized in the overall project described above, my thesis project is to explore two new strategies (Fig. 3.14). The corresponding two ligand systems will be prepared in two versions each, one that leads to the corresponding HS and the other to the LS complex. To the best of our knowledge, the LS complexes would be the first ever electroneutral ferrous complexes outside the context of porphyrin systems. The pursuit of these strategies is presented in detail in Chapter 4 and 5.

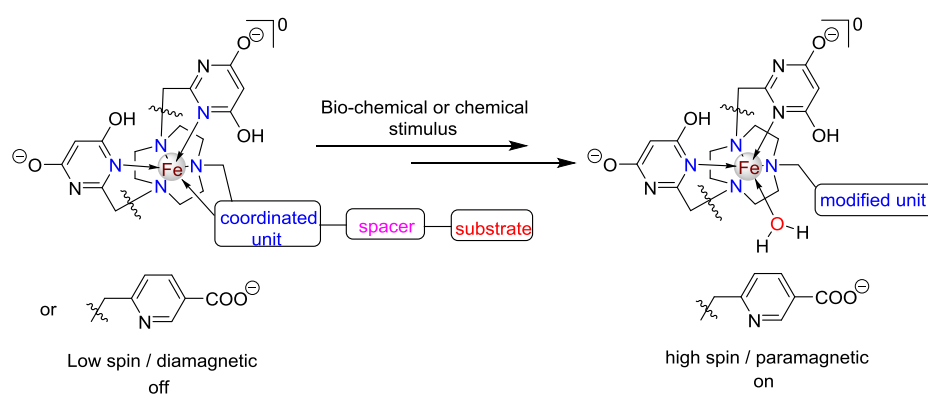


Fig. 3.14 Two strategies to achieve electroneutrality of MRI probes

### 3.6 References

- [1] König E., Ritter G., Kulshreshtha S. K. The Nature of Spin-State Transitions in Solid Complexes of Iron(II) and the Interpretation of Some Associated Phenomena. *Chem. Rev.*, 1985, 85, 219; Gülich P., Hauser A., Spiering H. Thermal and Optical Switching of Iron(II) Complexes. *Angew. Chem., Int. Ed. Engl.* 1994, 33, 2024; Gülich P., Garcia Y., Goodwin H. A. Spin crossover Phenomena in Fe(II) Complexes. *Chem. Soc. Rev.* 2000, 29, 419.
- [2] Halcrow M. A. The Spin-States and Spin-Transitions of Mononuclear Iron(II) Complexes of Nitrogen-Donor Ligands. *Polyhedron*, 2007, 26, 3523; Murray K. S. Advances in Polynuclear

- Iron(II), Iron(III) and Cobalt(II) Spin-Crossover Compounds. *Eur. J. Inorg. Chem.* 2008, 3101.
- [3] Nakamura M. Electronic Structures of Highly Deformed Iron(III) Porphyrin Complexes. *Coord. Chem. Rev.* 2006, 250, 2271.
- [4] Nihei M., Shiga T., Maeda Y., Oshio H. Spin Crossover Iron(III) Complexes. *Coord. Chem. Rev.* 2007, 251, 2606.
- [5] Gütllich P., Goodwin H. A. Spin Crossover in Transition Metal Compounds II. *Top. Curr. Chem.* 2004, 234, 23; Krivokapic I., Zerara M., Daku M. L., Vargas A., Enachescu C., Ambrus C., Tregenna-Piggott P., Amstutz N., Krausz E., Hauser A. Spin-Crossover in Cobalt(II) Imine Complexes. *Coord. Chem. Rev.* 2007, 251, 364.
- [6] König E. Structural Changes Accompanying Continuous and Discontinuous Spin-State Transitions. *Prog. Inorg. Chem.* 1987, 35, 527.
- [7] Kohler C. P., Jakobi R., Meissner E., Wiehl L., Spiering H., Gütllich P. Nature of the Phase Transition in Spin Crossover Compounds. *J. Phys. Chem. Solids* 1990, 51, 239.
- [8] Müller E. W., Spiering H., Gütllich P. On the Participation of Domains in the High Spin ( ${}^5T_2$ )  $\rightleftharpoons$  Low Spin ( ${}^1A_1$ ) Transition in Dithiocyanatobis (2, 2' - bi - 2 - Thiazoline) Iron(II). *J. Chem. Phys.* 1983, 79, 1439.
- [9] Franke P. L., Haasnoot J. G., Zuur A. P. Tetrazoles as ligands. Part IV. Iron(II) Complexes of Monofunctional Tetrazole Ligands, Showing High-spin ( ${}^5T_{2g}$ )  $\rightleftharpoons$  low-spin transitions. *Inorg. Chim. Acta* 1982, 59, 5.
- [10] Gütllich P., Goodwin H. A. Spin Crossover in Transition Metal Compounds I. *Top. Curr. Chem.* 2004, 233, 1.
- [11] Thies S., Sell H., Schutt C., Bornholdt I., Nather C., Tuczek F., Herges R. Light-Induced Spin Change by Photodissociable External Ligands: A New Principle for Magnetic Switching of Molecules. *J. Am. Chem. Soc.* 2011, 133, 16243.
- [12] Marignol L., Coffey M., Lawler M., Hollywood D. Hypoxia in prostate cancer: A Powerful Shield Against Tumour Destruction?. *Cancer Treat. Rev.* 2008, 34, 313.
- [13] Chaiswing L., Zhong W., Oberley T. D. Distinct Redox Profiles of Selected Human Prostate

- Carcinoma Cell Lines: Implications for Rational Design of Redox Therapy. *Cancers (Basel)* 2011, 3, 3557.
- [14] Beattie J. K. Dynamics of Spin Equilibria in Metal Complexes. *Adv. Inorg. Chem.* 1988, 32, 1.
- [15] Toftlund H. Spin Equilibria in Iron(II) Complexes. *Coord. Chem. Rev.* 1989, 94, 67.
- [16] Toftlund H. Spin Equilibrium in Solutions. *Monatshefte für Chemie/Chemical Monthly* 2001, 132, 1269.
- [17] Toftlund H., McGarvey J. J. Iron(II) Spin Crossover Systems with Multidentate Ligands. *Top. Curr. Chem.* 2004, 233, 151.
- [18] Shores M. P., Klug C. M., Fiedler S. R. In *Spin-Crossover Materials*. John Wiley & Sons Ltd, 2013, 281-301.
- [19] Ni Z., McDaniel A. M., Shores M. P. Ambient Temperature Anion-Dependent Spin State Switching Observed in “Mostly Low Spin” Heteroleptic Iron(II) Diimine Complexes. *Chem. Sci.* 2010, 1, 615.
- [20] Martin L. L., Hagen K. S., Hauser A., Martin R. L., Sargeson A. M. Spin Equilibria in Iron(II) Hexa-Amine Cages. *J. Chem. Soc., Chem. Commun.* 1988, 1313.
- [21] Martin L. L., Martin R. L., Sargeson A. M. The Ligand Field  $^1A_1$ - $^5T_2$  Spin Crossover with Iron(II) Encapsulated in Hexa-Amine Cages. *Polyhedron* 1994, 13, 1969.
- [22] Britovsek G. J. P., England J., White A. J. P. Non-heme Iron(II) Complexes Containing Tripodal Tetradentate Nitrogen Ligands and Their Application in Alkane Oxidation Catalysis. *Inorg. Chem.* 2005, 44, 8125.
- [23] England J., Britovsek G. J. P., Rabadia N., White A. J. P. Ligand Topology Variations and the Importance of Ligand Field Strength in Non-Heme Iron Catalyzed Oxidations of Alkanes. *Inorg. Chem.* 2007, 46, 3752.
- [24] Segaud N., Rebilly J. N., Senechal-David K., Guillot R., Billon L., Baltaze J. P., Farjon J., Reinaud O., Banse F. Iron Coordination Chemistry with New Ligands Containing Triazole and Pyridine Moieties. Comparison of the Coordination Ability of the N-Donors. *Inorg.*

*Chem.* 2013, 52, 691.

- [25] Sacconi L., Nannelli P., Campigli U. Complexes of Nickel(II) with Schiff Bases Formed from Salicylaldehydes and N-Substituted Ethylenediamines I. *Inorg. Chem.* 1965, 4, 818.
- [26] Vad M. S., Lennartson A., Nielsen A., Harmer J., McGrady J. E., Frandsen C., Morup S., McKenzie C. J. An Aqueous Non-Heme Fe(IV)oxo Complex with a Basic Group in the Second Coordination Sphere. *Chem. Commun.* 2012, 48, 10880.
- [27] Wainwright K. P. Chemistry of Structurally Developed Macrocycles. Part 1. Complexation Properties of NN'N''N'''-Tetra(2-Cyanoethyl)-1,4,8,11-Tetra-Azacyclotetradecane with Nickel(II). *J. Chem. Soc., Dalton Trans.* 1980, 2117.
- [28] Lippard S. J. The Chemistry of 1,4,7-Triazacyclononane and Related Tridentate Macrocyclic Compounds. *Prog. Inorg. Chem.* 2007, 35, 329.
- [29] Wilson P. J., Blake A. J., Schröder M. Syntheses and Structures of a New Class of Aza- and Thio-ether Macrocyclic  $d^0$  Imido Complexes. *Chem. Commun.* 1998, (9), 1007.
- [30] Hajela S., Schaefer W. P., Bercaw J. E. Highly Electron Deficient Group 3 Organometallic Complexes Based on the 1,4,7-Trimethyl-1,4,7-Triazacyclononane Ligand System. *J. Organomet. Chem.* 1997, 532, 45.
- [31] Zhen H. S., Wang C. M., Hu Y. H., Flood T. C. Reactions of (Trimethyltriazacyclononane) Rh(vinyl)<sub>3</sub>, -Rh(Z-propenyl)<sub>3</sub>, and -Rh(vinyl)<sub>2</sub>Me with Protic Acids. The Relative Migratory Aptitude of Methyl and Vinyl Groups to an (Ethyldiene)Rh Alkylidene Carbon. *Organometallics* 1998, 17, 5397.
- [32] Kaden T. A. Synthesis and Metal Complexes of Aza-macrocycles with Pendant Arms Having Additional Ligating Groups. *Top. Curr. Chem.* 1984, 121, 157.
- [33] Bernhardt P.V., Lawrance G. A. Complexes of Polyaza Macrocycles Bearing Pendant Coordinating Groups. *Coord. Chem. Rev.* 1990, 104, 297.
- [34] Wainwright K. P. Synthetic and Structural Aspects of the Chemistry of Saturated Polyaza Macrocyclic Ligands Bearing Pendant Coordinating Groups Attached to Nitrogen. *Coord. Chem. Rev.* 1997, 166, 35.

- [35] Kimura E., Kodama Y., Koike T., Shiro M. Phosphodiester Hydrolysis by a New Zinc(II) Macrocyclic Tetraamine Complex with an Alcohol Pendant: Elucidation of the Roles of Ser-102 and Zinc(II) in Alkaline Phosphatase. *J. Am. Chem. Soc.* 1995, 117, 8304.
- [36] Parker D. Tumour Targeting with Radiolabelled Macrocyclic–Antibody Conjugates. *Chem. Soc. Rev.* 1990, 19, 271.
- [37] Dischino D. O., Delancy E. J., Emswiler J. E., Gaughan G.T., Prasad J. S., Srivastava S. K., Tweedle M. F. Synthesis of Nonionic Gadolinium Chelates Useful as Contrast Agents for Magnetic Resonance Imaging: 1,4,7-Tris(carboxymethyl)-10-Substituted-1,4,7,10-Tetraazacyclododecanes and Their Corresponding Gadolinium Chelates. *Inorg. Chem.* 1991, 30, 1265.
- [38] Stavila V., Allali M., Canaple L., Stortz Y., Franc C., Maurin P., Beuf O., Dufay O., Samarut J., Janierd M., Hasserodt J. Significant Relaxivity Gap Between a Low-spin and a High-spin Iron(II) Complex of Structural Similarity: an Attractive Off-on System for the Potential Design of Responsive MRI Probes. *New J. Chem.* 2008, 32, 428.
- [39] Stavila, V., Stortz Y., Franc C., Pitrat D., Maurin P., Hasserodt J. Effective Repression of the Fragmentation of a Hexadentate Ligand Bearing an Auto-Immolable Pendant Arm by Iron Coordination. *Eur. J. Inorg. Chem.* 2008, (25), 3943.
- [40] Touti F., Maurin P., Canaple L., Beuf O., Hasserodt J. Awakening of a Ferrous Complex's Electronic Spin in an Aqueous Solution Induced by a Chemical Stimulus. *Inorg. Chem.* 2012, 51, 31.
- [41] Touti F., Maurin P., Hasserodt J. Magnetogenesis Under Physiological Conditions With Probes that Report on (bio-)chemical Stimuli. *Angew. Chem. Int. Ed.* 2013, 52, 4654.
- [42] Woods M., Caravan P., Gerald C. F. G. C., Greenfield M. T., Kiefer G. E., Lin M., McMillan K., Prata M. I. M., Santos A. C., Sun X., Wang J., Zhang S., Zhao P., Sherry A. D. The Effect of the Amide Substituent on the Biodistribution and Tolerance of Lanthanide(III) DOTA-Tetraamide Derivatives. *Invest Radiol.* 2008, 43, 861.
- [43] Gregorio E. D., Gianolio E., Stefania R., Barutello G., Digilio G., Aime S. On the Fate of

- MRI Gd-Based Contrast Agents in Cells. Evidence for Extensive Degradation of Linear Complexes upon Endosomal Internalization. *Anal. Chem.* 2013, 85, 5627.
- [44] Zhang Z., Nair S. A., McMurry T. J. Gadolinium Meets Medicinal Chemistry: MRI Contrast Agent Development. *Curr. Med. Chem.* 2005, 12, 751.
- [45] Pandya D. N., Bhatt N., An G. II, Ha Y. S., Soni N., Lee H., Lee Y. J., Kim J. Y., Lee W., Ahn H., Yoo J. Propylene Cross-Bridged Macrocyclic Bifunctional Chelator: A New Design for Facile Bioconjugation and Robust  $^{64}\text{Cu}$  Complex Stability. *J. Med. Chem.* 2014, 57, 7234.
- [46] Caravan P., Ellison J. J., McMurry T. J., Lauffer R. B. Gadolinium(III) Chelates as MRI Contrast Agents: Structure, Dynamics, and Applications. *Chem. Rev.* 1999, 99, 2293.
- [47] Dorazio S. J., Morrow J. R. The Development of Iron(II) Complexes as ParaCEST MRI Contrast Agents. *Eur. J. Inorg. Chem.* 2012, (12), 2006.
- [48] Touti F., Singh A. K., Maurin P., Canaple L., Beuf O., Samarut J., Hasserodt J. An Electroneutral Macrocyclic Iron(II) Complex that Enhances MRI Contrast In Vivo. *J. Med. Chem.* 2011, 54, 4274.

# Chapter 4 THESIS PROJECT: Achievement of electroneutrality of complexes based on pyridylcarboxylate

## 4.1 Introduction of the project

In view of the previous work, the new strategy to design a ligand has to serve the purpose of coordination and requirement of rendering negative charges. This ability is dependent on the pKa value of the moiety attached on the pendent arms. Normally the carboxylic acids occur to us due to their smaller pKa values than physiological pH. Combining coordination effect and carboxylic acid, the picolinic acid is a good choice.

M. Mazzanti et al.<sup>[1]</sup> reported the pKa values and thermodynamic stability of some Gd(III) and Ca(II) complexes bearing several carboxyl groups. Seen from the table, the pKa values of picolinic acid vary from 2.0 to 3.0 (Fig. 4.1 and Table. 4.1). These results provided us strong evidence and implication on designing electroneutral complexes.

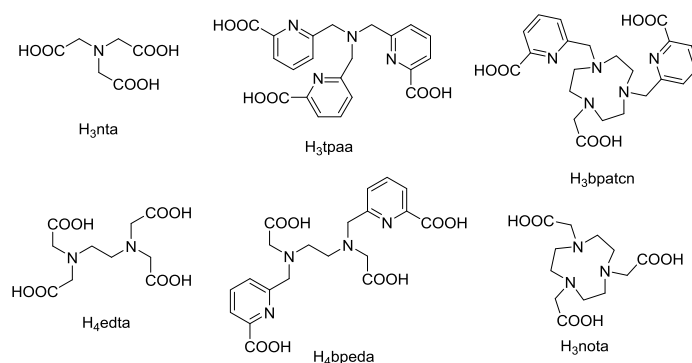


Fig. 4.1 The ligands bearing several carboxyl groups for coordination with Gd (II) and Ca (II).

Table 4.1 pKa values and coefficients of stability of six ligands (Fig. 4.1) binding to Gd (II) and Ca (II).

Ligand	pK <sub>a</sub>	Log K <sub>GdL</sub>	logK <sub>CaL</sub>
H <sub>3</sub> bpatch <sup>a</sup>	10.5, 5.42, 3.71, 2.3, 2.2	15.8	8.18
H <sub>3</sub> nota <sup>b</sup>	11.3, 5.6, 2.88	13.7	8.92
H <sub>4</sub> bpdea <sup>c</sup>	8.5, 5.2, 3.5, 2.9	15.1	9.4
H <sub>4</sub> edta <sup>b</sup>	10.19, 6.13, 2.69, 2.60	17.4	10.5
H <sub>3</sub> nta <sup>b</sup>	9.75, 2.64, 1.57	11.4	/
H <sub>3</sub> tpaa <sup>d</sup>	4.11, 3.3, 2.5	10.2	8.5

[a] *Chem. Eur. J.* 2006, 12, 7133. [b] *Coord. Chem. Rev.* 2000, 204, 309. [c] *Dalton Trans.* 2005, 1129. [d] *Inorg. Chem.* 2001, 40, 6737.

In view of that, our group chose to work with picolinate arms that can be introduced on a macrocyclic framework to improve thermodynamic stability and kinetic inertness of the resulting complex. In fact, one case of this type has already been published in 2013<sup>[2]</sup>. These authors investigated the acid-base behavior of the compound Hno1pa2py (Fig. 4.2) in aqueous solution and the pK<sub>a</sub> was determined by potentiometric titrations. Even though the ligand has seven basic centers (six nitrogen atoms and one carboxylate), only four protonation constants are exhibited. The first two (10.61, 5.25) respectively correspond to protonation of two of amines in the macrocycle, the second one of which presents a low value (5.25) due to the strong electrostatic repulsion of two charged amines which is caused by the small cavity size of the macrocycle. The other two (3.69, 1.61) are respectively attributed to the protonation of pyridyl and carboxylate. What is more, once the complex is formed, only deprotonated species exist at physiological pH. It may give us implication that coordination can decrease their basicity so that all of basic centers exist in the form of deprotonated species.

While it is well-known that picolinic acid or picolinate can be used as ligand with the nitrogen or oxygen atom or even both in coordination chemistry (Fig. 4.2)<sup>[3]</sup>. The

variety of coordination modes lead to versatile applications such as extracting agents for selective removal of lead from contaminated water.

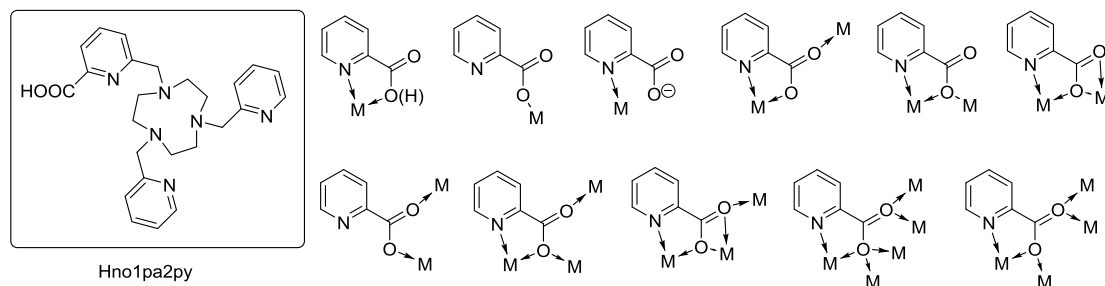


Fig. 4.2 Left, the structure of Hno1pa2py; right, possible coordination modes of picolinate to metal ions

However, 2-carboxyl group of picolinate can coordinate to metal ions and the oxygen atom just provides a weak field, which is unwanted to us. Herein, we only want to use nitrogen as coordination atom and use carboxyl group to provide negative charge to compensate the positive one of metal ions. Thus 3-picolinate attracts our interest in exploring our project (Fig. 4.3).

Consequently the low-spin state is targeted by introducing as third arm picolyl group and the high-spin one by use of benzyl or methyl group (Fig. 4.3). Their synthesis, measurement of magnetic moments and relaxivities are presented next because this data is essential to the assessment of their usefulness as MRI probe

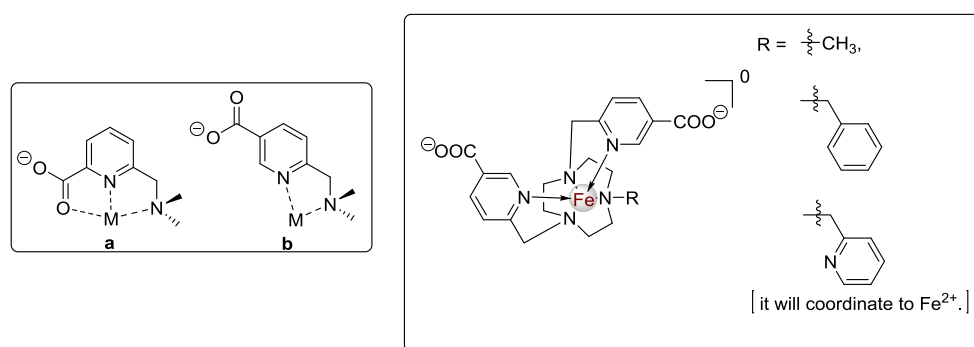


Fig. 4.3 Left, the coordination effect of 2-carboxypyridine (a) and 3-carboxypyridine (b); right, the designed complexes for achievement of electroneutrality

## 4.2 Synthesis of the designed complexes

The synthesis of pendant donor triazamacrocycles plays a very important role in the



Typically the three pyridine moieties as the pendent arms were introduced in the form of their halides. It is noticeable that the preparation of corresponding synthons is necessary.

#### 4.2.2.1 Synthesis of benzyl pyridinedicarboxylate

We envisaged the synthetic route for the synthon benzyl chloromethylpyridyl carboxylate. According to the literature<sup>[4]</sup>, the commercial product 2,5-pyridinedicarboxylic acid can be converted to benzyl dicarboxylate, which then can be selectively reduced to benzyl hydroxymethylpyridyl carboxylate, followed by the chloration to give the target. However, in fact it is not like ethyl dicarboxylate because of our starting material. Normally the difficulty of producing benzyl ester depends on the activity of the corresponding carboxylic acid. While 2,5-pyridinedicarboxylic acid is very inactive because of its poor solubility in alcohol or in thionyl chloride. Its synthesis through benzyl bromide on basic condition or condensation with alcohol in the presence of acidic catalyst<sup>[5]</sup> could not succeed (Table 4.2). When the thionyl chloride was mixed with benzyl alcohol and pyridinedicarboxylic acid together to carry out the reaction as the procedure of making ethyl ester, the efficiency was very low which may derived from the reaction between benzyl alcohol and thionyl chloride. Finally the separated two steps for making acyl chloride and ester could reach the goal.

Table 4.2 Synthesis of benzyl dicarboxylate

entry	conditions	results
1	Benzyl bromide, K <sub>2</sub> CO <sub>3</sub> , DMF	×
2	(cat.)[C]H <sub>2</sub> SO <sub>4</sub> , Benzyl alcohol	×
3	1) SOCl <sub>2</sub> ; 2) Benzyl alcohol	√

#### 4.2.2.2 Synthesis of benzyl hydroxymethylpyridylcarboxylate

Usually the compounds containing two ester groups like malonates have the problem of low yield for selectively reducing one with hydride reagents such as  $\text{LiAlH}_4$  and  $\text{NaBH}_4$ , thus the reductant  $\text{LiAl}(\text{O}-t\text{-Bu})_3\text{H}$  was often used for it<sup>[6]</sup>. Here this reagent is not necessary because the literature has reported that the ethyl ester group on the 2-position of pyridinedicarboxylate can be selectively reduced with  $\text{NaBH}_4/\text{CaCl}_2$  in alcohol. Based on the publication in 1982 about the relative reactivity of saline borohydrides ( $\text{LiBH}_4$ ,  $\text{NaBH}_4$ ,  $\text{Ca}(\text{BH}_4)_2$ ) for the reduction of carboxylic esters<sup>[7]</sup>, in ether solvents the order of reactivity is  $\text{LiBH}_4 > \text{Ca}(\text{BH}_4)_2 > \text{NaBH}_4$ , while in alcohol solvents it is  $\text{Ca}(\text{BH}_4)_2 > \text{LiBH}_4 > \text{NaBH}_4$ . That is why the researcher used  $\text{NaBH}_4/\text{CaCl}_2/\text{EtOH}$  condition which produced  $\text{Ca}(\text{BH}_4)_2$  to improve the reaction speed. However, benzyl pyridinedicarboxylate, unfortunately, almost could not be reduced no matter with  $\text{Ca}(\text{BH}_4)_2$  or  $\text{LiBH}_4$  in THF and in benzyl alcohol the efficiency of  $\text{NaBH}_4$  was surprisingly better than  $\text{NaBH}_4/\text{CaCl}_2$  ( $\text{Ca}(\text{BH}_4)_2$ ) (Table 4.3). Maybe it is related with the solubility of reductants in THF and benzyl alcohol, that is, in THF the solubility of both ( $\text{Ca}(\text{BH}_4)_2$  or  $\text{LiBH}_4$ ) are too poor to touch the ester and in benzyl alcohol the solubility of  $\text{NaBH}_4$  is better than that of  $\text{Ca}(\text{BH}_4)_2$ . Even though the selective reduction has been resolved, it could not complete in short time, and just gave a moderate yield (75%).

Table 4.3 Selective reduction of pyridinedicarboxylate

entry	Eq. of reductant	reductant	catalyst	solvent	temperature	time	Yield
1	0.6	$\text{NaBH}_4$	$\text{CaCl}_2$	THF	RT	5h	< 5% <sup>a</sup>
2	0.6	$\text{LiBH}_4$	$\text{CaCl}_2$	THF	RT	1h	< 5% <sup>a</sup>
3	1.2	$\text{LiBH}_4$	$\text{CaCl}_2$	THF	RT	4h	< 5% <sup>a</sup>
4	1.2	$\text{LiBH}_4$	$\text{CaCl}_2$	THF	65 °C	18h	< 5% <sup>a</sup>
5	0.6	$\text{LiBH}_4$	/	THF	RT	1h	< 5% <sup>a</sup>
6	1.2	$\text{LiBH}_4$	/	THF	RT	4h	< 5% <sup>a</sup>

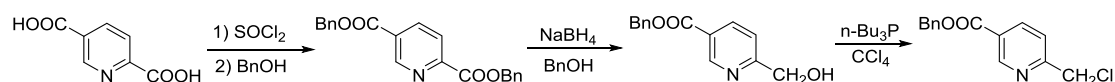
7	1.2	LiBH <sub>4</sub>	/	THF	65 °C	18h	< 5% <sup>a</sup>
8	0.6	L-selectride	/	THF	RT	1h	< 5% <sup>a</sup>
9	0.6	NaBH <sub>4</sub>	/	DMF	RT	17h	< 5% <sup>a</sup>
10	0.6	LiBH <sub>4</sub>	/	Et <sub>2</sub> O/Toluene	65 °C	3h	< 5% <sup>a</sup>
11	0.6	NaBH <sub>4</sub>	CaCl <sub>2</sub>	BnOH	60 °C	24h	35% <sup>b</sup>
12	1.2	NaBH <sub>4</sub>	CaCl <sub>2</sub>	BnOH	40 °C	24h	45% <sup>b</sup>
13	1.2	NaBH <sub>4</sub>	CaCl <sub>2</sub>	BnOH	RT	46h	60% <sup>b</sup>
14	1.2	NaBH <sub>4</sub>	/	BnOH	RT	16h	75% <sup>b</sup>

a. It was estimated by TLC monitoring the reaction; b. It was calculated after chromatography purification.

#### 4.2.2.3 Synthesis of benzyl chloromethylpyridylcarboxylate

Typically the hydroxyl group can be replaced by chlorine atom with SOCl<sub>2</sub><sup>[1]</sup>, but it usually takes 12 h to finish the reaction. There is another reagent Bu<sub>3</sub>P which can convert the hydroxy to chlorine in 15min at RT<sup>[8]</sup>.

In conclusion, the synthon was synthesized from the commercial 2,5-pyridinedicarboxylic acid which was treated with thionyl chloride and subsequent benzyl alcohol and then selective reduction afterwards chloration (Scheme 4.1). What should be mentioned is that the esterification and reduction require benzyl alcohol as solvent in case that transesterification occurs. This synthetic route was established after painstaking attempts (Compound **18b-20b**, in experimental part).

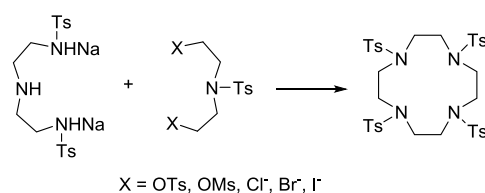


Scheme 4.1

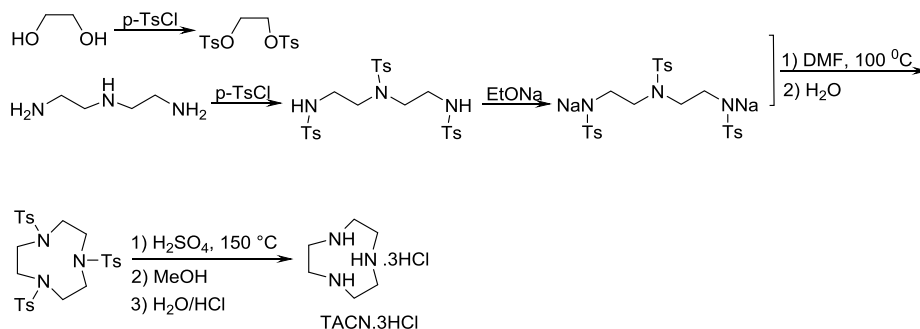
#### 4.2.3 Synthesis of the macrocycle TACN

The first common method to synthesize the macrocycles (i.e. (1,4,7,10-tetraazacyclododecan) was reported in 1954 by Stetter and ROOS<sup>[9]</sup>. They used bisulfonamide sodium salts and terminal dihalides to make cyclization, but the solution had to be highly dilute to avoid intermolecular reactions and normally three nitrogen atoms were protected with tosyl groups (Scheme 4.2). In spite of it, generally the cyclization reaction was performed in low yield. For example, a preparation of tritosylate of TACN was reported in 1972<sup>[10]</sup> its yield was about 57%. Afterwards J. E. Richman and T. J. Atkins<sup>[11]</sup> found the condensation of bisulfonamide sodium salts and sulfonate esters in a dipolar aprotic solvent could also give the corresponding products at the advantage of obviating the high dilution requirement and making the large-scale preparation practical. In our group F. TOUTI modified the preparation protocol so that TACN hydrochloride can be synthesized in 200 g scale.

In this thesis the product TACN hydrochloride was made following Faycal's protocol (Compound **5**, in experimental part). In detail the glycol and diethylenetriamine were protected with tosyl group, followed by cyclization in DMF and subsequent deprotection with concentrated sulfuric acid. Its hydrochloride was formed with concentrated hydrochloric acid in water (Scheme 4.3).



Scheme 4.2



Scheme 4.3

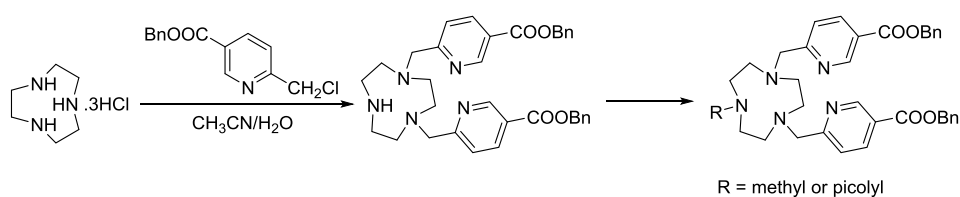
#### 4.2.4 Synthesis of the target ligands by alkylation of amines

*N,N,N*-functionalized TACN generally referred to the compounds that contains different moieties at three nitrogen atoms and that type of compounds as the ligands of some transition metals have been applied at the forefront of developments in several areas such as mimicing redox metalloenzymes (hemocyanin, galactose oxidase, tyrosinase)<sup>[12]</sup>, catalyzing oxidative organic transformations<sup>[13]</sup>, or effectively cleaving RNA or DNA<sup>[14-15]</sup>. However their preparation in good yield and excellent purity is always a challenge. Herein I will present my way to obtain this kind of ligands.

##### 4.2.4.1 Synthesis of the target ligands bearing benzyl ester groups and their deprotection

**The first strategy** to obtain the target ligands is to introduce the third arm after dialkylation of TACN (Scheme 4.4).

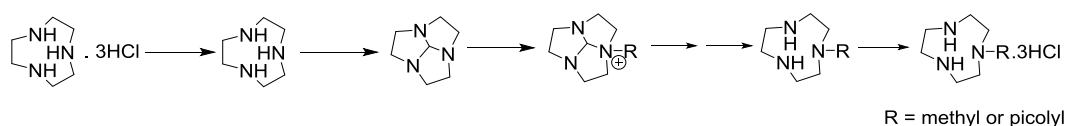
Dialkylation of TACN proceeded by TACN hydrochloride and the alkylating agent in the mixture of acetonitrile and water, and on the same condition picolyl group was introduced with picolyl hydrochloride (Compound **14b**, **13a** and **13b**). This kind of reactions should be set up with the right or less than required equivalents of alkylating agent, otherwise, they produced quaternary amines which brought some difficulty in purification. What is more, I could not harvest the target product in good yield because of the concomitant monoalkylated and trialkylated products which caused a waste of TACN at the same time.



Scheme 4.4

On this occasion, **the second strategy** was proposed on the concept of atom economy that the special group as the third arm which is crucial for the spin state of its corresponding complex was introduced firstly (Scheme 4.5).

As far as synthesis of the *N*-functionalized TACN is concerned, a clean route was developed by Weisman and his co-workers. They made this type of compounds through the reaction of orthoamide 1,4,7-triazacyclo[5.2.1.0<sup>4,10</sup>]-decane with the appropriate alkyl halide and the hydrolysis of the obtained quaternary amine<sup>[16-18]</sup>.



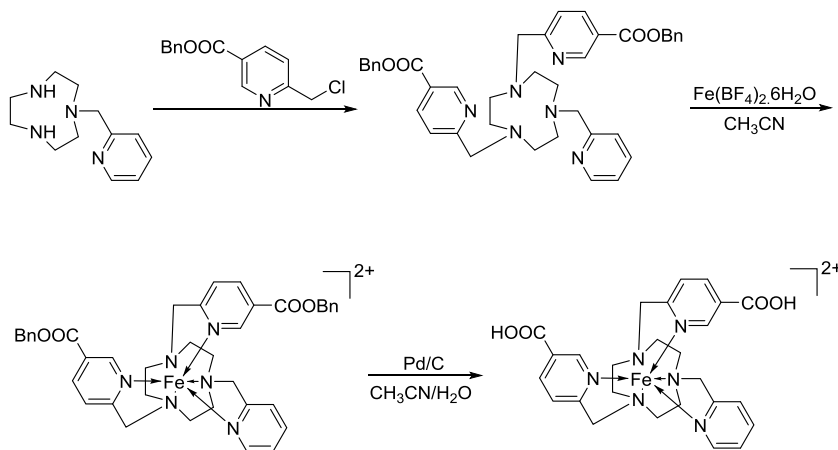
Scheme 4.5

Normally most of literatures reported all kinds of monoalkylated TACN were prepared and directly used for their next steps and the next product was purified easily<sup>[19-20]</sup>. In my case, purification of complexes is limited by the potential oxidation and the good solubility of water. Thus the task of purification has to be completed before complexation. As long as monoalkylated TACN was absolutely pure, it is possible that I could get the target compound of the following step in good yield and excellent purity.

TACN hydrochloride was neutralized with sodium hydroxide in the mixture of water and toluene with the equipment of Dean-Stark due to its good solubility in water. Then the TACN reacted with *N,N*-dimethyl formamide dimethyl acetal to give its orthoamide<sup>[21-22]</sup>, which was used for preparation of required quaternary amines. Subsequently hydrolysis and removal of formyl group led to *N*-monoalkylated TACN, which was transformed into its hydrochloride salt in a suitable alcohol (Compound **11a** and **11c**, in experimental part). This method benefits excellent purity, easy handling and avoiding their oxidation.

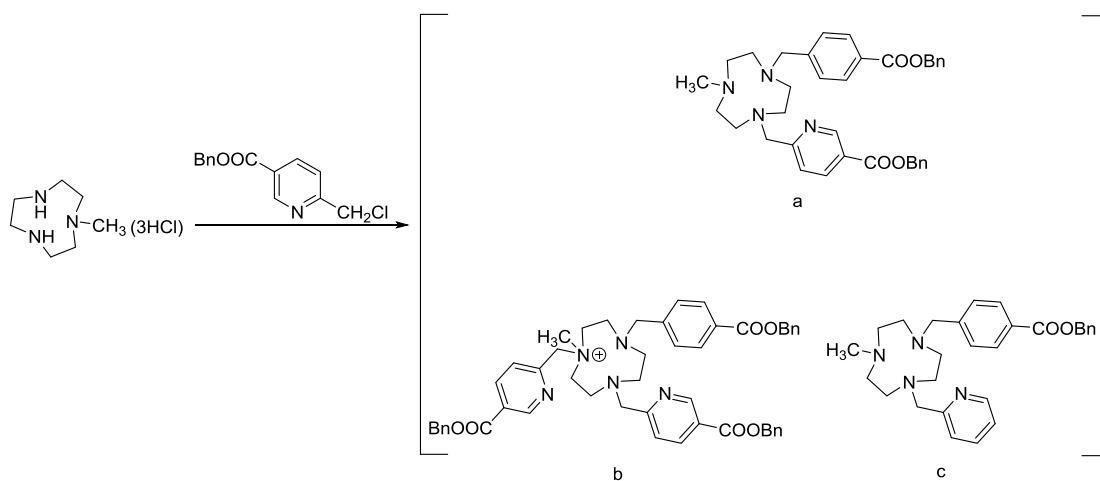
The picolinate could be successfully introduced to *N*-picolyl TACN, and the synthesis of its complex was carried out in acetonitrile then the catalyzed hydrogenolysis

proceeded in a mixture of acetonitrile and water (Compound **16a** and **16c**) (Scheme 4.6).



Scheme 4.6

while it was not a good way to *N*-methyl TACN. Because no matter the reaction was carried out in homogenous solution or heterogenous mixture (Table 4.4), it always produced the target compound as well as quaternary amine which resulted from introduction of three picolinate groups, and when NaH was used as the base, the decarboxylated product was produced. (Scheme 4.7).



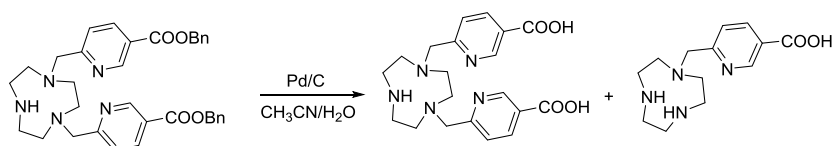
Scheme 4.7

Table 4.4 The conditions to introduce picolinate to monomethylated TACN

reactant	condition	products
----------	-----------	----------

<i>N</i> -methyl TACN.3HCl	K <sub>2</sub> CO <sub>3</sub> , CH <sub>3</sub> CN/H <sub>2</sub> O, 50 °C	a, b
<i>N</i> -methyl TACN	K <sub>2</sub> CO <sub>3</sub> , CH <sub>3</sub> CN, 50 °C	a, b
<i>N</i> -methyl TACN	DIPEA, CH <sub>3</sub> CN, 50 °C	a, b
<i>N</i> -methyl TACN	NaH, THF, 50 °C	a, c
<i>N</i> -methyl TACN	NaH, THF/DMF, RT	a, c

Seeing from the table, we deduced that decarboxylated product was caused by relatively strong base and the quaternary amine was produced maybe because of lack of steric hindrance from methyl group. In that case, the bulky group was supposed to work to avoid the difficulty in separating those polyamines. Considering the activity of alkylating agent reacting with monosubstituted TACN and its size that can prevent producing the quaternary amine, benzyl group should be a good candidate to meet these requirements. However it cannot be used because of benzyl ester whose deprotection may also remove it according to an indirect proof published in 2003<sup>[23]</sup>. If the hydrogenolysis of benzyl ester based on the ligand before its complexation, it should have been a good solution. However, the reality is not always in accord with the design. Hydrogenation of the ligand also cleaved the bond between nitrogen atom of TACN and picolyl group (Scheme 4.8), which could be monitored by LCMS. And the attempt to separate them by C<sub>18</sub> was proved impossible because of their similar properties.



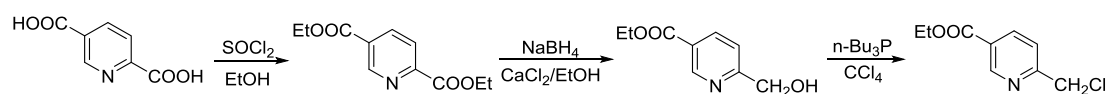
Scheme 4.8

#### 4.2.4.2 Synthesis of the target ligands bearing ethyl ester groups and their deprotection

In view of that, I attempted to switch the protecting group with ethyl ester which is

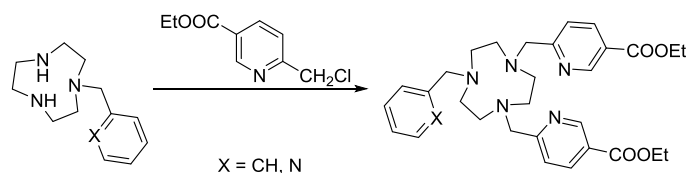
supposed to be hydrolyzed easily then benzyl group can also become an option to replace methyl group.

The synthon ethyl chloromethylpyridylcarboxylate was synthesized more easily than that of benzyl ester. It was also cooked from the commercial 2,5-pyridinedicarboxylic acid which was treated with thionyl chloride and selective reduction afterwards chlorination (Compound **18a-20a**, in experimental part) (Scheme 4.9).



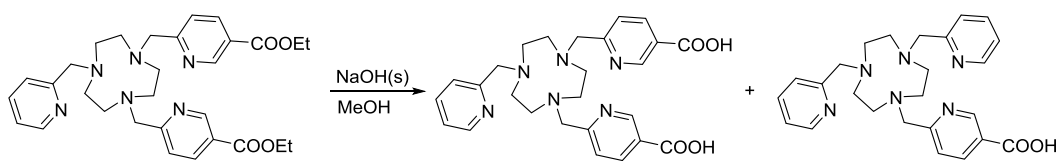
Scheme 4.9

The monobenzylated TACN was synthesized in the same way with *N*-picolyl or *N*-methyl TACN. Then its hydrochloride was removed before integration with picolinate (Compound **11b** and **12a-b**, in experimental part) (Scheme 4.10).



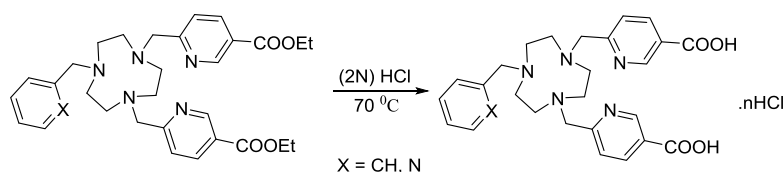
Scheme 4.10

Hydrolysis of ethyl ester normally can be achieved under a basic or acidic condition. Herein decarboxylation accompanied the process of the basic hydrolysis neither at 70 °C nor at room temperature, which was monitored by LCMS (Scheme 4.11). What is more, the information from LCMS showed signals of the decarboxylated and target compounds not only during the reaction process but also purification by C<sub>18</sub> cartridge, and the different ratios of signal intensities between them. It convinced us that it is not the ionization for MS which caused the appearance of fragments. Unfortunately those two products behaved in similar way so that the reverse chromatography could not completely separate them.



Scheme 4.11

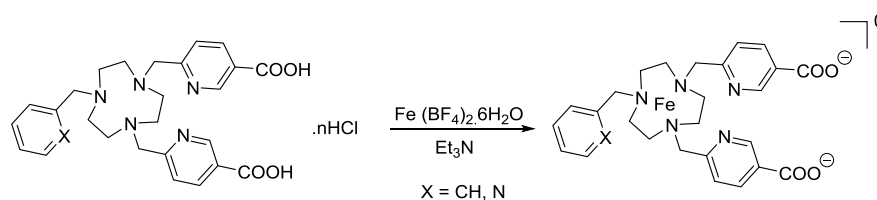
That naturally brought me to the other way to hydrolyze it. As we have known, the acidic catalyzed hydrolysis is reversible and the reaction speed is quite slow so that heating is necessary to accelerate it (Compound **15a-b**, in experimental part) (Scheme 4.12).



Scheme 4.12

#### 4.2.5 Synthesis of the target complexes

Synthesis of the low-spin complex was carried out in ethanol in the presence of triethylamine and the high-spin one was synthesized in the mixture of methanol (used for dissolution) and acetonitrile (for coordination). All the solvents should be degassed and all the operations should be carried out under argon (Compound **16c-d**, in experimental part).



Scheme 4.13

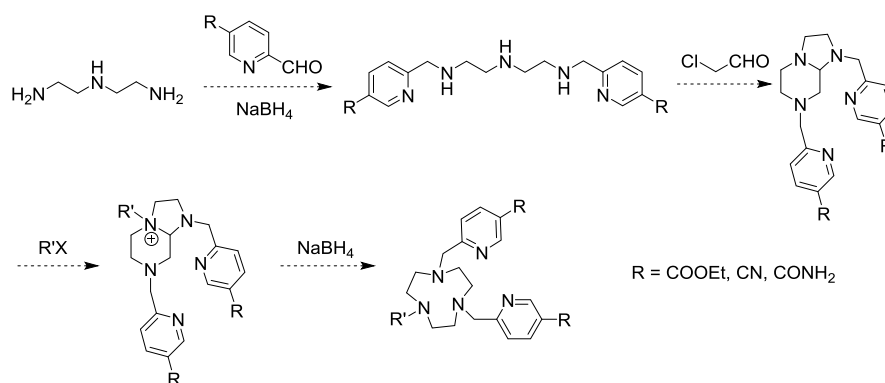
The red powder was obtained as the low-spin complex and it was crystallized in acetonitrile with 5% water, and the light yellow powder was prepared as the high-spin one, but unfortunately the crystals with good enough quality could not be

obtained so that there was no its X-Ray Diffraction for characterization. Only a little needle crystals for MRI session, relaxation time and magnetic moment measurements.

#### **4.2.6 Synthesis of the ligands by reductive amination**

Even though this method works well, inevitable absolutely anhydrous operations are not so welcome because of hydroscopic quaternary amine when the picolyl or benzyl group was introduced to TACN and it took much even more time depending on activity of alkylating agent. For example, it took seven days at RT when picolyl chloride reacted with orthamide of TACN.

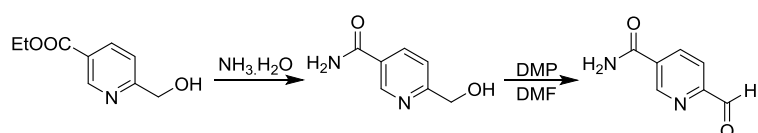
Thus another attempt to make big quantities of the ligands was also done. This strategy was proposed according to Denat's work<sup>[24]</sup>. As the patent said, the usual synthesis previously mentioned has some disadvantages. For example, cyclization takes long reaction time, the use of tosyl groups does not conform to the atom economy rule and its elimination requires hard conditions. What is the worse is the overall yield of less than 12%. This patent presented an efficient and versatile preparation method for N- and/or C- functionalized TACN derivatives by the intermediate product imadazo[1, 2-a]pyrazin4-ium salts. In our case, the picolinaldehyde was used. The two amino groups of diethylenetriamine have prior reactive activity with aldehydes to give their corresponding reductive aminated compounds in the presence of a reductant. This product reacted with chloroacetaldehyde to give the tertiary amine which was subsequently transformed to quaternary amine on the special nitrogen atom with certain halogenated agent. Afterwards it was reduced to macrocyclic product as a TACN derivative. Given that a reductant has to be used twice, the ester should be avoided or the soft reductant should be chosen in case of esters (Scheme 4.14).



Scheme 4.14

#### 4.2.6.1 Synthesis of the synthon 2-formylpyridine-5-yl-amide

In view of that I tried to make the synthon picolinaldehyde bearing amide group from ethyl 2-hydroxymethylenepyridyl carboxylate which was transformed into amide and subsequently was oxidized with DMP to the aldehyde. However, once the ester was transformed to amide, the solubility changed a lot. Its poor solubility in dichloromethane and chloroform really limited its oxidation which therefore could be carried out only in DMF (Compound **34**, in experimental part) (Scheme 4.15).



Scheme 4.15

In fact at the beginning a lot of activated manganese dioxide was used on several conditions for oxidation but did not give good yields, and DMP gave only 60% yield after silica gel chromatography (Table 4.5) which could not be managed easily, nor performed in a big scale due to its still poor solubility in ethyl acetate, dichloromethane and chloroform.

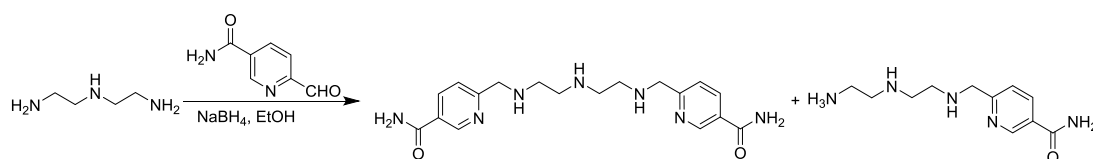
Table 4.5 The conditions for synthesis of 2-formylpyridine-5-yl-amide

Oxidant	Quantity (eq.)	Condition	Yield (%)
MnO <sub>2</sub>	10	DMF, RT, 24h	10

MnO <sub>2</sub>	10	DMF/CHCl <sub>3</sub> , RT, 24h	10
MnO <sub>2</sub>	10	CHCl <sub>3</sub> , 60 °C, 24h	10
MnO <sub>2</sub>	20	DMF, RT, 24h	20
DMP	1.5	DMF, RT, 24h	60

#### 4.2.6.2 Synthesis of the ligands bearing amide groups

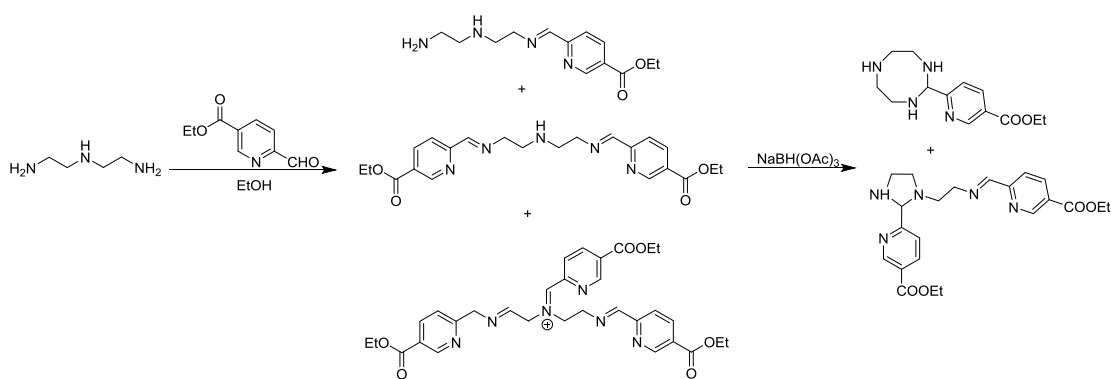
Its reductive amination with diethylenetriamine gave the compound which was produced by reacting with one equivalent of diethylenetriamine besides of the target product (Scheme 4.16). Those two compounds are more soluble in water than in organic solvents so that they could not be extracted. In that case, another problem about separation was raised because the aqueous solution also contained other sodium salts. Thus maybe the strategy that an ester group is used instead of the amide can avert this tough work.



Scheme 4.16

#### 4.2.6.3 Synthesis of the ligands bearing ethyl ester groups

However even though esters have better solubility in organic solvents than amides, and the weak reductant (sodium triacetoxyborohydrid) was used to prevent the reduction of ester group, the products were still a mixture caused not only by reactions of triamine with different equivalents of aldehyde but also by another reason that after reduction the intramolecular interaction between one nitrogen atom and the C=N double bond made a cycle in the molecule (Scheme 4.17).

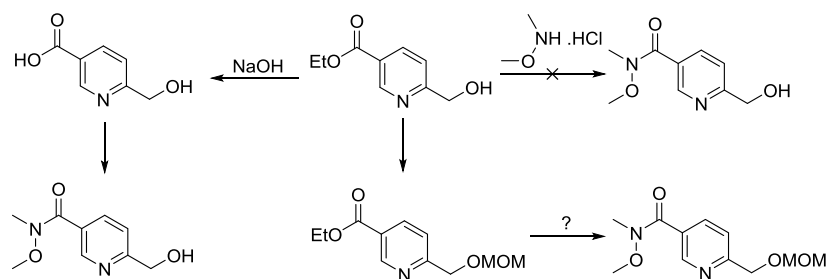


Scheme 4.17

#### 4.2.7 Synthesis of the ligands bearing weinreb amide groups

Weinreb amides normally are inert to the reductants and maybe they are more soluble in organic solvent than the amides because of its methyl and methoxyl groups on the nitrogen atom. Moreover, the weinreb amide is easy to form the corresponding carboxylic acid by the treatment of *t*BuOK in the mixture of diethyl ether and water<sup>[25-26]</sup>. In view of that, the weinreb amide is also an option to protect carboxyl group of the pyridine.

Normally the synthesis of weinreb amides is not difficult according to the literature<sup>[27-28]</sup>. However, as far as the 2-hydroxymethyl-pyridyl-5-carboxylic acid is concerned, it is not available and I had to prepare it by hydrolysis of the ethyl ester. As a result, the carboxylic acid was mixed with sodium hydroxide after evaporation of water, which was directly used for condensation with *N*-methoxymethylamine hydrochloride in the presence of EDC and HOBT (Compound **38**, in experimental part). While the direct treatment of ethyl ester with *N*-methoxymethylamine hydrochloride could not give the target compound. Another way is that the hydroxy was protected before hydrolysis of the ester (Scheme 4.18). In that case the condition should be very special in order to keep the protecting group, which is under trying.



Scheme 4.18

## 4.3 Results and discussion

The ligands obtained through the acidic hydrolysis of ethyl ester were used for complexation. Then the complexes were applied for the measurements for characterization of magnetism and cytotoxicity, and their electrochemistry, even attempts for detection of pKa values.

### 4.3.1 Magnetic moment measurements

Evans' method was used for measurement of magnetic moments in solution and the experiments were generally carried out in mixture of 90 % H<sub>2</sub>O and 10 % D<sub>2</sub>O (treated as solvent) containing of 2 % *t*BuOH. Herein the total volume can be calculated directly by addition of two, where the difference between the real and the calculated was neglected, as well as that between density of solution and pure solvent. Bruker 300 MHz instrument and coaxial NMR tubes which consist of inner and outer tube were used. The signals of *t*BuOH from two tubes give different chemical shifts due to the presence of a complex only in one tube (The concentration typically is 5 mM).

The following equation is used by the Evans' method to determine the number of unpaired electrons of a given paramagnetic compound by first calculating the magnetic moment  $\mu_{eff}$  and then applying it to the spin-only formula. This formula is only valid for transition elements of the first row with low *Z* (spin-orbit coupling

negligible) and for the  $^1A_1$  ground state. This is the case for the low-spin and high-spin iron(II) compounds studied herein.

$$2.828 \sqrt{\frac{T \times \delta_0}{\nu_0 \times S_f \times C}} = \mu_{eff} = 2\sqrt{S(S+1)}$$

Where  $T$  is the temperature (K),  $S_f$  is the symmetry factor of the coil ( $4\pi/3$  for a cylindrical sample in a superconducting magnet with sample axis parallel to the magnetic field),  $C$  is the molar concentration ( $\text{mol}\cdot\text{cm}^{-3}$ ),  $\nu_0$  is the  $^1\text{H}$  NMR spectrometer frequency and  $\delta_0$  is the frequency shift (Hz) compared to the reference. No diamagnetic correction was introduced into the calculations for paramagnetic compounds. However, they can be evaluated either 1) by using this same procedure to also determine the diamagnetic contribution for the corresponding diamagnetic complex with a different metal ion. or 2) by use of Pascal's constants.

So I used crystals of low-spin or high-spin complex to prepare this kind of solutions previously mentioned, then measured the  $^1\text{H}$  NMR signal of *t*BuOH.

The frequency shift of *t*BuOH respectively in the presence of the low-spin complex or high-spin complex is as following:

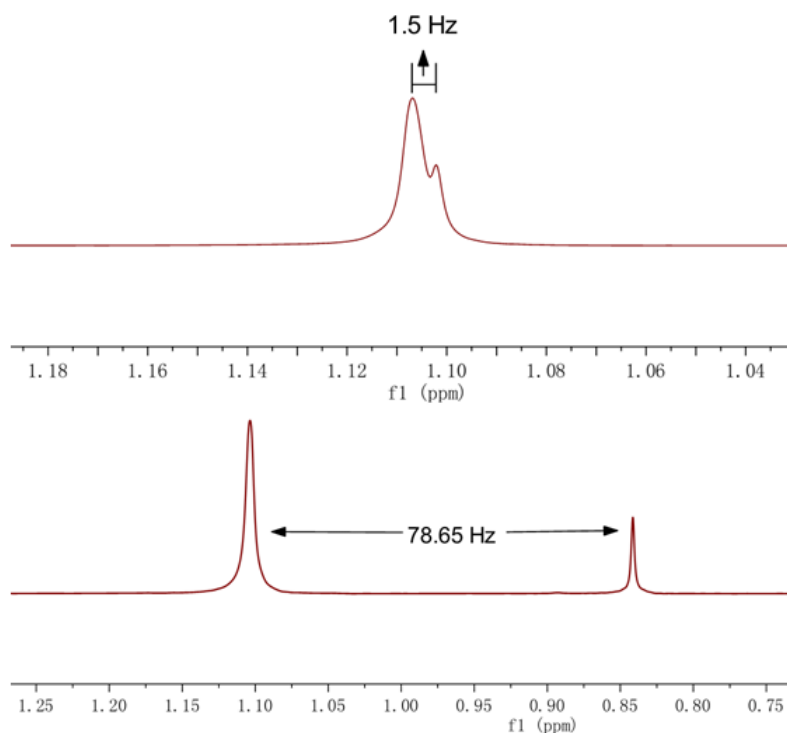


Fig. 4.5 Chemical shifts of the signals from *t*BuOH caused by low-spin and high-spin complexes. Seen from the spectra, the low-spin complex could not affect the signal of *t*BuOH very much, conversely the high-spin complex made it shift much. In addition, after preparation of high-spin complex in acetonitrile, acetonitrile molecule was supposed to coordinate to iron(II) so that it should be low-spin. Once it was dissolved in water, the acetonitrile molecule should be replaced by water molecule very quickly to make the complex high-spin. This statement was proved by measurements with respect to time. The data from the table showed us that the frequency shift of *t*BuOH under the effect of high-spin complex did not change, which demonstrated quite fast exchange between acetonitrile and water molecule. The magnetic moment was calculated according to the formula (Table 4.6) (Experimental parameters:  $T = 298$  K;  $g_0 = 300$  MHz).

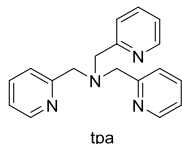
Table 4.6 The magnetic moments of two complexes.

compound	LS	HS		
Concentration (mM)	5.0	5.0		
Time (h)	0	0	0.5	336
Frequency shift (Hz)	1.5	78.65	77.78	77.76
Magnetic moment (BM)	0.76	5.38	5.35	5.35

The values can be compared with those published in the literature<sup>[29]</sup> which described that three Fe<sup>2+</sup>-complexes could show different spin states in acetonitrile and acetone (Table 4.7). Because the acetonitrile molecule could not replace the two coordinated chloride ions so that the complex **3** in acetonitrile still show its high-spin state, while acetone molecule could replace the two coordinated acetonitrile molecules so that complex **1** and **2** showed their high-spin states in acetone. And the magnetic moment values of high-spin complexes belong to the range of 5.0-6.0 BM, on the contrary, those of low-spin ones lie in the range of 0-1.0 BM. Thus herein the magnetic moment values are in the normal range.

Table 4.7 The magnetic moment values published in the literature.

Compound	1	2	3	1	2	3
solvent	CH <sub>3</sub> CN			CH <sub>3</sub> COCH <sub>3</sub>		
$\mu_{\text{eff}}$ (BM)	0.74	0.834	5.29	5.07	5.33	5.46



Complex 1: Fe(tpa)(CH<sub>3</sub>CN)<sub>2</sub>(ClO<sub>4</sub>)<sub>2</sub>  
 2: Fe(tpa)(CH<sub>3</sub>CN)<sub>2</sub>(CF<sub>3</sub>SO<sub>3</sub>)<sub>2</sub>  
 3: Fe(tpa)(Cl)<sub>2</sub>

### 4.3.2 Relaxivity measurements

Relaxivity is the natural property of the complexes that can stand for their potential to be MRI CAs and probes. It can be measured by NMR instrument or in MRI session. Herein the crystals of two complexes were used for their relaxivity measurements.

#### 4.3.2.1 Relaxation time measured by Bruker NMR instrument

The relaxation time of water protons was measured by Bruker NMR instrument in the magnetic field 300MHz. And that of the high-spin complex with respect to time was also measured, which showed the fast exchange between acetonitrile and water molecule (Table 4.8).

Table 4.8  $T_1$  measured by NMR instrument

Compound	LS	HS			
Concentration (mM)	4.0	4.0			
Time (min)	0	0	30	60	90
$T_1$ (s)	2.168	0.55	0.50	0.49	0.48

As we have known, even though at lower magnetic field strength (e.g., 1.5 T) the electronic correlation relaxation time  $T_{1e}$  of iron(II) center is not in favor of lowering  $T_1$  of the surrounding water proton, at higher field strength,  $T_{1e}$  for iron(II) decreases with the square of the field<sup>[30-31]</sup> so that exchange rate between the bulk water and coordinated water molecules becomes a key relevant parameter which is high to  $10^{-10}$ - $10^{-7}$  s in the same range of lanthanide ions<sup>[32]</sup>. Consequently ferrous ion can still

decrease  $T_1$  and it is reasonable that it does not work so well as gadolinium ion. Generally the tests conducted in the NMR spectrometer (at 4 mM, 500MHz), the  $T_1$  of surrounding water protons in the presence of high-spin complex is about 3.5 s and that of low-spin one is about 0.35 s<sup>[33]</sup>.

The herein relaxation times obtained stand in the range of normal values which are satisfactory. It is a great success that they can show the big difference of relaxation time between high-spin and low-spin complexes. Their more reasonable and comparable relaxivities will be shown subsequently.

#### 4.3.2.2 Relaxation time measured in MRI

Both  $T_1$  and  $T_2$  were measured *in vitro* at four concentrations by using  $[\text{Gd}(\text{DOTA})]^{-1}$  (Dotarem) and Fe(TPTACN) as references and water in the absence of any complex for the negative control.  $T_1$  values obtained in two different ways ( $T_1$  FISP and  $T_1$  RARE) do not make much differences (Fig. 4.6 and Fig. 4.7). FISP is the abbreviation of the fast imaging with steady-state precession and the RARE means Rapid Acquisition Relaxation Enhancement. It is obvious that the relaxation time is related to the concentration. Typically according to the formula (1) and (3) presented in chapter 2, the relationship between the reciprocal of relaxation time and concentration is linear and the slope should be the relaxivity of the complex.

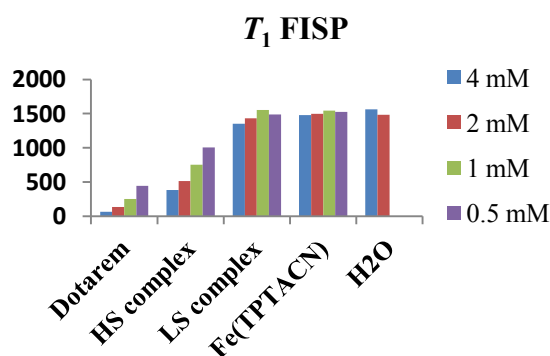


Fig. 4.6

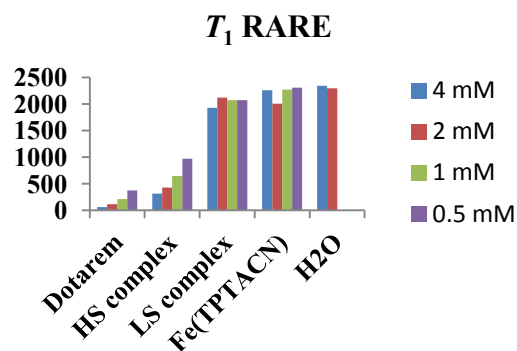


Fig. 4.7

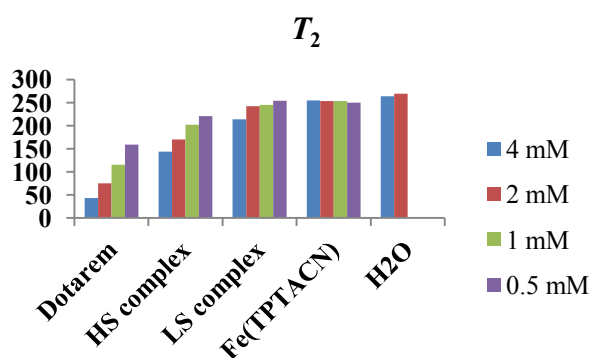


Fig. 4.8

Thus the relaxivity of high-spin and low-spin complexes were calculated by the fitted straight line according to the Fig. 4.6 and Fig 4.8 ( $T_1$  FISP and  $T_2$ ), then compared them with Fe(TPTACN).

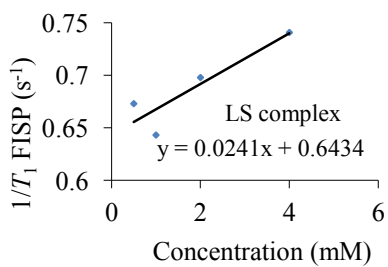


Fig. 4.9

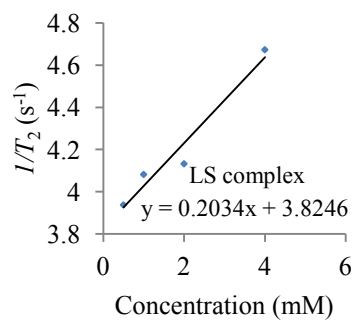


Fig. 4.10

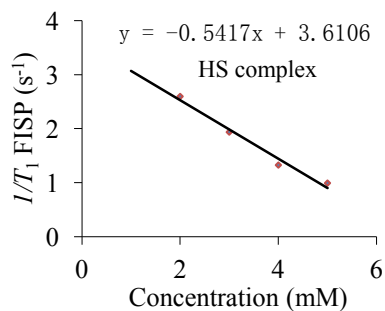


Fig. 4.11

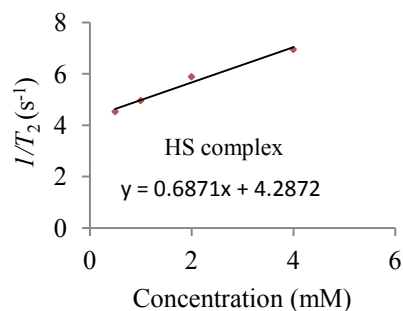


Fig. 4.12

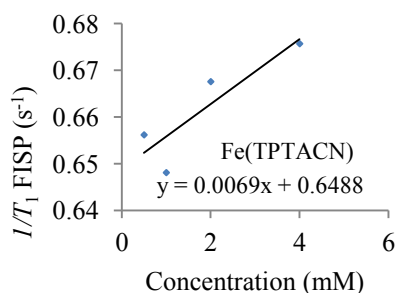


Fig. 4.13

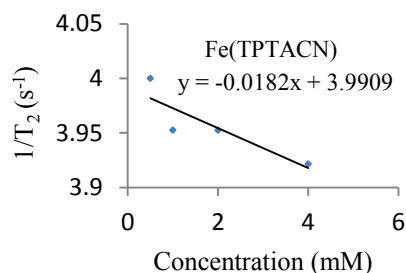


Fig. 4.14

Based on the figures from Fig. 4.9 to Fig. 4.14, the relaxivities of both low-spin and high-spin complexes in PBS are concluded in Fig. 4.15. compared to Fe(TPTACN). The longitudinal and transverse relaxivities of low-spin complex respectively are 0.02 and  $0.2 \text{ mM}^{-1}\text{s}^{-1}$ , which are similar with those of low-spin complex Fe(TPTACN) ( $0.007, 0.02 \text{ mM}^{-1}\text{s}^{-1}$ ), and those of high-spin complex are  $0.54, 0.69 \text{ mM}^{-1}\text{s}^{-1}$ . What is exciting, the longitudinal relaxivity  $r_1$  which are bigger than that of low-spin complex by 27 times.

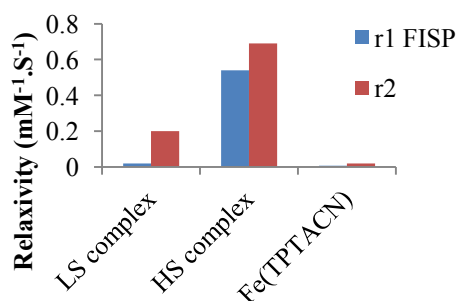


Fig. 4.15

In addition, compared to the electroneutral complex bearing two tetrazole moieties

prepared by F. Touti in 2011 (the longitudinal relaxivity is about  $0.57 \text{ mM}^{-1} \text{ s}^{-1}$  at  $7 \text{ T}^{[34]}$ ), it is obvious that the longitudinal relaxivity of the high-spin complex is totally in accord with its value.

#### 4.4 Cytotoxicity tests

MTS cell viability assay was conducted to test cytotoxicity. It is a colorimetric method for sensitive quantification of viable cells. MTS contains a tetrazolium moiety which can be reduced by NADPH or NADH generated by dehydrogenase enzymes in active cells to a colored formazan product (Scheme 4.18). The formazan which stands for cell viability can be quantified by the absorbance at 490-500 nm of the cell culture media because of its presence.

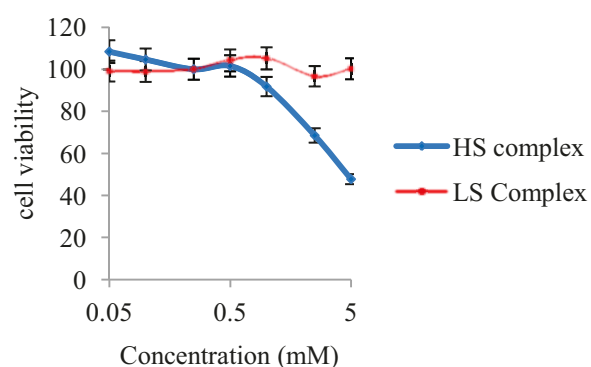
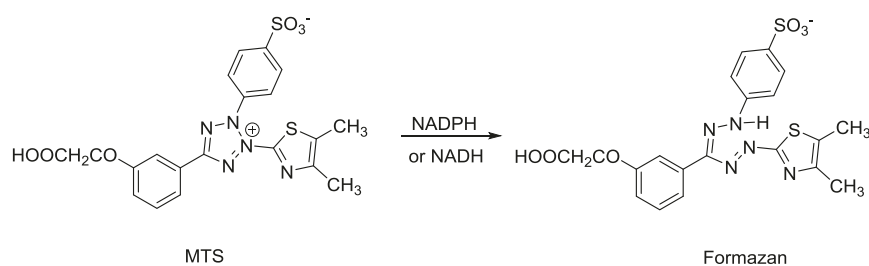


Fig. 4.16

Seen from the figure, the low-spin complex is not toxic because of its stability resulting from the relatively strong coordination effect provided by the hexadentate ligand. As far as the high-spin complex is concerned, it is hardly toxic at the concentration 1.0 mM (92% cells were alive) and the viability is about 50% at the

concentration 5.0 mM, which is very gratifying and encouraging because the electroneutral complex bearing two tetrazoles is very toxic (Almost all the cells died when the solution of the complex at concentration smaller than 0.5 mM, this unacceptable result is not published but known in the group.).

## 4.5 UV-vis spectrum analysis

UV-vis spectroscopy is very useful in chemistry for quantitative analysis of some transition metal ions or conjugated organic compounds in solution according to Beer-Lambert law and it is often used for quantitative characterization. In my thesis, I tried to measure pKa values of the complexes by observing the changes of their UV-vis absorbances.

### 4.5.1 UV-vis absorptions

Both crystals of two complexes were used for measurement of UV-vis spectra (Fig. 4.17).

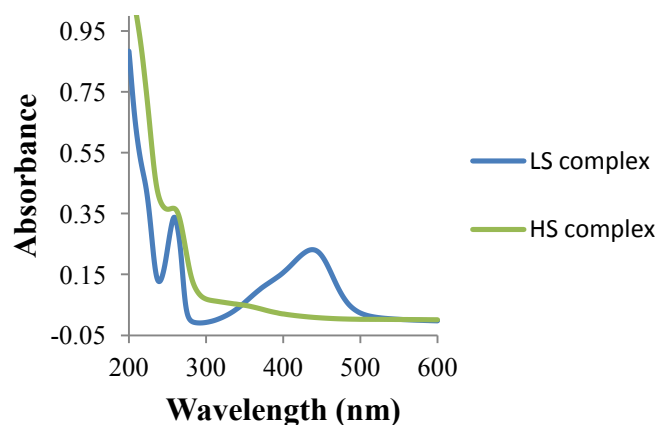


Fig. 4.17

According to the literature<sup>[35]</sup>, both LS and HS Fe(II) complexes show high energy transitions between 340 and 440 nm that are assigned as metal-to-ligand charge transfers (MLCT), and those of HS is much less strong than those of the LS complexes (i.e.  $\epsilon$  1650 vs 4700); energy feature below 300 nm in the absorption

spectra likely results from metal-independent  $\sigma\text{-}\sigma^*$  transitions within Pyridine.

In my case, seen from the UV spectrum of LS complex the strong absorptions are observed at 438 nm and at 259 nm, which are attributed to MLCT and metal-independent  $\sigma\text{-}\sigma^*$  transitions within picolinate; while in the HS spectrum,  $\sigma\text{-}\sigma^*$  transitions within picolinate is weak, at the same time the absorption hardly exists at 438 which can also be explained by the words "much less strong" given that the one of LS complex is neither so strong. Maybe it is attributed to the weak coordination effect of the HS complex. This is almost in accord with the literature and the results are relatively acceptable.

#### **4.5.2 UV-vis spectra for determination of pKa values**

Theoretically when the carboxyl groups in the periphery of the complexes are deprotonated or protonated, the charge transfer differs dramatically so that the absorption band shifts on the UV-vis spectra.

##### **4.5.2.1 UV-vis spectra of low-spin complexes at different pHs**

The experimental measurement of the UV-vis absorption spectra of the crystalline low-spin complex was performed in water at concentration of 0.02 mM varying the apparent pH from 6.71 to 12.93 for basic titration by 4 M NaOH (aq) and from 6.71 to 0 for acidic titration by 4 M HCl (aq). The spectra obtained were shown in Fig. 4.18 and Fig. 4.19

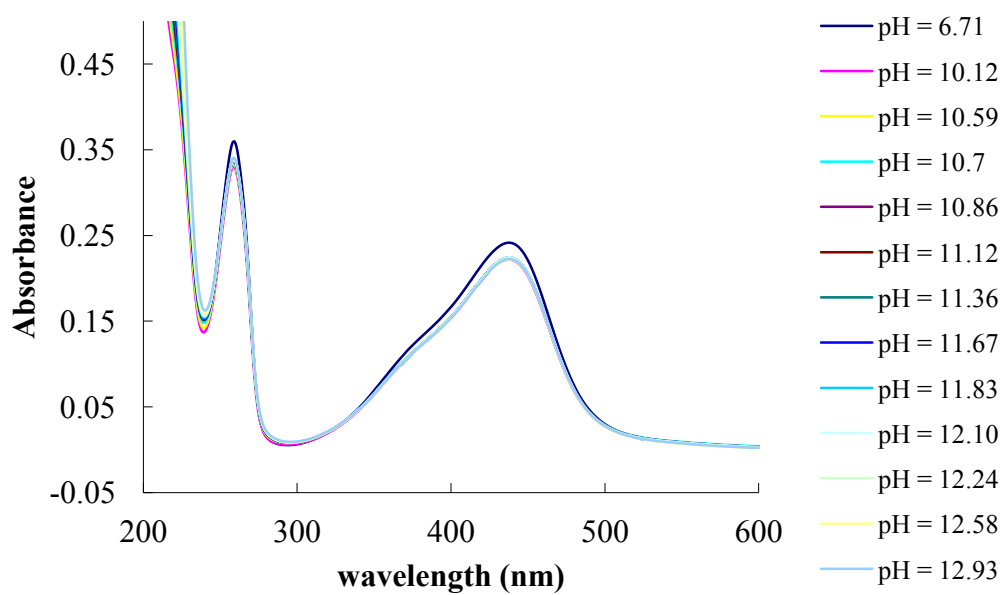


Fig. 4.18

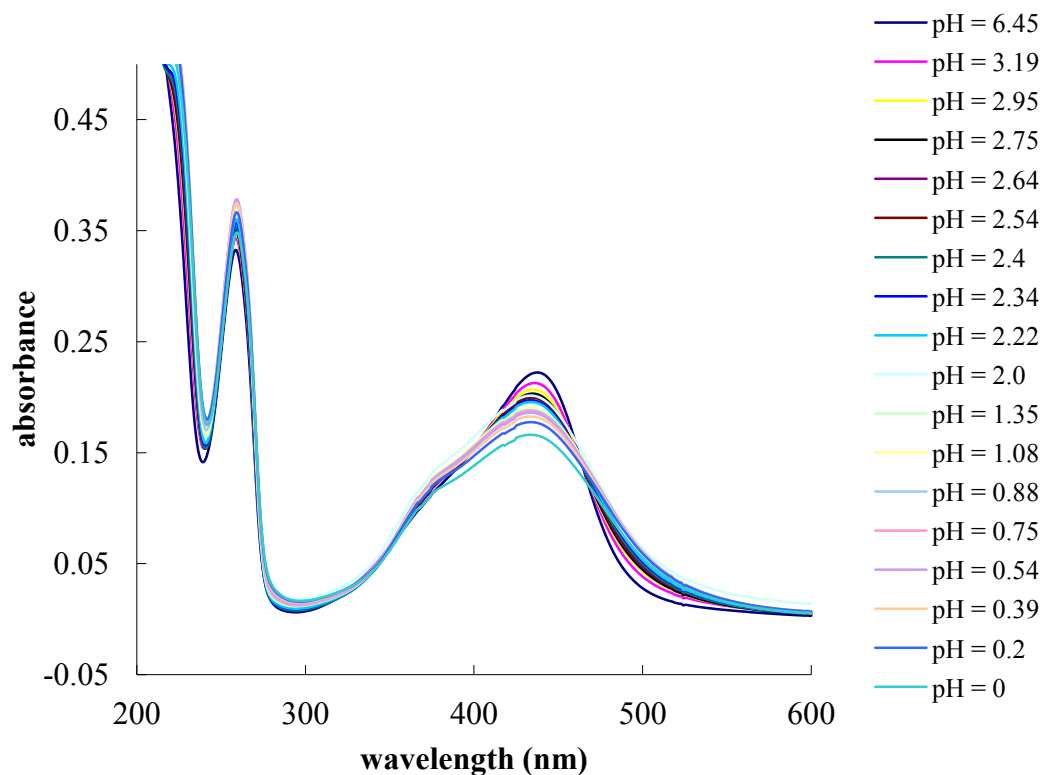


Fig. 4.19

The UV spectral development during basic titration does not show significant evolution when being brought from neutral pH to pH 13. This supports the notion that

the complex already exists as an electroneutral species at pH 7 and no further deprotonation can take place. The results also show that no degradation appears to take place during this process.

When being acidified, the low-spin complex is supposed to experience successive protonation of the carboxylates. But this has a limited and mute measurable influence on the MLCT band, as seen in Fig. 4.19. If only one protonation takes place in the pH interval explored, then isosbestic points can be expected.

Thus the UV-vis spectra of the low-spin complex at different pH values can be concluded and shown as following (Fig. 4.20):

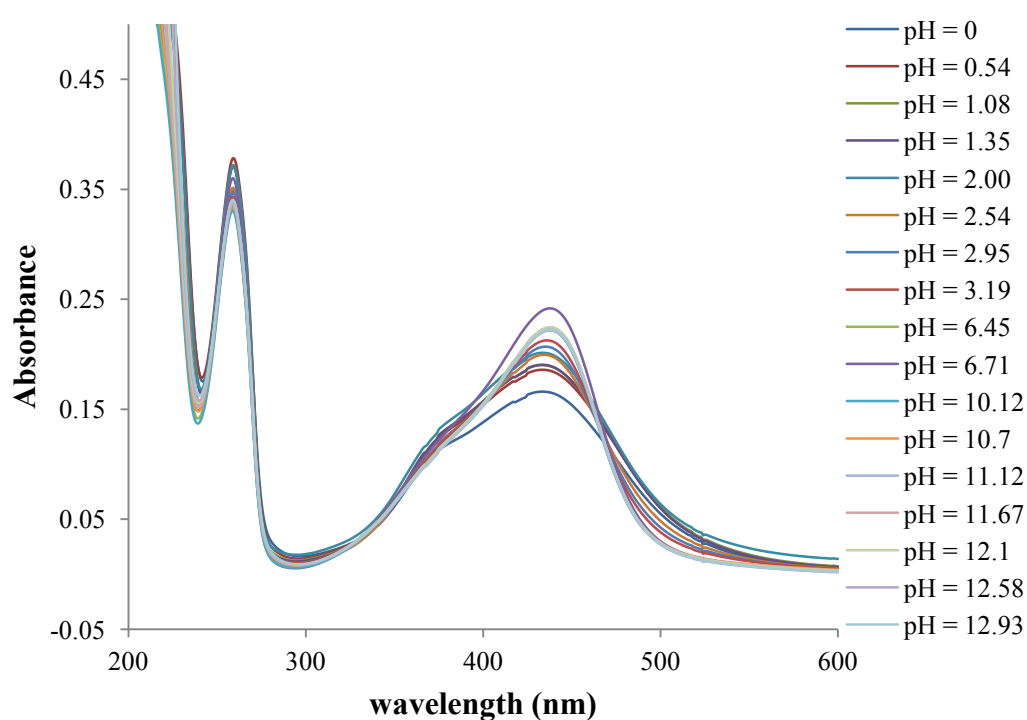


Fig. 4.20

#### 4.5.2.2 UV-vis spectra of high-spin complexes at different pHs

The experimental measurement of the UV-vis absorption spectra of the high-spin complex (powder) was performed in water at concentration of 0.02 mM varying the apparent pH from 5.92 to 13.15 for basic titration by 4 M NaOH (aq) and from 6.76 to 0. for acidic titration by 4 M HCl (aq). The spectra obtained were shown in Fig. 4.21 and Fig. 4.22.

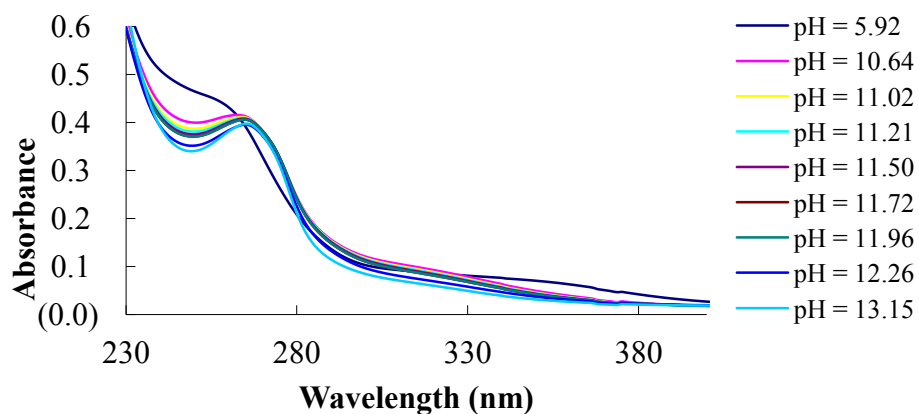


Fig. 4.21

When high-spin complex is brought to high pH with NaOH, a spectral change is observed that can be rationalized with the deprotonation of one inner sphere water molecule to yield the hydroxide complex.

Acidification of high-spin complex leads to a significant change of the UV spectrum, too. Here, the speciation analysis can be expected to be more complex: the two carboxylates can be successively protonated like the LS complex; but the sixth coordination site may experience either hydroxide protonation or even OH exchange with another sample component at lower pH such as chloride.

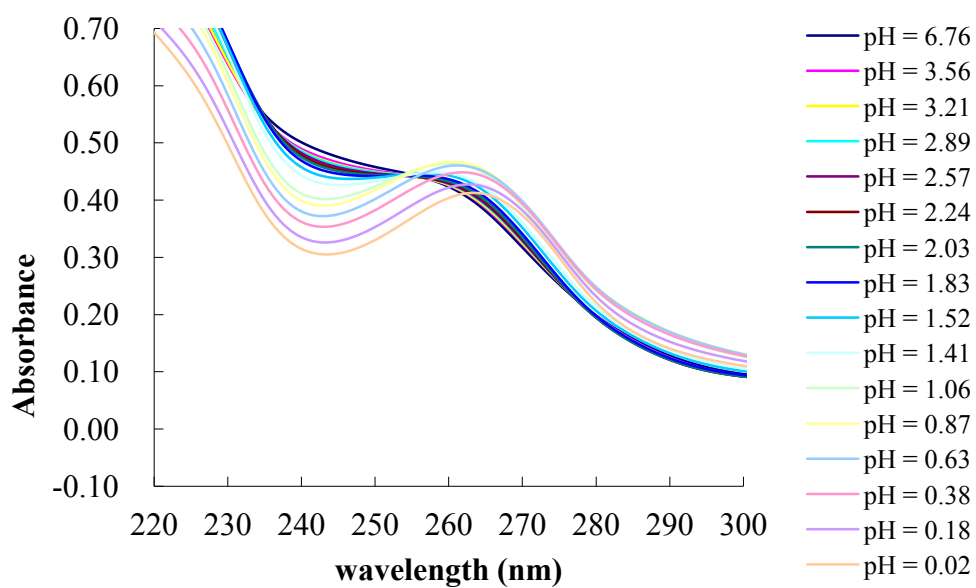


Fig. 4.22

Thus the UV-vis spectra of the high-spin complex at different pH values can be concluded and shown as following (Fig. 4.23):

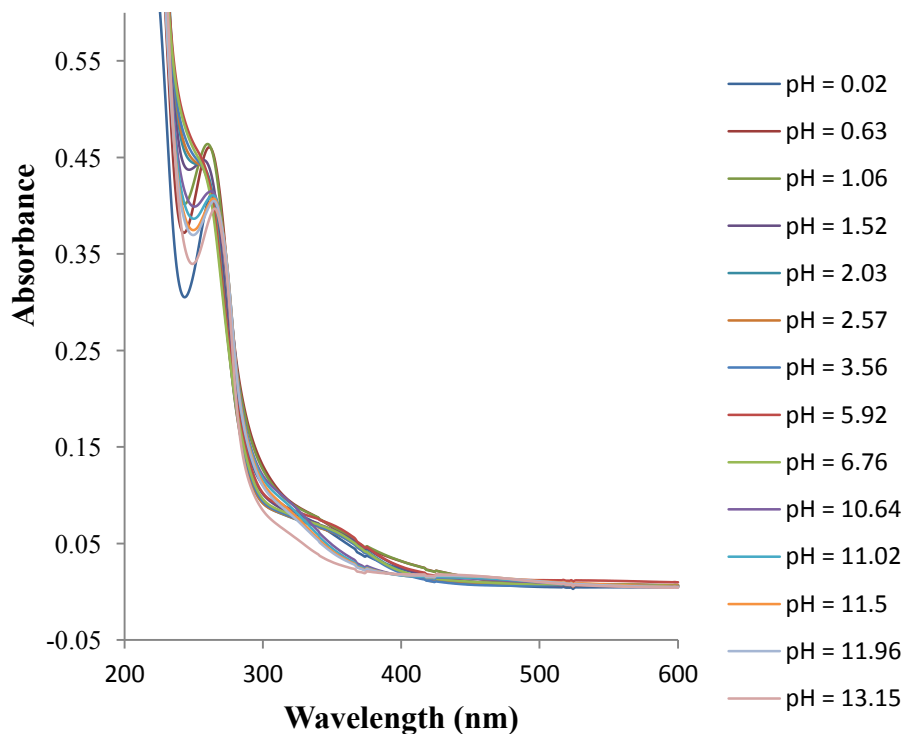


Fig. 4.23

In conclusion, seeing from the UV-visible spectra, I deduce that the pKa values of pyridylcarboxylic acid of the two complexes are quite low because of the coordination effect and coulombic attraction so that the two complexes are electroneutral at physiological pH. During basic titration, OH may coordinate to iron(II) of the HS complex causing its spectral change. When they are acidified, both of two complexes experience successive protonation, but it has a weak influence on the MLCT band as for the LS complex, while the significant change of the HS complex may be attributed to a relatively complex reason such as successive protonation of the carboxylates, protonation of hydroxide and exchange between OH and Cl.

#### **4.6 Cyclic voltammograms**

Cyclic voltammetry (CV) is well-known for its utility of studying the electrochemical properties of an analyte in solution. Cyclic voltammograms are plotted with current ( $i$ ) versus applied potential ( $E$ ) provides information about redox potentials of the analyte and its electrochemical reaction rates. And the ideal value of  $E_{pc}-E_{pa}$  is equal to  $56.5$  (mV) divided to the number of electrons during the process in a reversible CV. It is possible that the wave is irreversible because of a subsequent chemical process or a physical process like precipitation. At present CV has become an important technique to study a variety of redox processes and electron transfer kinetics, also determine the stability of reaction products.

In my case, cyclic voltammetry measurements of both complexes were carried out at the concentration of 1 mM in PBS and any support electrolyte was not added. The working electrode was glassy carbon (3mm) and the reference was saturated calomel electrode (SCE).

For low-spin complex the scan rate was 100 mV/s and the CV is irreversible (Fig. 4.24); and for high-spin complex the experiments were performed with a series of scan rates (from 25 mV to 20 V/s) and all of them provided irreversible waves (Fig.

4.25).

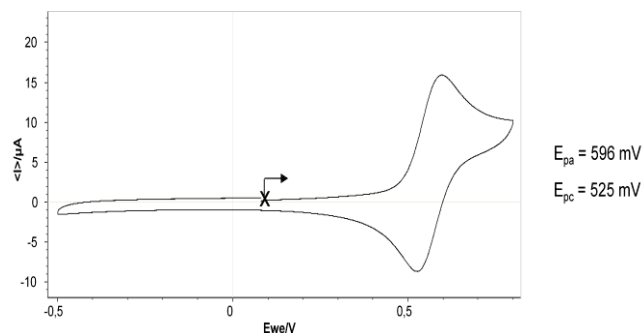


Fig. 4.24

According to the presentation above, 56 mV is the ideal value of difference between the oxidation potential and reduction one in a standard reversible CV. In an irreversible CV the value is bigger than 56 mV. In our case, an irreversible CV was observed due to the difference 71 mV. We can also see that the oxidation potential has more intensity of current than the latter. What makes us satisfied is that there is only one wave both in oxidation and reduction process.

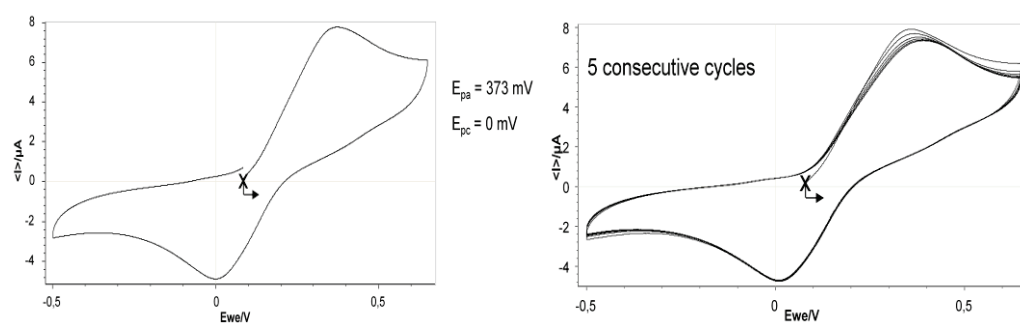


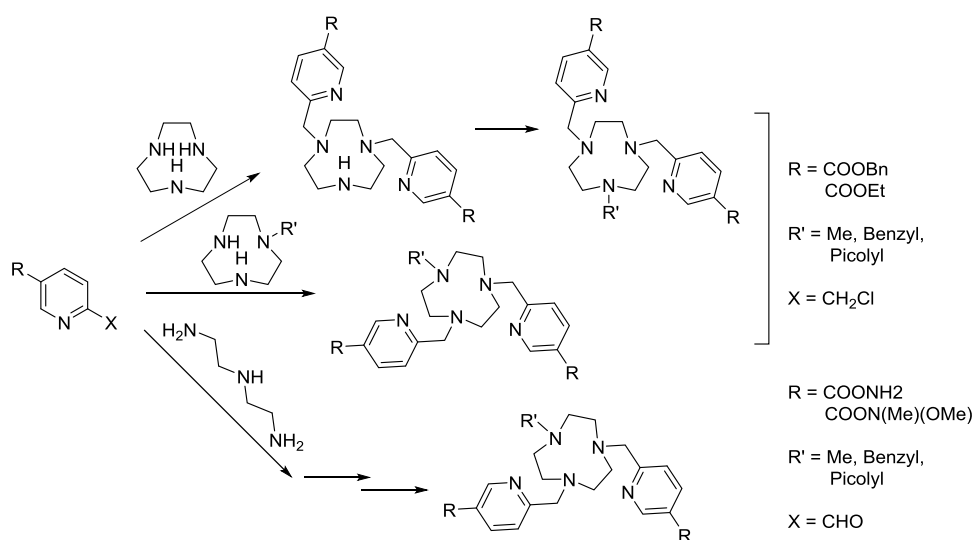
Fig 4.25

For the high-spin complex, it is also an irreversible CV no matter how many the scan rate is. The oxidation potentials are slightly increasing with the acceleration of scan rate, and it is obviously smaller than that of the low-spin one by 0.2 V. What is the important is the difference between the oxidation and reduction potential is so big, which implies that there exists some rearrangement of the oxidized Fe(III) complex to stabilize it so that its reduction to Fe(II) species more difficult.

## 4.7 Summary and perspective

In conclusion, four protecting groups (COOBn, COOEt, CONH<sub>2</sub>, CON(Me)(OMe)) for carboxyl and three ways (two alkylations and one reductive amination) for combination with TACN were tried (Scheme 4.19), then the ligands bearing the ethyl ester groups were successfully obtained which were subsequently hydrolyzed under acidic condition for complexation with iron (II) salt.

The obtained complexes were characterized by HRMS and the low-spin one has its <sup>1</sup>H NMR and X-Ray Diffraction. Both were used for measurement of their properties such as relaxivities, magnetic moment, UV-vis absorptions, pH titration, cytotoxicity, and cyclic voltammetry.



Scheme 4.19

The results of pH titration implied us that the complexes should be electroneutral at physiological pH. And their relaxivities and magnetic moments prove that the N6 type complexes bearing carboxyl groups are potential to be designed as MRI probes because the N5O1 type complexes are high-spin, and the probes are promising in application in biology field due to their low toxicity.

## 4.8 References

- [1] Nonat A., Gateau C., Fries P. H., Mazzanti M. Lanthanide Complexes of a Picolinate Ligand Derived from 1,4,7-Triazacyclononane with Potential Application in Magnetic Resonance Imaging and Time-resolved Luminescence Imaging. *Chem. Eur. J.* 2006, 12, 7133.
- [2] Roger M., Lima L. M. P., Frindel M., Platas-Iglesias C., Gestin J.-F., Delgado R., Patinec V., Tripier R. Monopicolinate-dipicolyl Derivative of Triazacyclononane for Stable Complexation of  $\text{Cu}^{2+}$  and  $^{64}\text{Cu}^{2+}$ . *Inorg. Chem.* 2013, 52, 5246.
- [3] Huang D., Wang W., Zhang X., Chen C., Chen F., Liu Q., Liao D., Li L., Sun L. Synthesis, Structural Characterizations and Magnetic Properties of a Series of Mono-, Di- and Polynuclear Manganese Pyridinecarboxylate Compounds. *Eur. J. Inorg. Chem.* 2004, 1454.
- [4] Kojima T., Hayashi K., Iizuka S., Tani F., Naruta Y., Kawano M., Ohashi Y., Hirai Y., Ohkubo K., Matsuda Y., Fukuzumi S. Synthesis and Characterization of Mononuclear Ruthenium(III) Pyridylamine Complexes and Mechanistic Insights into Their Catalytic Alkane Functionalization with *m*-Chloroperbenzoic Acid. *Chem. Eur. J.* 2007, 13, 8212.
- [5] Schiffner J. A., Wöste T. H., Oestreich M. Enantioselective Fujiwara–Moritani Indole and Pyrrole Annulations Catalyzed by Chiral Palladium(II)–NicOx Complexes. *Eur. J. Org. Chem.* 2010, 174.
- [6] Ayers T. A. New Methods for the Selective Reduction of Disubstituted Malonates to the Corresponding Hydroxy-ester Derivatives. *Tetrahedron Lett.* 1995, 40, 5467.
- [7] Brown H. C., Narasimhan S., Choi Y. M. Selective Reductions. 30. Effect of Cation and Solvent on the Reactivity of Saline Borohydrides for Reduction of Carboxylic Esters. Improved Procedures for the Conversion of Esters to Alcohols by Metal Borohydrides. *J. Org. Chem.* 1982, 47, 4702.
- [8] N’Goka V., Stenbøl T. B., Krogsgaard-Larsen P., Schlewer G. Synthesis and GABA Uptake Inhibitory Properties of 6-Aryl Iminoxymethyl Substituted Nipecotnic Acids. *Eur. J. Med. Chem.* 2004, 39, 889.

- [9] Stetter H., Roos E.-E. Eine Synthese Makro-cyclischer, Stickstoffhaltiger Ringsysteme. *Chem. Ber.* 1954, 87, 566.
- [10] Koyama H., Yoshino T. Syntheses of Some Medium Sized Cyclic Triamines and Their Cobalt(III) Complexes. *Bull. Chem. Soc. Jpn.* 1972, 45, 481.
- [11] Richman J. E., Atkins T. J. Nitrogen Analogs of Crown Ethers. *J. Am. Chem. Soc.* 1974, 96, 2268.
- [12] (a) Chaudhuri P., Wieghardt K. The Chemistry of 1,4,7-Triazacyclononane and Related Tridentate Macrocyclic Compounds. *Prog. Inorg. Chem.* 2007, 35, 329. (b) Wieghardt K. The Active Sites in Manganese-Containing Metalloproteins and Inorganic Model Complexes. *Angew. Chem., Int. Ed. Engl.* 1989, 28, 1153. (c) Tolman W. B. Making and Breaking the Dioxygen O–O Bond: New Insights from Studies of Synthetic Copper Complexes. *Acc. Chem. Res.* 1997, 30, 227.
- [13] (a) de Vos D. E., Meinershagen J. L., Bein T. Highly Selective Epoxidation Catalysts Derived from Intrazeolite Trimethyltriazacyclononane-Manganese Complexes. *Angew. Chem., Int. Ed. Engl.* 1996, 35, 2211. (b) Zondervan C., Hage R., Feringa B. L. Selective Catalytic Oxidation of Benzyl Alcohols to Benzaldehydes with a Dinuclear Manganese(IV) Complex. *Chem. Commun.* 1997, 419.
- [14] (a) Hegg E. L., Burstyn J. N. Copper(II) Macrocycles Cleave Single-Stranded and Double-Stranded DNA under Both Aerobic and Anaerobic Conditions. *Inorg. Chem.* 1996, 35, 7474. (b) Young M. J., Chin J. Dinuclear copper(II) complex that hydrolyzes RNA. *J. Am. Chem. Soc.* 1995, 117, 10577.
- [15] (a) Rossi P., Felluga F., Tecilla P., Formaggio F., Crisma M., Toniolo C., Scrimin P. A Bimetallic Helical Heptapeptide as a Transphosphorylation Catalyst in Water. *J. Am. Chem. Soc.* 1999, 121, 6948. (b) Sissi C., Rossi P., Felluga F., Formaggio F., Palumbo M., Tecilla P., Toniolo C., Scrimin P. Dinuclear  $Zn^{2+}$  Complexes of Synthetic Heptapeptides as Artificial Nucleases. *J. Am. Chem. Soc.* 2001, 123, 3169. (c) Rossi, P.; Felluga, F.; Tecilla, P.; Formaggio, F.; Crisma, M.; Scrimin, P. An Azacrown-Functionalized Peptide as a Metal Ion

- Based Catalyst for the Cleavage of a RNA-model Substrate. *Pept. Sci.* 2000, 55, 496.
- [16] Weisman G. R., Vachon D. J., Johnson V. B., Gronbeck D. A. Selective N-protection of medium-ring triamines. *J. Chem. Soc., Chem. Commun.* 1987, 886.
- [17] Blake A. J., Fallis I. A., Parsons S., Ross S. A., Schroder M. Asymmetric Functionalisation of Aza Macrocycles. Syntheses, Crystal Structures and Electrochemistry of  $[\text{Ni}(\text{Bz}[9]\text{aneN}_3)_2][\text{PF}_6]_2$  and  $[\text{Pd}(\text{Bz}[9]\text{aneN}_3)_2][\text{PF}_6]_2 \cdot 2\text{MeCN}$  ( $\text{Bz}[9]\text{aneN}_3 = 1\text{-benzyl-1,4,7-triazacyclononane}$ ). *J. Chem. Soc., Dalton Trans.* 1996, (4), 525.
- [18] Blake A. J., Fallis I. A., Gould S., Parsons S., Ross S. A., Schroder M. Stacked Amido Macrocylic Complexes: Synthesis and Single Crystal X-ray Structure of  $\text{Na}[\text{Cu}(\text{L})(\text{NCMe})](\text{BF}_4)_2(\text{NO}_3)[\text{L} = 1\text{-formyl-4,7-bis(2-hydroxy-2-methylpropyl)-1,4,7-triazacyclononane}]$ . *J. Chem. Soc., Chem. Commun.* 1994, 2467.
- [19] McGowan P. C., Podesta T. J., Thornton-Pett M. N- Monofunctionalized 1,4,7-Triazacyclononane Macrocycles as Building Blocks in Inorganic Crystal Engineering. *Inorg. Chem.* 2001, 40, 1445.
- [20] Ellis D., Farrugia L. J., Hickman D. T., Lovatt P. A., Peacock R. D. A General Route for the Synthesis of Triazacyclononane Functionalised with One, Two or Three Pendant Phosphine Arms: Crystal Structure of  $[\text{Zn}_2\text{L}_2\text{C}_{13}][\text{C}_{104}]$ ,  $\text{L} = \text{N}(\text{-diphenylphosphinopropyl})\text{-1,4,7-Triazacyclononane}$ . *Chem. Commun.* 1996, 1817.
- [21] (a) Atkins T. J. Tricyclic Trisaminomethanes. *J. Am. Chem. Soc.* 1980, 102, 6364. (b) Weisman G. R., Johnson V., Fiala R. E. Tricyclic Orthoamides: Effects of Lone-pair Orientation upon NMR Spectra. *Tetrahedron Lett.* 1980, 21, 3635.
- [22] Weisman G. R., Vachon D. J., Johnson V. B., Gronbeck D. A. Selective N-Protection of Medium-ring Triamines. *J. Chem. Soc., Chem. Commun.* 1987, 886.
- [23] Kang J., Jo J. H. The Synthesis of 1,4,7-Triazacyclononane Conjugated Amyloid-phillic Compound and Its Binding Affinity to the  $\beta$ -Amyloid Fibril. *Bull. Korean Chem. Soc.* 2003, 24, 1403.
- [24] Denat F., Desogere P., Bernhard C., Rousselin Y., Boschetti F. Synthesis of Imidazo[1,

- 2-A]Pyrazin-4-ium Salts for the Synthesis of 1,4,7-Triazacyclononane (TACN) and N- and/or C-functionalized Derivatives Thereof. US 2014/0142298 A1.
- [25] Rodriques K. E. A Novel Route to Cyclopropyl Ketones, Aldehydes, and Carboxylic Acids. *Tetrahedron Lett.* 1991, 32, 1275.
- [26] Gassmart P. C., Hodgson P. K. G., Balchunis R. J. Base-Promoted Hydrolysis of Amides at Ambient Temperatures. *J. Am. Chem. Soc.* 1976, 98, 1275.
- [27] Miyakoshi H., Miyahara S., Yokogawa T., Endoh K., Muto T., Yano W., Wakasa T., Ueno H., Chong K. T., Taguchi J., Nomura M., Takao Y., Fujioka A., Hashimoto A., Itou K., Yamamura K., Shuto S., Nagasawa H., Fukuoka M. 1,2,3-Triazole-Containing Uracil Derivatives with Excellent Pharmacokinetics as a Novel Class of Potent Human Deoxyuridine Triphosphatase Inhibitors. *J. Med. Chem.* 2012, 55, 6427.
- [28] Yamada S., Abe M. Selective Deprotection and Amidation of 2-Pyridyl Esters via N-Methylation. *Tetrahedron* 2010, 66, 8667.
- [29] Furukawa S., Hitomi Y., Shishido T., Tanaka T. Efficient Aerobic Oxidation of Hydrocarbons Promoted by High-spin Nonheme Fe(II) Complexes Without Any Reductant. *Inorg. Chim. Acta* 2011, 378, 19.
- [30] Lauffer R. B. Paramagnetic Metal-complexes as Water Proton Relaxation Agents for NMR Imaging: Theory and Design. *Chem. Rev.* 1987, 87, 901.
- [31] Caravan P., Ellison J. J., McMurry T. J., Lauffer R. B. Gadolinium(III) Chelates as MRI Contrast Agents: Structure, Dynamics, and Applications. *Chem. Rev.* 1999, 99, 2293.
- [32] Frausto Da Silva J. J. R., Williams R. J. P. *The Biological Chemistry of the Elements*, 2nd ed.; Oxford University Press: New York, 2001; Chapter 9.
- [29] Touti F., Maurin P., Hasserodt J. Magnetogenesis Under Physiological Conditions With Probes that Report on (bio-)chemical Stimuli. *Angew. Chem. Int. Ed.* 2013, 52, 4654.
- [33] Touti F., Singh A. K., Maurin P., Canaple L., Beuf O., Samarut J., Hasserodt J. An Electroneutral Macrocyclic Iron(II) Complex that Enhances MRI Contrast In Vivo. *J. Med.*

*Chem.* 2011, 54(12), 4274.

- [34] Goldsmith C. R., Jonas R. T., Cole A. P., Stack T. D. P. A Spectrochemical Walk: Single-Site Perturbation within a Series of Six-Coordinate Ferrous Complexes. *Inorg. Chem.* 2002, 41, 4642.

## **Chapter 5 Achievement of electroneutrality of complexes based on pyrimidinediol**

### **5.1 Introduction of the project and design of the target complexes**

Pyrimidine as a kind of azabenzene ring is the precursor of cytosine, thymine, and uracil in DNA or RNA<sup>[1]</sup>. It is not surprising that pyrimidine and its derivatives attract much interest due to their diverse biological and clinical applications and pyrimidine is often used as a synthon to make all kinds of biologically active compounds such as anticonvulsant, antidepressant and antimalarial agents<sup>[2-5]</sup>. Thus most of researchers put emphasis on synthesis of its derivatives. At the same time, it has to be recognized that the pyrimidine and its derivatives are appealing in the field of coordination chemistry due to the coordination ability resulting from nitrogen atoms or six-member  $\pi$  ring which give  $\sigma$ - or  $\pi$ -type configurations respectively<sup>[6-9]</sup>.

Moreover, this kind of compound draws our attention not only because of their coordination capacities but also the pKa values. It is reported that typically the pKa values of malonyl heterocycles such as 4-hydroxy-6-pyrimidones, 4-hydroxy-2-pyrones and 4-hydroxy-coumarins and so on rang between 4.0-6.0<sup>[10]</sup> and that of 4,6-dihydroxypyrimidine (4,6-DHP) is 5.4<sup>[11]</sup>, which inspires us to think of the 2-methyl-4,6-dihydroxypyrimidine (DHMP). It has three pKa values (0.21, 6.35 and 12.9)<sup>[12-13]</sup>, the lowest one of which (0.21) is attributed to the protonated cation heterocycle losing its proton, 6.35 corresponds to two hydroxyl groups of the heterocycle and 12.9 is assigned to the CH of the heterocycle. This reasonable theoretical evidence proves that pyrimidinediol is a good candidate to be explored as part of macrocyclic TACN-based ligand that renders its complex with iron (II) electroneutral at physiological pH.

In addition, the negative charge localized in the malonate anion moiety of the pyrimidinediol can be compensated internally by the nitrogen atom yielding zwitterionic or mesoionic form.

Consequently the target complexes were designed as following (Fig. 5.1):

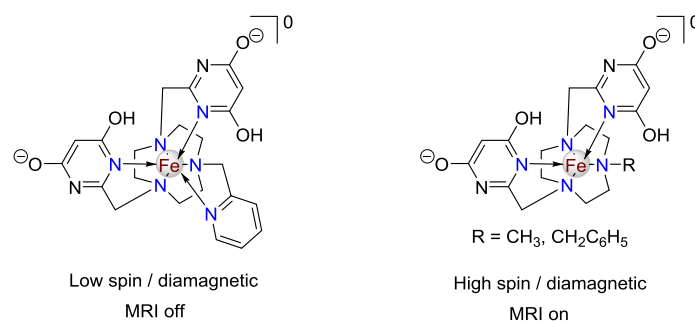


Fig. 5.1

## 5.2 Synthesis of the target ligands bearing pyrimidinediol

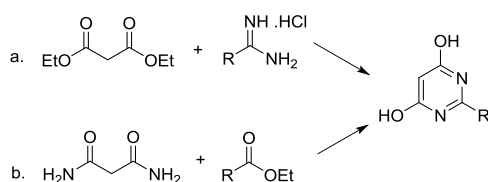
The attempt of preparing a ligand which can be negatively charged is designed by introduction of 4,6-DHP to TACN. While the coordination of TACN and pyrimidine at the same time requires its flexible structure. That is to say, at least one CH<sub>2</sub> is necessary between pyrimidine ring and the nitrogen atom of TACN. So 2-methyl-4,6-dihydroxypyrimidine (DHMP) is suitable to our project.

### 5.2.1 Synthesis of the synthon bromomethylpyrimidine

In order to joint TACN and pyrimidine ring together, it is imperative to synthesize the synthon of pyrimidine as alkylating agent. Then the strategy was proposed that firstly the pyrimidinediol ring DHMP should be prepared, followed by synthesis of halomethylpyrimidinediol.

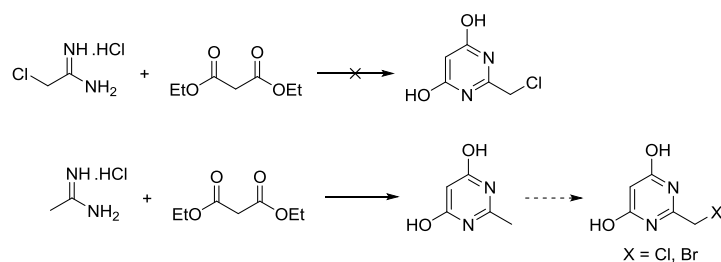
The pioneer E. L. Pinner<sup>[14]</sup> published the preparation of 2-phenyl-4,6-dihydroxypyrimidine which was made by the condensation of benzamidine with malonic ester (Scheme 5.1 a). However he did not report the

aliphatic amidine to synthesize the corresponding compounds. Until 1911, F. G. P. Remfry<sup>[15]</sup> used malonamide and substituted malonic esters to prepare this kind of pyrimidines, even afterwards R. Hull<sup>[16]</sup> and D. J. Brown<sup>[17]</sup> also synthesized 4,6-dihydroxypyrimidine and its 5-ethyl and 5-phenyl derivatives using ethyl formate or other esters and malondiamidine (Scheme 5.1 b). In spite of this, the method presented by E. L. Pinner. was not forgotten. L. P. Ferris II and A. R. Ronzio<sup>[18]</sup> synthesized a series of 2-methyl-5-alkyl-4,6-dihydroxypyrimidine by the method. Since that, those two methods have been the classic synthesis way of 4,6-DHP and its 2- or 5-substitued derivatives.



Scheme 5.1

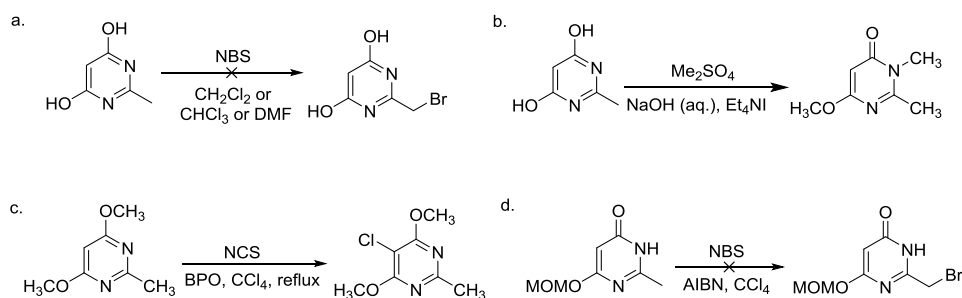
Therefore it is natural and easy to condense 2-chloroacetamidine with diethyl malonate to directly obtain the 2-chloromethyl-4,6-pyrimidinediol. However, maybe the bond Cl-CH<sub>2</sub> was easily cleaved during the reaction process so that making the product by this method was not successful. Then the second synthetic route was proposed that firstly the DHMP was made then bromation or chloration was performed (Scheme 5.2).



Scheme 5.2

Thus the preparation of DHMP was successful following the protocol given by the literature mentioned previously about synthesis of 4,6-dihydroxypyrimidine (Compound **21**, synthesis I in experimental part).

Afterwards the halo-substitution of the DHMP was a problem because its solubility in most of organic solvents is so poor that its direct bromination is no way carried out even in DMF. What is worse, even though it works, the product could not be extracted and thus it mixed with 4,6-dihydroxypyrimidine and the succinimide from *N*-bromosuccinimide (NBS) because of their similar solubility. Therefore, I failed to separate them (Scheme 5.3 a).

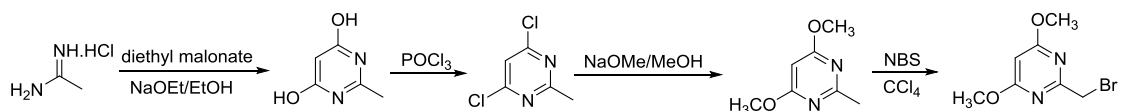


Scheme 5.3

Then protection of hydroxyl groups was proposed to improve its solubility. Typically Tosyl group cannot be used considering that its own methyl group on aromatic ring can bring side reactions. Among the aliphatic protecting groups, the methyl group gets preferential consideration due to its convenient synthesis. There is a way to prepare it by dimethyl sulfate in aqueous solution of sodium hydroxide. Unfortunately methyl group was introduced on the nitrogen atom of pyrimidine ring (Scheme 5.3 b) seen from its  $^1\text{H}$  NMR. In that case, it had to be synthesized by two steps, the first one of which was chlorine atoms replaced the two hydroxyl groups with the reagent phosphorus oxytrichloride, followed by the replacement of methoxyl groups to give 2-methyl-4,6-dimethoxypyrimidine which was halogenated afterwards<sup>[19-21]</sup>. The chloration was tried in the presence of the initiator benzoyl peroxide (BPO) which unexpectedly resulted in an introduction of chlorine on the heterocycle (Scheme 5.3 c). The bromination condition with NBS based on BPO that was initiated by light (500 W) gave a complicate consequence so that I could not isolate the target compound from the mixture. Even though the azodiisobutyronitrile (AIBN) initiated by heating<sup>[20]</sup>

could induce this reaction and produce relatively simple mixture of mono- and di-bromomethylenepyrimidine, the yield is fairly low (30%).

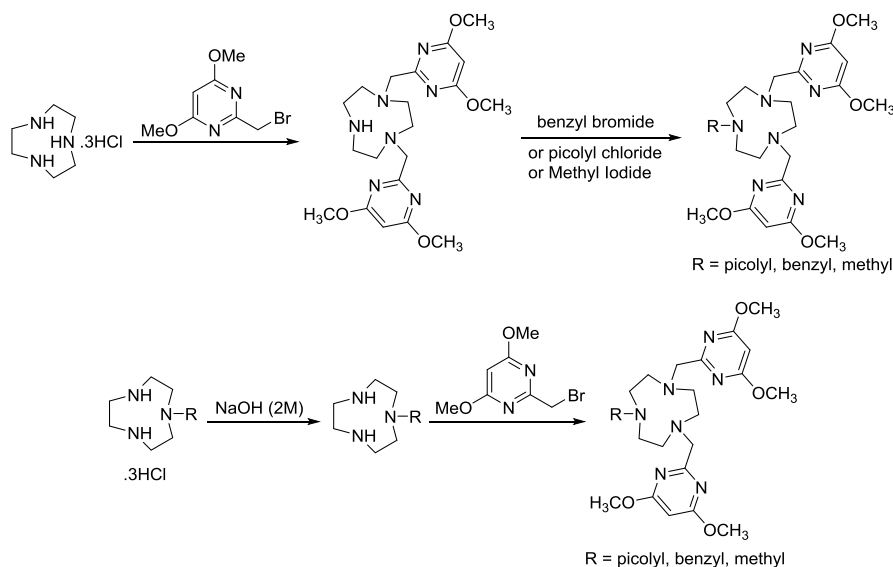
In view of that, the synthetic route for 2-bromomethyl-4,6-dimethoxypyrimidine was chosen as following in spite of the low yield in the last step (Scheme 5.4). (Compound **22-24**, synthesis II in experimental part)



Scheme 5.4

### 5.2.2 Synthesis of the target ligands

According to my previous presentation, the alkylation of TACN with the synthon (2-bromomethyl-4,6-dimethoxypyrimidine) and introduction of methyl, benzyl or picolyl group can be done in two ways (Scheme 5.5).



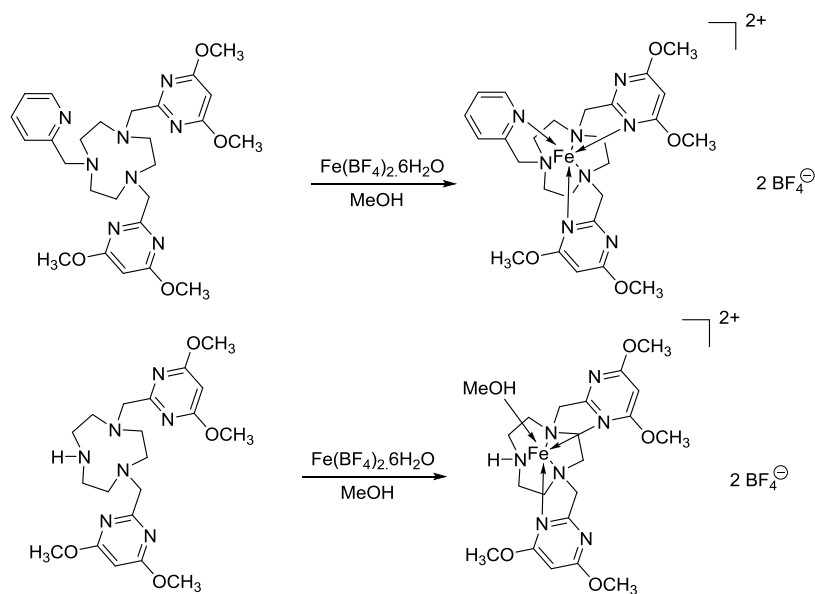
Scheme 5.5

When R is picolyl group (Compound **27**, in experimental part), two ways were tried. The first way of firstly dialkylation then nucleophilic substitution of picolyl chloride

always faced the low yield and a waste of the precious synthon. The second way contains some anhydrous operations when the *N*-picolyl TACN was synthesized and difficulty in separation of the target compound from the quaternary amine when pyrimidine ring was introduced on the other two nitrogen atoms of *N*-picolyl TACN. As what has been presented previously, the quaternary amine was produced when 3.0 eq. pyrimidine ring was introduced. In spite of these disadvantages, both could give the target compound. When R is benzyl or methyl group, the corresponding ligands are preparing. I have not yet obtained them.

### 5.2.3 Synthesis of the complexes bearing protecting groups

After the N6 type ligand with protecting groups was synthesized, it was used for complexation with Fe(II) in methanol (Scheme 5.6). The one bearing picolyl group was a little green and this N6 type complex was crystallized and characterized by X-Ray Diffraction (Its XRD structure is shown in Chapter 5.3) while the one bearing methyl group is being synthesizing. At the same time the N5O1 type one without methyl group on nitrogen atom was synthesized for comparison (Compound **29** and **30**, in experimental part). However, it could not yield crystals of sufficient quality.



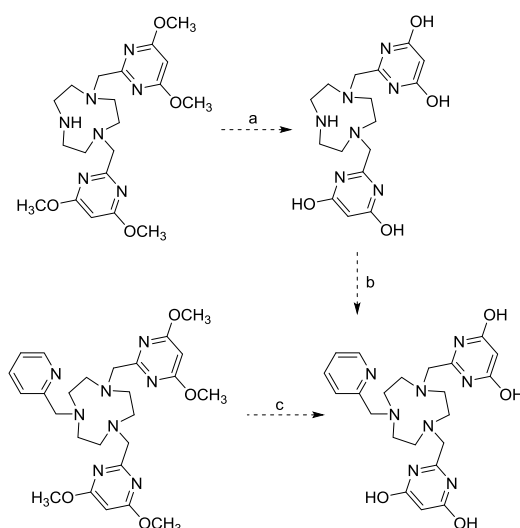
Scheme 5.6

## 5.2.4 Synthesis of the ligands without protecting groups

In order to synthesize the electroneutral complexes, the ligands should be deprotonated to provide negative charges to compensate the positive ones of the metal ion. Thus the deprotection is necessary to the ligands.

### 5.2.4.1 Removal of four methyl groups of the ligands

I planned two ways to get the deprotected ligands. According to the literature<sup>[22-26]</sup>, different conditions (Table 5.2) were tried for step a (Fig. 5.7). The results showed that the removal of methyl groups to obtain pyrimidinediol was a real problem that could not be resolved easily. Basic conditions could remove only one methyl group from each pyrimidine ring. The iodotrimethylsilane (TMSI) and its analogous mixture of reagents, chlorotrimethylsilane (TMSCl) with sodium iodide (NaI)<sup>[27-28]</sup>, could make me reach the goal, but the latter failed to allow the fully deprotected compound far from the inorganic salts.



Scheme 5.7

Table 5.2 Conditions for removing methyl groups

entry	reagents	temperature (°C)	time	results
1	AlCl <sub>3</sub> /DCM	25 then 40	24 h	× <sup>a</sup>

2	BBr <sub>3</sub> /DCM	-50 then 25	24 h	× <sup>a</sup>
3	BBr <sub>3</sub> /DCE	60	16 h	monoketo-monomethoxy <sup>b</sup>
4	NaOH (2 M)	100	4.6 d	monoketo-monomethoxy <sup>b</sup>
5	NaOH (6 M)	100	3.6 d	monoketo-monomethoxy <sup>b</sup>
6	NaOH (6 M) then HCl (2 M)	100	3.6 d <sup>d</sup>	monoketo-monomethoxy <sup>b</sup>
7	NaOH (2 M)/Ph <sub>2</sub> O	120	16 h	× <sup>a</sup>
8	HCl (2 M)	100	24 h	× <sup>a</sup>
9	Me <sub>3</sub> SiCl/NaI	80	24 h	√ <sup>c</sup>
10	Me <sub>3</sub> SiI	80	24 h	√ <sup>c</sup>

a. It means the reaction did not give any deprotected compound no matter how many methyl groups were removed. b. It means only one methyl group was removed from one arm. c. It means that the reaction gave the completely deprotected compound. d. This reaction was carried out just after the reaction 5.

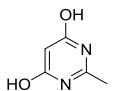
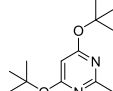
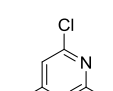
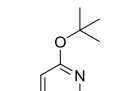
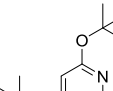
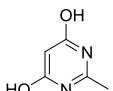
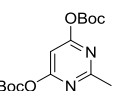
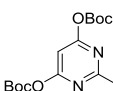
As far as the step b was concerned, LCMS showed that two picolyl groups were introduced in the presence of triethylamine in methanol. The product may be quaternary amine because two picolyl groups were present on the same nitrogen atom or respectively on two different nitrogen atoms, or it was the compound produced by the reaction of the second equivalent picolyl chloride with one hydroxyl group. The step c was completed by iodotrimethylsilane in acetonitrile at 80 °C (Compound **28**, in experimental part). But once the product was obtained in the form of powder, it could not be easily dissolved in MeOH or EtOH even acetonitrile again so that its complexation could not be carried out. Maybe addition of some base can resolve this problem. At present I have not tried this way.

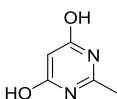
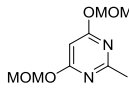
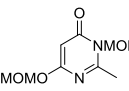
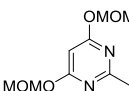
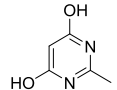
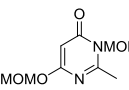
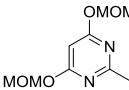
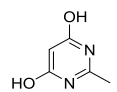
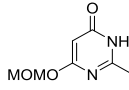
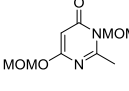
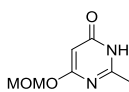
#### 5.2.4.2 Other protecting groups as options

At the same time of trying to remove methyl groups, other protecting groups such as *t*-butyl, Boc and MOM were also considered because they allow acidic deprotection (Table 5.1). The isobutylene<sup>[29]</sup> was used for protecting hydroxyl groups in the

presence of acidic catalyst, but it did not succeed in giving the protected compound, which was still originated from the poor solubility. If it was made in the same way with dimethoxypyrimidine, potassium *tert*-butoxide was supposed to be used. But it has been known that the nucleophilicity of potassium *tert*-butoxide is weaker than that of sodium methoxide, thus it is easy to understand why potassium *tert*-butoxide just caused one replacement. Boc group was introduced easily in moderate yield, and its deprotection under acidic condition worked very well. However, the Boc groups maybe can make the 2-methyl of the compound inactive so that it did not react with NBS. The MOM protected compound was prepared using potassium carbonate<sup>[30]</sup> in acetone in low yield because MOM was also introduced on the nitrogen atom of the ring. Maybe the relatively strong base *N,N*-diisopropylethylamine (DIPEA)<sup>[31]</sup> could deprotonate both hydroxy preferentially to prevent the byproduct. In fact this way gave only the byproduct. If one hydroxy exist in the form of keto and the other in the form of protected hydroxy, it is also an option for the following synthesis of the ligands and their complexes. However when only one equivalent MOMCl was used, the product was also a mixture and the target compound was obtained in 25% yield. What is more, even though the mono-MOM compound was obtained and could be brominated with NBS in CCl<sub>4</sub> in the next step (Scheme 5.3 d), the yield of this step has been a fatal weakness in overall synthesis.

Table 5.1 Attempts of changing the protecting groups

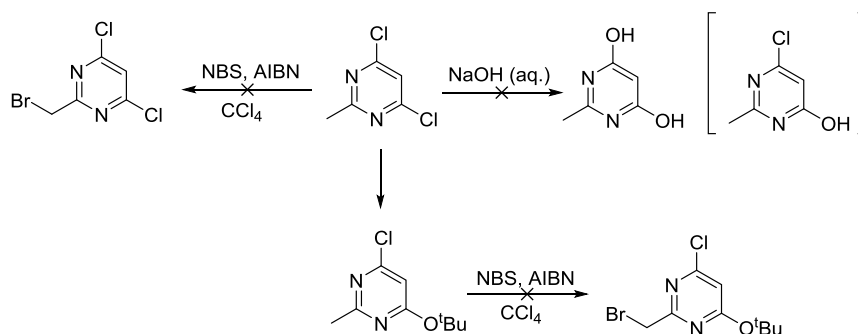
protecting group	starting material	conditions	products	target compound	yield (%) <sup>a</sup>
tert-butyl		isobutylene, [H <sup>+</sup> ], DCM	/		0
		<i>t</i> BuOK, <i>t</i> BuOH			0
Boc		(Boc) <sub>2</sub> O, 4-DMAP, THF			67

		2.0 eq. MOMCl, K <sub>2</sub> CO <sub>3</sub> , Acetone	 		21
MOM		2.0 eq. MOMCl, DIEA, CH <sub>3</sub> CN			0
		1.0 eq. MOMCl, DIEA, CH <sub>3</sub> CN	 		25

a. it is referred to the yield of target compound.

### 5.2.4.3 Other attempts for the ligands without protecting groups

Based on the experiences during the synthesis of 2-bromomethyl-4,6-dimethoxypyrimidine, the other ways to achieve the goal of making the ligands without protecting groups. For example, it was found two chlorine atoms of the 2-methyl-4,6-dichloropyrimidine not only can be replaced by some strong nucleophilic reagents such as methoxy or ethoxy, amine and so on, but also one chlorine atom is very easy to be replaced by hydroxy when POCl<sub>3</sub> treated the 2-methyl-4,6-pyrimidinediol to make 2-methyl-4,6-dichloropyrimidine. I tried to take advantage of this observation and proposed to bromate the 2-methyl-4,6-dichloropyrimidine then use sodium or potassium hydroxide solution to make it return back to pyrimidinediol after conjugation with TACN. Unfortunately, this strategy was a failure because its bromation under the condition of NBS in CCl<sub>4</sub> in the presence of AIBN could not give the target product and the sodium hydroxide solution just replaced only one chlorine atom (Scheme 5.8).

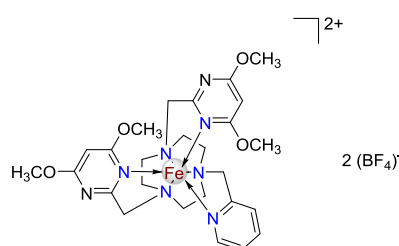
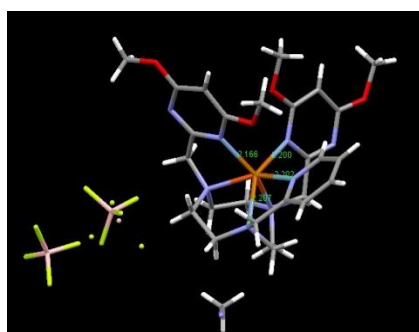


Scheme 5.8

Since potassium *tert*-butoxide just caused one replacement of 4,6-dichloropyrimidine, It was hypothesized that maybe the other chlorine atom which was not replaced by *tert*-butoxide can be hydrolyzed after alkylation of its bromated product and TACN, then the remaining *tert*-butyl group can be removed under acidic condition. However, the bromation did not succeed again.

### 5.3 Results and discussion

The XRD structure of N6 type complex is shown as following:



Seen from its structure, the length of the Fe-N bond (the distance from the yellow to the blue atom) is about 2.2 Å. However, It is reported that the bond N-Fe(II) of low-spin complexes should be between 1.96 and 2.0 Å, and that of high-spin complexes should be around 2.2 Å<sup>[32]</sup>. Thus this complex displayed as high-spin nature in the solid state. The measurement of its magnetic moment in solution by Evans' method accordingly yielded a value of 5.93 BM in contrast to that of the

low-spin complex which should be lower than 1.0 BM.

We deduced that this result may derive (a) from the steric hindrance of four methoxyl groups on two pyrimidine arms and (b) from the absence of coulombic attraction as would be likely present in the electroneutral target complex (thus generating a stronger ligand field).

## 5.4 Summary and Perspectives

In conclusion, two complexes bearing four methyl groups were prepared, and the N6 type complex showed us its high-spin property. The definitely reasonable explanation should be given by its comparison with the deprotected one. The deprotection of the N6 type ligand is also successful by using the condition of Me<sub>3</sub>SiI/CH<sub>3</sub>CN at 80 °C (Compound **28**, in the experimental part) after many attempts (which have been presented above), but its poor solubility in MeOH, EtOH and acetonitrile hinders its complexation. Thus some work in perspective is proposed. The reagent Me<sub>3</sub>SiI should be fresh enough and CH<sub>3</sub>CN should be anhydrous, also the reaction should be carried out under inert gas and the reaction should be kept for enough time (24 h) to make sure all the methyl groups are removed or a suitable method for LCMS should be found to monitor the reaction (In my experience, the product could not give its signals by LCMS may due to the difficulty in ionization). As far as its complexation is concerned, addition of some base is suggested to make the ligand be dissolved in MeOH, EtOH or acetonitrile. Meanwhile other protecting groups were tried but most of them failed in bromation which is also one considering aspect for the coming research. Maybe the better protecting group can be found once the bromation works.

## 5.5 References

- [1] Brown D. J. The Chemistry of Heterocyclic Compounds. The Pyrimidines; Wiley: New York, 1962.

- [2] Wang H., Zhang Q., Zhang J., Li L., Zhang Q., Li S., Zhang S., Wu J., Tian Y. Synthesis, Two-Photon Absorption Properties and Bioimaging Applications of Mono-, Di- and Hexa-Branched Pyrimidine Derivatives. *Dyes Pigm.* 2014, 102, 263.
- [3] Moffatt J. S. Contributions to the Chemistry of Synthetic Antimalarials. Part IX. Some Pyrimidine Derivatives. *J. Chem. Soc.* 1950, 1603.
- [4] King F. E., King T. J. New Potential Chemotherapeutic Agents. Part VI. Derivatives of 1:3-Diam-acridine. *J. Chem. Soc.* 1947, 726.
- [5] Lauria A., Patella C., Abbate I., Martorana A., Almerico A. M. Lead Optimization Through VLAK Protocol: New Annelated Pyrrolo-Pyrimidine Derivatives as Antitumor Agents. *Eur. J. Med. Chem.* 2012, 55, 375.
- [6] Coelho A. L., Toma H. E., Malin J. M. Pentacyanoferrate(II) Complexes of Pyrimidine and Quinoxaline. *Inorg. Chem.* 1983, 22, 2703.
- [7] Alisir S. H., Demir S., Sariboga B., Buyukgungor O. A Disparate 3-D Silver(I) Coordination Polymer of Pyridine-3,5-Dicarboxylate and Pyrimidine with Strong Intermetallic Interactions: X-ray Crystallography, Photoluminescence and Antimicrobial Activity. *J. Coord. Chem.* 2015, 68, 155.
- [8] Bushuev M. B., Gatilov Y. V., Krivopalov V. P., Shkurko O. P. Tetra- and Polynuclear Cadmium(II) Complexes with 3,5-Bis(pyrimidin-2-yl)-4H-1,2,4-triazol-4-amine. Synthesis, Polymorphism, Lone pair- $\pi$  Interactions and Luminescence. *Inorg. Chim. Acta* 2015, 425, 182.
- [9] Shao P., Kuang X.-Y., Ding L.-P. Probing the Structural, Bonding, and Magnetic Properties of Cobalt Coordination Complexes: Co-Benzene, Co-Pyridine, and Co-Pyrimidine. *J. Phys. Chem. A* 2013, 117, 12998.
- [10] Habib N. S., Kappe T. Ylids of Heterocycles. VII. I-, N-, P- and S-Ylides of Pyrimidones. *J. Heterocycl. Chem.* 1984, 21, 385.
- [11] Brown D. J., Teitei T. Simple Pyrimidines VII. The Fine Structure of 4,6-Dihydroxypyrimidine. *Aust. J. Chem.* 1964, 17, 567.
- [12] Luke, T. L., Mohan H., Jacob T. A., Manoj V. M., Manoj P., Mittal J. P., Destailats H.,

- Hoffmann M. R., Aravindakumar C. T. Kinetic and Spectral Investigation of the Electron and Hydrogen Adducts of Dihydroxy- and Dimethyl-Substituted Pyrimidines: a Pulse Radiolysis and Product Analysis Study. *J. Phys. Org. Chem.* 2002, 15, 293.
- [13] Hurst D. T. An Introduction to the Chemistry and Biochemistry of Pyrimidines, Purines and Pteridines. John Wiley & Sons: Chichester, 1980, 18.
- [14] Pinner E. L. Über 2-Phenyl-4,6-dioxy-pyrimidin. *Chem. Ber.* 1908, 41, 3517-3519.
- [15] Remly F. G. P. LXIX.-Chemical Constitution and Hypnotic Action. Acid Amides and Products of the Condensation of Malonamides and Malonic Esters. *J. Chem. Soc. Trans.* 1911, 99, 610-625.
- [16] Hull R. Notes. New Synthesis of 4, 6-Dihydroxypyrimidines. *J. Chem. Soc.* 1951, 2207.
- [17] Brown D. J. Pyrimidine Reactions. Part I. Pyrimidines from Malondiamide. *J. Chem. Soc.* 1956, 2312.
- [18] Ferris II L. P., Ronzio A. R. A Series of 2-Methyl-5-alkyl-4,6-dihydroxypyrimidines. *J. Am. Chem. Soc.* 1940, 62, 606.
- [19] Delia T. J., Stark D., Glenn S. K. 2,4,6-Trichloropyrimidine. Reaction with Ethanolamine and Diethanolamine. *J. Heterocycl. Chem.* 1995, 32, 1177.
- [20] El-Kerdawy M. M., El-Emam A. A., El-Subbagh H. I. Synthesis of Certain Substituted Pyrimidines as Potential Schistosomicidal Agents. *J. Heterocyclic Chem.* 1989, 26, 913.
- [21] Czeskis B. A. Synthesis of Triple [<sup>14</sup>C]-Labeled Moxonidine. *J. Label Compd. Radiopharm.* 2004, 47, 699.
- [22] Han A. Q., Wang E., Gauss C., Xie W., Coburn G., Demuys J.-M. Antiviral Pyrimidines. WO 2010/1183567 A2.
- [23] Li T., Wu Y. L. Facile Regio- and Stereoselective Total Synthesis of Racemic Aklavinone. *J. Am. Chem. Soc.* 1981, 103, 7007.
- [24] Soni A., Dutt A., Sattigeri V., Cliffe I. A. Efficient and Selective Demethylation of Heteroaryl Methyl ethers in the presence of Aryl Methyl Ethers. *Synthetic Communications: An International Journal for Rapid Communication of Synthetic Organic Chemistry*, 2011, 41,

1852.

- [25] Parsy C. C., Alexandre F.-R., Leroy F., Convard T., Surleraux D. Macrocyclic Serine Protease Inhibitors Useful Agent Viral Infections, Particularly HCV. WO 2011/017389 A1.
- [26] Spadaro A., Frotscher M., Hartmann R. W. Optimization of Hydroxybenzothiazoles as Novel Potent and Selective Inhibitors of 17 $\beta$ -HSD1. *J. Med. Chem.* 2012, 55, 2469.
- [27] Hull J. F., Himeda Y., Fujita E., Muckerman J. T. Bimetallic Catalysts for CO<sub>2</sub> Hydrogenation and H<sub>2</sub> Generation from Formic Acid and/or Salts Thereof. WO 2013/040013 A2.
- [28] Eastwood P. R., Gonzalez R. J., Bach-Tana J., Pages S., Lluís M., Taltavull-Moll J. Imidazopyridine Derivatives as Jak Inhibitors. WO 2011/076419 A1.
- [29] Messmore B. W., Hulvat J. F., Sone E. D., Stupp S. I. Synthesis, Self-Assembly, and Characterization of Supramolecular Polymers from Electroactive Dendron Rodcoil Molecules. *J. Am. Chem. Soc.* 2004, 126, 14452.
- [30] Scopton A., Kelly T. R. Synthesis of Azacridone A. *Org. Lett.* 2004, 6, 3869.
- [31] Miyakoshi H., Miyahara S., Yokogawa T., Endoh K., Muto T., Yano W., Wakasa T., Ueno H., Chong K. T., Taguchi J., Nomura M., Takao Y., Fujioka A., Hashimoto A., Itou K., Yamamura K., Shuto S., Nagasawa H., Fukuoka M. 1,2,3-Triazole-containing Uracil Derivatives with Excellent Pharmacokinetics as a Novel Class of Potent Human Deoxyuridine Triphosphatase Inhibitors. *J Med. Chem.* 2012, 55, 6427.
- [32] (a) Gutlich P., Hauser A., Spiering H. Thermal and Optical Switching of Iron (II) Complexes *Angew. Chem. Int. Ed. Engl.* 1994, 33, 2024. (b) Beattie, J. K. Dynamics of Spin Equilibria in Metal Complexes. *Adv. Inorg. Chem.* 1988, 32, 1-53. (c) Toftlund, H. Spin Equilibria in Iron(II) Complexes. *Coord. Chem. Rev.* 1989, 94, 67. (d) Xia H.-L., Ardo S., Sarjeant A. A. N., Huang S.-X., Meyer G. J. Photodriven Spin Change of Fe(II) Benzimidazole Compounds Anchored to Nanocrystalline TiO<sub>2</sub> Thin Films. *Langmuir* 2009, 25, 13641.

## Part III Experimental section

### General Introductions

Available reagents and solvents were purchased from Aldrich, Acros, and Alfa Aesar and used without further purification. All the solvents for complexation were dried by activated molecular sieves and degassed with the method "freeze-pump-thaw". Column chromatography was performed using Merck silica gel Si-60 (40~63  $\mu\text{m}$ ) or Acros activated neutral Alumina (60  $\text{\AA}$ , 50~200  $\mu\text{m}$ ).

$^1\text{H}$  and  $^{13}\text{C}$  NMR spectra were acquired on a Bruker DPX 300 or 500 instrument (300 or 500, and 75 or 100 MHz, respectively) at 298 K. Chemical shifts ( $\delta$ ) are reported in ppm (s = singlet, d = doublet, t = triplet, m = multiplet, br = broad) and referenced to solvent peak. NMR coupling constants ( $J$ ) are reported in hertz.

High resolution mass spectrometry (HRMS) were performed by the "Centre Commun de Spectrometrie de Masse" of the University Claude Bernard in Lyon (France). Low resolution mass spectra obtained on an Agilent 1100 Series LC/MSD apparatus was used for monitoring some reactions. Usually the samples were directly injected then vaporized at 300  $^{\circ}\text{C}$  and ionized in ESI mode. Subsequently the molecular mass signals ( $m/z$ ) were reported in their cationic forms such as  $\text{M}+\text{H}$ ,  $\text{M}+\text{Na}$  and  $\text{M}+\text{K}$  with an intensity of the peak which were relative to the highest one (100 %). During the whole process, the solvent was used consisting of acetonitrile and water mixed at the ratio 98:2 (for the molecules which are very soluble in acetonitrile.) or 50:50 (for the molecules which are very soluble in water like the complexes.) Normally water contains very little of ammonium formate which sometimes causes some signals due to the cations of the complexes binding to the formate. 70 and 150 eV as fragmentation voltages were applied. UV-vis spectra were scanned at RT with a V-670 Jasco spectrophotometer.

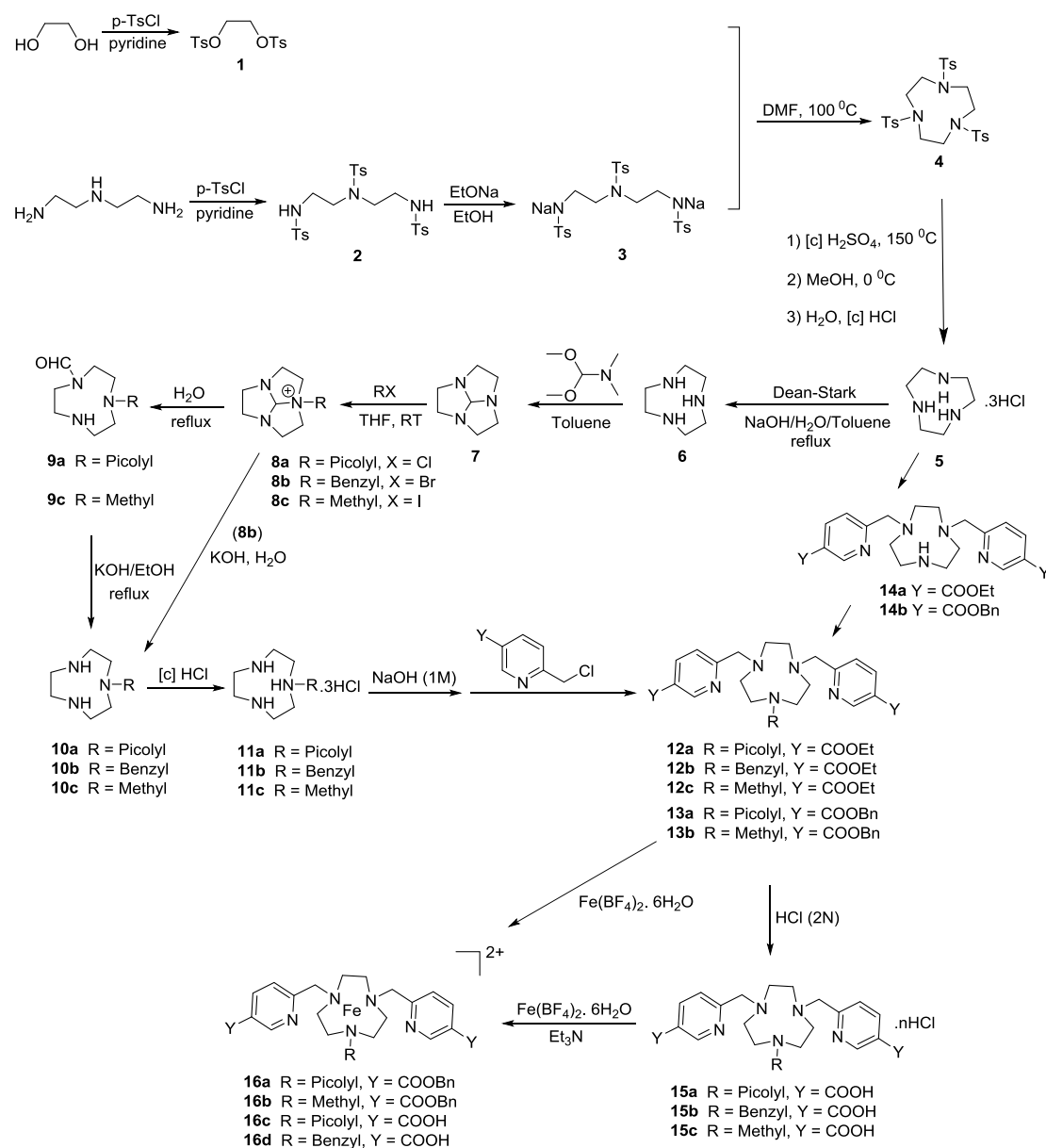
Cyclic voltammetry experiments were conducted in a standard electrolytic cell consisting of three electrodes (vitreous carbon as the working one, saturated calomel electrode (SCE) as reference one and Pt-wire as the counter one) and the solution of the samples in PBS in a compartment. The biologic ESP300 potentiostat was used and no other chemical salt as support was added. The CVs of the complexes (1 mM) were scanned at the rate of 100 mV/s for the low-spin one and the rate from 25 mV to 20 V/s for high-spin one.

The X-Ray Diffraction was acquired by Erwann Jeanneau who is working in the Centre de Diffractométrie Henri Longchambon (France).

MRI relaxation time was measured by Laurence Canaple in the "Institut de Genomique Fonctionnelle de Lyon" (France).

## Synthesis I

The following scheme is showing the synthetic route of the ligands and the complexes based on the pyridylcarboxylic acid.



### Synthesis of the *N*-functionalized TACN (11a-c)

#### Compound 1

Ethylene glycol (22.6 mL, 0.41 mol) was dissolved in 190 mL anhydrous pyridine in

2 L flask with one neck, to which p-TsCl (154.03 g, 0.81 mol) was added slowly at 0 °C. After all the p-TsCl was completely added, the mixture could not be stirred any more, 170 mL anhydrous pyridine was added and kept it stirred at 0 °C for 1.5 h. Subsequently the ice bath was removed away and the mixture was stirred at RT for 2 h. The reaction was monitored with TLC. When ethylene glycol was completely converted to the protected product, diluted HCl solution, which was prepared with 215 mL concentrated HCl (37%) and 700 mL ice, was added slowly in the flask and the mixture was stirred overnight. The white precipitate was filtered, then put in 300 mL anhydrous MeOH and heated to reflux for 15 min, subsequently the mixture was cooled down at RT for 3 h and 0 °C for 2 h. Finally the white precipitate was filtered and washed with cold methanol and made dry under vacuum. 117.45 g white powder as the product **1** was obtained in yield 78.3%. <sup>1</sup>H NMR (300 MHz, CDCl<sub>3</sub>) δ 7.72 (2H, dd, *J* = 6.6, 1.8 Hz), 7.32 (2H, dd, *J* = 8.5, 0.6 Hz), 4.18 (2H, s), 2.45 (3H, s); <sup>13</sup>C NMR (75 MHz, CDCl<sub>3</sub>) δ 145.28, 132.37, 129.97, 127.98, 66.69, 21.69

#### Compound **2**

P-TsCl (201.7 g, 1.06 mol) was dissolved in 445 mL anhydrous pyridine in 1 L three-neck flask. Then the solution of Diethylenetriamine (38.4 mL, 0.35 mol) in 53 mL anhydrous pyridine was dropwise added during 2 h. The obtained mixture was heated to 50 °C for 3 h, which was subsequently transferred to 2 L Erlen flask and 400 mL water was added then stirred overnight. After that the suspension was put in ice bath for 2 h and filtered, washed with water and cold 95% ethanol and some ethyl ether, finally made dry under vacuum to give 190.99 g light yellow powder as the product **2** in yield 95.5%. <sup>1</sup>H NMR (300 MHz, DMSO-d<sub>6</sub>) δ 7.70-7.65 (6H, m), 7.54 (2H, d, *J* = 8.3 Hz), 7.42-7.36 (6H, m), 3.01 (4H, t, *J* = 7.2 Hz), 2.81 (4H, t, *J* = 6.8 Hz), 2.40 (6H, s), 2.39 (3H, s); <sup>13</sup>C NMR (75 MHz, DMSO-d<sub>6</sub>) δ 143.93, 143.23, 137.86, 135.82, 130.35, 130.15, 127.30, 127.00, 48.84, 42.04, 21.44

#### Compound **3**

The compound **2** (190.0 g, 0.34 mol) and 470 mL absolutely anhydrous Ethanol was added in a flask. To this suspension, fresh EtONa solution (prepared by adding Sodium (15.47 g, 0.67 mol) slowly to 470 mL anhydrous EtOH) was added under argon. All of the compound **2** was almost dissolved during 5min to give clear solution which was subsequently filtered quickly. The filtrate was kept in a fridge overnight to produce a lot of precipitate which was filtered and washed with cold anhydrous EtOH then made dry under vacuum by oil pump for 4 d to give 203.0 g white powder as the product **3** in yield 99.1%. It was not characterized and directly used for next step.

#### Compound **4**

Compound **3** (103.0 g, 0.17 mol) was dissolved in 1.1 L anhydrous DMF and it was heated to 100 °C. Then the solution of compound **1** in 350 mL anhydrous DMF was dropwise added during 4 h. Afterwards the mixed solution was cooled down to RT. and added 600 mL water to give a suspension which was kept in a fridge overnight. It was filtered and washed with water, anhydrous EtOH and Et<sub>2</sub>O, and made dry by oil pump for 2 d to give 77.2 g light yellow powder as the product **4** in yield 77.2%. <sup>1</sup>H NMR (300 MHz, CDCl<sub>3</sub>) δ 7.68 (2H, d, *J* = 7.9 Hz), 7.31 (2H, d, *J* = 7.9 Hz), 3.42 (4H, s), 2.43 (3H, s); <sup>13</sup>C NMR (75 MHz, CDCl<sub>3</sub>) δ 143.91, 134.62, 129.89, 127.52, 51.87, 21.54

#### Compound **5**

Compound **4** (73.0 g, 0.12 mol) was added to the hot concentrated H<sub>2</sub>SO<sub>4</sub> at 150 °C during 3 min, and the dark mixture was kept at 150 °C for 40 min. Then it was cooled down and added dropwise to 500 mL anhydrous MeOH at 0 °C during 6 h to give a suspension which was kept in a fridge overnight at -20 °C. The gray precipitate was obtained by filtration then it was dissolved in 40 mL water and heated to 100 °C for 1 h. After it was cooled down at RT, 40 mL concentrated HCl was dropwise added to produce much precipitate which was subsequently filtered and washed with 95% EtOH and Et<sub>2</sub>O to give 24.0 g gray powder as the product **5** in yield 82%. <sup>1</sup>H NMR

(300 MHz, D<sub>2</sub>O)  $\delta$  3.37 (s)

#### Compound **6**

Compound **5** (9.84 g, 0.041 mol) was dissolved in 17.0 mL water, to the solution NaOH (4.32 g) and 60 mL toluene was added. Afterwards the mixture was equipped to Dean-Stark which is filled with toluene and heated to reflux for 3 h. The solution in the flask was decanted out and another 2.3 g NaOH (s) and 20 mL toluene was added to the residue, then it was heated to reflux again for 2 h with Dean-Stark. The solution was decanted again and the residue was washed with toluene. All the toluene solution was combined together and dried by evaporator to give 4.6 oil as product **6** in yield 86%. The oil became colorless crystals when it was put in the fridge. <sup>1</sup>H NMR (300 MHz, CDCl<sub>3</sub>)  $\delta$  2.57 (s)

#### Compound **7**

To the solution of compound **6** (1.5 g, 11.6 mmol) in 15 mL toluene, *N,N*-dimethylformamide dimethyl acetal (1.62 mL, 12.2 mmol) was added. It was heated to 70 °C for 1 h. 1.3 g light yellow oil as product **7** was obtained in yield 81% after evaporation of toluene. <sup>1</sup>H NMR (300 MHz, CDCl<sub>3</sub>)  $\delta$  5.01 (1H, s), 3.04-3.06 (6H, m), 2.76-2.79 (6H, m).

#### Compound **11a**

Picolyl chloride hydrochloride (3.2 g, 19.51 mmol) was neutralized with 40 mL NaOH (1 M) and extracted with Et<sub>2</sub>O three times. Then the Et<sub>2</sub>O solution was washed with brine and dried with anhydrous Na<sub>2</sub>SO<sub>4</sub>, subsequently solvent was removed by evaporator to give 2.4 g pink oil as picolyl chloride in yield 98%.

To the solution of Compound **7** (2.0 g, 14.37 mmol) in 5 mL THF, was dropwise added the solution of picolyl chloride (1.81 g, 14.37 mmol) in 4 mL THF at 0 °C under argon. There was some white precipitate produced. After finishing addition the system was kept stirred at RT for 4 d. The precipitate was filtered and washed with dry THF to give white powder (product **8a**) which was subsequently dissolved in 15

mL H<sub>2</sub>O and heated to 100 °C overnight. Water was removed by evaporator, then the residue (the crude product **9a**) was dissolved in 15 mL EtOH. Afterwards 2.0 g KOH was added, and the suspension was refluxed overnight. Ethanol was removed and 15 mL water was added, then it was extracted with Et<sub>2</sub>O and the organic solution was washed with brine and washed with anhydrous Na<sub>2</sub>SO<sub>4</sub>. Finally it was concentrated and dried under vacuum. The obtained light yellow oil (the crude product **10a**) was dissolved in 20 mL anhydrous EtOH and added 6 mL concentrated HCl to give brown solution. Then all volatiles were removed by evaporator and 40 mL EtOH was added to produce precipitate which was subsequently filtered and washed with Et<sub>2</sub>O to give 4.14 g pink powder as product **11a** in yield 93.5%. <sup>1</sup>H NMR (300 MHz, D<sub>2</sub>O) δ 8.62 (1H, dd, *J* = 5.4, 0.8 Hz), 8.42 (1H, t, *J* = 7.9 Hz), 7.92 (1H, d, *J* = 8.0 Hz), 7.84 (1H, t, *J* = 6.8 Hz), 4.17 (2H, s), 3.57 (4H, s), 3.25 (4H, t, *J* = 5.6 Hz), 2.98 (4H, t, *J* = 5.6 Hz); <sup>13</sup>C NMR (75 MHz, D<sub>2</sub>O) δ 150.56, 146.94, 142.22, 127.99, 126.42, 55.32, 48.06, 43.87, 42.52; ESI-MS: calcd. for C<sub>12</sub>H<sub>21</sub>N<sub>4</sub>[M + H] 221.1761; found 221.1762.

#### Compound **11b**

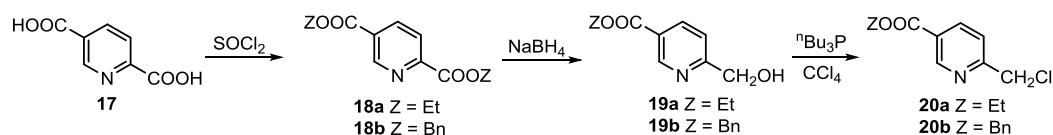
Compound **7** (1.70 g, 12.2 mmol) was dissolved in 8 mL anhydrous THF, then the solution of benzyl bromide (2.0 g, 12.2 mmol) in 5 mL THF was dropwise added at 0 °C. The solution was kept stirred at RT for 1d, and the white precipitate (product **8b**) was filtered and washed with anhydrous THF. Afterwards the white powder was dissolved in 15 mL H<sub>2</sub>O and 2.1 g KOH (s) was added. The solution was kept stirred at 100 °C overnight then extracted with Et<sub>2</sub>O three times and dried with anhydrous Na<sub>2</sub>SO<sub>4</sub>. Then Et<sub>2</sub>O was removed by evaporator to give oil (the crude product **10b**) which was dissolved in 20 mL anhydrous EtOH again and added 5 mL concentrated HCl. After that all volatiles were removed to give some white powder which was washed with 30 mL EtOH and Et<sub>2</sub>O. Finally 2.52 g product **11b** was obtained in yield 63%. <sup>1</sup>H NMR (300 MHz, D<sub>2</sub>O) δ 7.34 (5H, s), 3.82 (2H, s), 3.51 (4H, s), 3.10 (4H, t, *J* = 5.8 Hz), 2.92 (4H, t, *J* = 5.8 Hz); <sup>13</sup>C NMR (75 MHz, D<sub>2</sub>O) δ 135.25, 130.23,

128.83, 128.33, 59.08, 47.68, 43.61, 42.20; ESI-MS: calcd. for C<sub>13</sub>H<sub>22</sub>N<sub>3</sub> [M + H]<sup>+</sup> 220.1808; found 220.1804.

### Compound **11c**

Compound **7** (3.2 g, 23.0 mmol) was dissolved in 12 mL anhydrous THF, then the solution of iodomethane (1.43 mL, 23.0 mmol) in 10 mL THF was dropwise added at 0 °C. The solution was kept stirred at RT for 1 d, and the white precipitate (product **8c**) was filtered and washed with anhydrous THF. The obtained white powder was dissolved in 30 mL H<sub>2</sub>O and kept it at 100 °C for 10 h. After water was removed and 30 mL EtOH and 5.0 g KOH was added to the mixture (the crude product **9c**). The suspension was kept stirred at 80 °C overnight. Ethanol was removed and 15 mL water was added, then it was extracted with Et<sub>2</sub>O and the organic solution was washed with brine and washed with anhydrous Na<sub>2</sub>SO<sub>4</sub>. Finally it was concentrated and dried under vacuum. The obtained light yellow oil (the crude product **10c**) was dissolved in 15 mL anhydrous MeOH and added 8 mL concentrated HCl to give white precipitate which was subsequently filtered and washed with MeOH and Et<sub>2</sub>O to give 4.09 g pink powder as product **11c** in yield 70.76%. <sup>1</sup>H NMR (300 MHz, D<sub>2</sub>O) δ 3.39 (4H, s), 3.20 (4H, t, *J* = 5.8 Hz), 2.92 (4H, t, *J* = 5.8 Hz), 2.47 (3H, s); <sup>13</sup>C NMR (75 MHz, D<sub>2</sub>O) δ 50.23, 42.77, 42.59, 41.76; ESI-MS: calcd. for C<sub>7</sub>H<sub>18</sub>N<sub>3</sub> [M + H]<sup>+</sup> 144.1495; found 144.1492.

### Synthesis of the synthons (20a-b)



### Compound **18a**

Compound **17** (20 g, 0.12 mol) was put in a 500 mL flask with 200 mL anhydrous EtOH, then thionyl chloride (66 mL, 0.91 mol) was dropwise added to the suspension

at RT. Afterwards the mixture was refluxed at 80 °C for 16 h. Excess SOCl<sub>2</sub> was distilled off then the left solution was poured on ice and extracted with DCM three times. The combined organic phase was washed with saturated NaHCO<sub>3</sub> twice and with brine once, then it was dried with anhydrous Na<sub>2</sub>SO<sub>4</sub> and was concentrated under vacuum, subsequently the obtained oil was washed with petroleum ether to give the target compound **18a** (25 g) in 93.6% yield. <sup>1</sup>H NMR (300 MHz, CDCl<sub>3</sub>) δ 9.33 (1H, *J* = 1.7 Hz), 8.44 (1H, dd, *J* = 8.1, 2.0 Hz), 8.20 (1H, d, *J* = 8.1 Hz), 4.56-4.43 (4H, m), 1.50-1.42 (6H, m); <sup>13</sup>C NMR (75 MHz, CDCl<sub>3</sub>) δ 164.54, 164.46, 151.13, 150.82, 138.19, 128.78, 124.60, 62.40, 61.93, 14.30, 14.24

#### Compound **19a**

Compound **18a** (5.0 g, 0.02 mol) was dissolved in 50 mL anhydrous EtOH, to the solution NaBH<sub>4</sub> (0.5 g, 0.013 mol) and anhydrous CaCl<sub>2</sub> (2.49 g, 0.02 mol) was added. The suspension was stirred at RT overnight then removed EtOH by evaporator. The obtained mixture was purified by chromatography on silica gel to give compound **19a** (3.36 g) in 82.7% yield. <sup>1</sup>H NMR (300 MHz, CDCl<sub>3</sub>) δ 9.15 (1H, d, *J* = 1.5 Hz), 8.28 (1H, dd, *J* = 8.1, 2.0 Hz), 7.38 (1H, d, *J* = 8.1 Hz), 4.84 (2H, s), 4.38 (2H, q, *J* = 7.1 Hz), 3.90 (1H, s), 1.40 (3H, t, *J* = 7.1 Hz); <sup>13</sup>C NMR (75 MHz, CDCl<sub>3</sub>) δ 165.15, 163.59, 149.91, 137.76, 125.18, 119.99, 64.30, 61.45, 14.27

#### Compound **20a**

Compound **19a** (1.75 g, 9.65 mmol) was mixed with 15 mL CCl<sub>4</sub>, to the suspension <sup>n</sup>Bu<sub>3</sub>P was dropwise added. The solution was stirred at RT for 30 min. The reaction was monitored by TLC. Afterwards solvent was removed by evaporator and the residual oil was purified by chromatography on silica gel to give 1.82 g light yellow oil as product **20a** in 94.3% yield. <sup>1</sup>H NMR (200 MHz, CDCl<sub>3</sub>) δ 9.03 (1H, s), 8.17 (1H, dd, *J* = 8.2, 2.0 Hz), 7.44 (1H, d, *J* = 8.2 Hz), 4.60 (2H, s), 4.24 (2H, q, *J* = 7.1 Hz), 1.26 (3H, t, *J* = 7.1 Hz); <sup>13</sup>C NMR (50 MHz, CDCl<sub>3</sub>) δ 164.34, 160.10, 150.05, 137.69, 125.16, 121.79, 61.07, 45.74, 13.82

### Compound **18b**

2, 5-pyridinedicarboxylic acid **17** (3.0 g, 0.018 mol) was added to 100 ml flask, to which 20 mL SOCl<sub>2</sub> was added. Compound **17** was not soluble in SOCl<sub>2</sub>. The mixture was refluxed for 24 h at 80 °C. The solid gradually disappeared. After that excess SOCl<sub>2</sub> was distilled off. To the obtained residue, 15 mL Benzyl Alcohol was added slowly and kept the reaction at 50 °C for 2 h. Distilled excess Benzyl alcohol off under vacuum by oil pump. The residue was dissolved with CHCl<sub>3</sub>, and washed with saturated Na<sub>2</sub>CO<sub>3</sub> solution. Once the Na<sub>2</sub>CO<sub>3</sub> solution was added, some precipitate was produced. I filtered it and separated the organic phase, then washed with saturated NaCl solution and dried with anhydrous Na<sub>2</sub>SO<sub>4</sub>, afterwards, removed solvent under vacuum to obtain the crude product which was washed with petroleum ether to get the target product **18b** without further purification in 85% yield. <sup>1</sup>H NMR (300 MHz, CDCl<sub>3</sub>) δ 9.38 (1H, dd, *J* = 2.0, 0.7 Hz), 8.44 (1H, dd, *J* = 8.1, 2.1 Hz), 8.20 (1H, dd, *J* = 8.1, 0.7 Hz), 7.53-7.36 (10H, m), 5.50 (2H, s), 5.44 (2H, s); <sup>13</sup>C NMR (75 MHz, CDCl<sub>3</sub>) δ 164.28, 151.06, 151.02, 138.32, 135.29, 135.18, 128.76, 128.68, 128.60, 128.42, 124.78, 67.95, 67.56; ESI-MS: calcd. for C<sub>21</sub>H<sub>18</sub>NO<sub>4</sub> [M + H] 348.1230; found 348.1222.

### Compound **19b**

To the solution of Dibenzylester **18b** (3.47 g, 0.01 mol) in 50 mL BnOH, NaBH<sub>4</sub> (0.45 g, 0.012 mol) was added at RT and kept it stirred for 16 h. After that 20 mL water was added and extracted the product with CH<sub>2</sub>Cl<sub>2</sub> three times. The organic phase was washed with saturated NaCl solution and dried with anhydrous Na<sub>2</sub>SO<sub>4</sub>. After Evaporation of CH<sub>2</sub>Cl<sub>2</sub>, the solution of the product in BnOH was put on the silica column, petroleum ether was used as eluent to remove BnOH, and CHCl<sub>3</sub> : MeOH = 30 : 1 to get the target compound **19b** in 80% yield. **OR** After Evaporation of CH<sub>2</sub>Cl<sub>2</sub>, the solution of the product in BnOH was treated to distill off most of BnOH under vacuum by oil pump, then purified the product by silica gel

chromatography.  $^1\text{H}$  NMR (300 MHz,  $\text{CDCl}_3$ )  $\delta$  9.20 (1H, s), 8.30 (1H, dd,  $J = 8.2, 2.0$  Hz), 7.46-7.34 (6H, m), 5.40 (2H, s), 4.83 (2H, s);  $^{13}\text{C}$  NMR (75 MHz,  $\text{CDCl}_3$ )  $\delta$  164.99, 163.54, 150.04, 137.85, 135.49, 128.71, 128.54, 128.35, 124.95, 119.97, 67.15, 64.21; ESI-MS: calcd. for  $\text{C}_{14}\text{H}_{14}\text{NO}_3$  [M + H] 244.0968; found 244.0969.

#### Compound **20b**

To the suspension of Compound **19b** (3.0 g, 0.012 mol) in 15 mL  $\text{CCl}_4$ , 4.6 mL  $^n\text{Bu}_3\text{P}$  was dropwise added. The solution was stirred at RT for 30 min. Evaporated  $\text{CCl}_4$  and purified the product by silica column to get the target compound **20b** in 90% yield.  $^1\text{H}$  NMR (300 MHz,  $\text{CDCl}_3$ )  $\delta$  9.18 (1H, dd,  $J = 2.1, 0.7$  Hz), 8.29 (1H, dd,  $J = 8.1, 2.1$  Hz), 7.52 (1H, d,  $J = 8.1$  Hz), 7.44-7.32 (5H, m), 5.37 (2H, s), 4.68 (2H, s);  $^{13}\text{C}$  NMR (75 MHz,  $\text{CDCl}_3$ )  $\delta$  164.68, 160.78, 150.65, 138.28, 135.47, 128.70, 128.53, 128.32, 125.32, 122.28, 67.18, 46.16; ESI-MS: calcd. for  $\text{C}_{14}\text{H}_{13}\text{ClNO}_2$  [M + H] 262.0629; found 262.0629.

### Synthesis of the ligands (**12a**, **13a**) from TACN hydrochloride

#### Compound **14a**

Hydrochloride of TACN **5** (0.5 g, 2.1 mmol) was dissolved in 15 mL solvent ( $\text{CH}_3\text{CN} : \text{H}_2\text{O} = 2 : 1$ ), to which the solution of ethyl chloromethylenepyridyl carboxylate (0.84 g, 4.2 mmol) in 25 mL solvent ( $\text{CH}_3\text{CN} : \text{H}_2\text{O} = 2 : 1$ ) was added, followed by another 20 mL  $\text{CH}_3\text{CN}$ . After the mixture was heated to  $60\text{ }^\circ\text{C}$ , the solution of  $\text{K}_2\text{CO}_3$  (1.45 g, 10.5 mmol) in 10 mL  $\text{H}_2\text{O}$  was dropwise added by syringe pump at the rate of 0.4 mL/h and the reaction was monitored by LCMS. When 2.8 mL basic solution was added, LCMS showed that the target compound was major. Afterwards it was continued to be added for 6 h at rate of 0.2 mL/h. (In all 4.0 mL  $\text{K}_2\text{CO}_3$  solution was added.) Heating was stopped then the mixture was cooled down and extracted with DCM (30 mL $\times$ 3). The combined organic phase was washed with brine and dried with anhydrous  $\text{Na}_2\text{SO}_4$ . Finally it was concentrated and purified by alumina

chromatography (DCM : MeOH = 50 : 1) to obtain 0.25 g dialkylated product **14a** (yellow oil) in yield 26.2%. <sup>1</sup>H NMR (300 MHz, CDCl<sub>3</sub>) δ 9.18 (1H, d, *J* = 1.5 Hz), 8.15 (1H, dd, *J* = 8.1, 2.1 Hz), 7.30 (1H, d, *J* = 8.1 Hz), 4.36 (2H, q, *J* = 7.1 Hz), 3.95 (2H, s), 3.26 (2H, t, *J* = 5.3 Hz), 3.02 (2H, t, *J* = 5.4 Hz), 2.70 (2H, s), 1.37 (3H, t, *J* = 7.1 Hz); <sup>13</sup>C NMR (75 MHz, CDCl<sub>3</sub>) δ 165.00, 162.46, 150.62, 137.79, 125.32, 122.41, 61.52, 60.75, 52.28, 49.39, 45.04, 14.26; ESI-MS: calcd. for C<sub>24</sub>H<sub>34</sub>N<sub>5</sub>O<sub>4</sub> [M + H] 456.2605; found 456.2600.

#### Compound **12a**

Compound **14a** (0.5 g, 1.10 mmol) was dissolved in the mixture of 5 mL CH<sub>3</sub>CN and 1 mL H<sub>2</sub>O, to the solution picolyl chloride hydrochloride (0.28 g, 1.65 mmol) and K<sub>2</sub>CO<sub>3</sub> (0.23 g, 1.65 mmol) was added. The solution was heated to 50 °C and kept it overnight. 5 mL water was added to the system and extracted with DCM three times, then washed with brine and dried with anhydrous Na<sub>2</sub>SO<sub>4</sub>. The obtained crude product after evaporation was purified by alumina chromatography and big TLC then 0.07 g yellow oil as the product **12a** in yield 11.6%. Its characterization was given later.

#### Compound **14b**

It was prepared through two ways from TACN:

Method a:

Hydrochloride of TACN **5** (0.5 g, 2.1 mmol) was dissolved in 15 mL solvent (CH<sub>3</sub>CN : H<sub>2</sub>O = 2 : 1), to which the solution of Benzyl chloromethylenepyridyl carboxylate (1.10 g, 4.2 mmol) in 25 mL solvent (CH<sub>3</sub>CN : H<sub>2</sub>O = 2 : 1) was added, followed by another 20 mL CH<sub>3</sub>CN. After the mixture was heated to 60 °C, the solution of K<sub>2</sub>CO<sub>3</sub> (1.45 g, 10.5 mmol) in 10 mL H<sub>2</sub>O was dropwise added by syringe pump at the rate of 0.4 mL/h and the reaction was monitored by LCMS. When 2.8 mL basic solution was added, the rate was changed to 0.2 mL/h and it was continued to be added for 5 h at that rate. (In all 3.8 mL K<sub>2</sub>CO<sub>3</sub> solution was added.) Heating was stopped then the

mixture was cooled down and extracted with DCM (30 mL×3). The combined organic phase was washed with brine and dried with anhydrous Na<sub>2</sub>SO<sub>4</sub>. Finally it was concentrated and purified by alumina chromatography (DCM : MeOH = 50 : 1) to give 0.16 g dialkylated product **14b** (yellow oil) in yield 13.1% and 0.5 g Benzyl chloromethylenepyridyl carboxylate was recycled.

Method b:

Hydrochloride of TACN **5** (0.5 g, 2.1 mmol) was dissolved in 20 mL solvent which consisted of 20 mL mixture (CH<sub>3</sub>CN : H<sub>2</sub>O = 2 : 1) and 10 mL CH<sub>3</sub>CN (100%), and it was heated to 60 °C. Then the solution of Benzyl chloromethylenepyridyl carboxylate (1.10 g, 4.2 mmol) in 10 mL solvent CH<sub>3</sub>CN and that of K<sub>2</sub>CO<sub>3</sub> (1.45 g, 10.5 mmol) in 10 mL H<sub>2</sub>O was at the same time dropwise added by syringe pump at the rate of 0.4 mL/h. The reaction was monitored by LCMS and alumina TLC. When 4.8 mL basic solution was added, the rate was changed to 0.1 mL/h and it was continued to be added for 20 h at that rate. (In all 6.8 mL K<sub>2</sub>CO<sub>3</sub> solution was added.) Heating was stopped then the mixture was cooled down and extracted with DCM (30 mL×3). The combined organic phase was washed with brine and dried with anhydrous Na<sub>2</sub>SO<sub>4</sub>. Finally it was concentrated and purified by alumina chromatography (DCM : MeOH = 50 : 1) to obtain 0.29 g dialkylated product **14b** (yellow oil) in yield 23.8% and 0.42 g Benzyl chloromethylenepyridyl carboxylate was recycled.

<sup>1</sup>H NMR (300 MHz, CDCl<sub>3</sub>) δ 9.26 (1H, d, *J* = 1.6 Hz), 8.23 (1H, dd, *J* = 8.1, 2.1 Hz), 7.51-7.36 (6H, m), 5.42 (2H, s), 4.00 (2H, s), 3.19 (2H, t, *J* = 5.5 Hz), 3.04 (2H, t, *J* = 5.3 Hz), 2.74 (2H, s); <sup>13</sup>C NMR (125MHz, CDCl<sub>3</sub>) δ 164.64, 163.05, 150.39, 137.50, 135.28, 128.42, 128.19, 128.04, 124.59, 122.30, 66.79, 61.06, 52.10, 49.83, 45.06; ESI-MS: calcd. for C<sub>34</sub>H<sub>38</sub>N<sub>5</sub>O<sub>4</sub> [M + H] 580.2918; found 580.2916.

Compound **13a**

Compound **14b** (0.4 g, 0.69 mmol) was dissolved in the mixture of 5 mL CH<sub>3</sub>CN and 1 mL H<sub>2</sub>O, to the solution picolyl chloride hydrochloride (0.17 g, 1.04 mmol) and

K<sub>2</sub>CO<sub>3</sub> (0.14 g, 1.04 mmol) was added. The solution was heated to 50 °C and kept it overnight. 5 mL water was added to the system and extracted with DCM three times, then washed with brine and dried with anhydrous Na<sub>2</sub>SO<sub>4</sub>. The obtained crude product after evaporation was purified by alumina chromatography and 0.38 g yellow oil as the product **13a** in yield 82.6%. Its characterization was given later.

The compound **13b** could not be prepared by using this method because of the production of the corresponding quaternary amine.

### Synthesis of the ligands (**15a-c**, **13a-b**) from *N*-functionalized TACN

#### Compound **12a**

Compound **11a** (0.6 g, 1.82 mmol) was dissolved in 10 mL NaOH (1 M), then it was extracted with DCM three times and the organic phase was washed with saturated NaCl solution and dried with anhydrous Na<sub>2</sub>SO<sub>4</sub>, subsequently it was concentrated and dried under vacuum to give 0.4 g light yellow oil which was directly used for alkylation.

The obtained oil (0.4 g, 1.82 mmol) was dissolved in 16 mL CH<sub>3</sub>CN and 4 mL H<sub>2</sub>O, to the solution ethyl chloromethylenepyridylcarbonate **20a** (0.54 g, 2.73 mmol) and K<sub>2</sub>CO<sub>3</sub> (0.5 g, 3.64 mmol) was added. The mixture was heated to 50 °C for 2 h. Afterwards it was added 10 mL H<sub>2</sub>O and extracted with DCM (20 mL×3). The obtained DCM solution was washed with brine and dried with anhydrous Na<sub>2</sub>SO<sub>4</sub>. After evaporation the crude product was purified by alumina chromatography (EA : MeOH = 100 : 5) to give 0.65 g yellow oil as the target product **12a** in overall yield 87.8% for two steps. <sup>1</sup>H NMR (300 MHz, CDCl<sub>3</sub>) δ 9.02 (2H, s), 8.42 (1H, d, *J* = 4.1 Hz), 7.57 (2H, d, *J* = 8.0 Hz), 7.65-7.57 (3H, m), 7.52 (1H, s), 7.13 (1H, t, *J* = 5.8 Hz), 4.31 (4H, q, *J* = 7.1 Hz), 3.98 (6H, s), 2.91 (12H, br), 1.33 (6H, t, *J* = 7.1 Hz) <sup>13</sup>C NMR (75MHz, CDCl<sub>3</sub>) δ 165.15, 150.26, 149.07, 137.43, 136.69, 128.62, 128.25, 124.92, 122.90, 61.34, 53.46, 14.23; ESI-MS: calcd. for C<sub>30</sub>H<sub>39</sub>N<sub>6</sub>O<sub>6</sub> [M + H]

547.3027; found 547.3029.

### Compound **15a**

The product **12a** (0.17 g, 0.31 mmol) was added 7 mL HCl (2 N), then heated to 70 °C and LCMS monitored the reaction. 34 h later heating was stopped and the reaction was cooled down to RT. Then all the volatiles were removed by evaporator and some toluene was used for complete removal of water to give 0.15 g pink power as product **15a** in yield 68.2%. <sup>1</sup>H NMR (300 MHz, D<sub>2</sub>O) δ 9.11 (2H, d, *J* = 1.5 Hz), 8.59 (1H, d, *J* = 2.0 Hz), 8.57 (1H, d, *J* = 2.0 Hz), 8.53 (1H, dd, *J* = 5.9, 1.0 Hz), 8.36 (1H, td, *J* = 7.9, 1.5 Hz), 8.06 (1H, d, *J* = 8.0 Hz), 7.85-7.80 (3H, m), 4.44 (4H, s), 4.23 (2H, s), 3.19 (4H, s), 3.13-3.09 (4H, m), 2.92-2.91 (4H, m); <sup>13</sup>C NMR (75 MHz, D<sub>2</sub>O) δ 166.32, 155.27, 152.14, 147.08, 146.95, 143.17, 141.34, 128.03, 127.45, 126.24, 125.74, 56.91, 55.54, 50.74, 48.50, 47.58; ESI-MS: calcd. for C<sub>26</sub>H<sub>31</sub>N<sub>6</sub>O<sub>4</sub> [M + H] 491.2401; found 491.2377.

### Compound **12b**

Compound **11b** (0.6 g, 1.83 mmol) was dissolved in 10 mL NaOH (1 M), then it was extracted with DCM three times and the organic phase was washed with saturated NaCl solution and dried with anhydrous Na<sub>2</sub>SO<sub>4</sub>, subsequently it was concentrated and dried under vacuum to give 0.4 g light yellow oil which was directly used for alkylation.

The obtained oil (0.4 g, 1.83 mmol) was dissolved in 16 mL CH<sub>3</sub>CN and 4 mL H<sub>2</sub>O, to the solution ethyl chloromethylenepyridylcarboxylate **20a** (0.27 g, 1.38 mmol) and K<sub>2</sub>CO<sub>3</sub> (0.55 g, 2.75 mmol) was added. The mixture was heated to 50 °C for 2 h. Afterwards it was added 10 mL H<sub>2</sub>O and extracted with DCM (20 mL×3). The obtained DCM solution was washed with brine and dried with anhydrous Na<sub>2</sub>SO<sub>4</sub>. After evaporation the crude product was purified by alumina chromatography (EA : MeOH = 100 : 4) to give 0.55 g yellow oil as the target product **12b** in overall yield

55.0% for two steps.  $^1\text{H}$  NMR (300 MHz,  $\text{CDCl}_3$ )  $\delta$  9.09 (2H, s), 8.22 (2H, d,  $J = 8.1$  Hz), 7.57 (2H, d,  $J = 8.2$  Hz), 7.27-7.29 (5H, m), 4.34 (4H, qd,  $J = 7.1, 1.1$  Hz), 3.86 (4H, s), 3.59 (2H, s), 2.92-2.71 (12H, m), 1.35 (6H, td,  $J = 7.1, 1.1$  Hz);  $^{13}\text{C}$  NMR (75 MHz,  $\text{CDCl}_3$ )  $\delta$  165.36, 165.18, 150.20, 140.05, 137.27, 129.02, 128.13, 128.09, 126.83, 124.54, 122.57, 64.48, 63.42, 61.21, 55.90, 55.82, 55.78, 14.30; ESI-MS: calcd. for  $\text{C}_{31}\text{H}_{40}\text{N}_5\text{O}_4$  [ $\text{M} + \text{H}$ ] 546.3075; found 546.3067.

#### Compound **15b**

The product **12b** (0.55 g, 1.01 mmol) was added 25 mL HCl (2 N), then heated to 70 °C and LCMS monitored the reaction. 28 h later heating was stopped and the reaction was cooled down to RT. Then all the volatiles were removed by evaporator and some toluene was used for complete removal of water to give 0.54 g pink power as product **15b** in yield 79.4%.  $^1\text{H}$  NMR (300 MHz,  $\text{D}_2\text{O}$ )  $\delta$  8.91 (2H, d,  $J = 2.0$  Hz), 8.58 (2H, dd,  $J = 8.2, 2.0$  Hz), 7.58 (2H, d,  $J = 8.2$  Hz), 7.44-7.32 (5H, m), 4.41 (2H, s), 4.21 (4H, s), 3.48 (4H, s), 3.17 (4H, br), 2.91 (4H, s);  $^{13}\text{C}$  NMR (75 MHz,  $\text{D}_2\text{O}$ )  $\delta$  166.13, 156.49, 146.43, 143.69, 130.94, 130.63, 129.69, 129.30, 128.20, 125.88, 60.52, 57.59, 51.16, 49.78, 47.97; ESI-MS: calcd. for  $\text{C}_{27}\text{H}_{32}\text{N}_5\text{O}_4$  [ $\text{M} + \text{H}$ ] 490.2449; found 490.2437.

#### Compound **12c**

Compound **11c** (0.8 g, 3.18 mmol) was dissolved in 8 mL NaOH (1 M), then it was extracted with DCM three times and the organic phase was washed with saturated NaCl solution and dried with anhydrous  $\text{Na}_2\text{SO}_4$ , subsequently it was concentrated and dried under vacuum to give 0.4 g colorless powder which was directly used for alkylation.

The obtained oil (0.4 g, 2.79 mmol) was dissolved in 16 mL  $\text{CH}_3\text{CN}$  and 4 mL  $\text{H}_2\text{O}$ , to the solution ethyl chloromethylenepyridylcarboxylate **20a** (0.84 g, 4.20 mmol) and  $\text{K}_2\text{CO}_3$  (0.77 g, 5.59 mmol) was added. The mixture was heated to 50 °C for 2 h. Afterwards it was added 10 mL  $\text{H}_2\text{O}$  and extracted with DCM (20 mL $\times$ 3). The

obtained DCM solution was washed with brine and dried with anhydrous  $\text{Na}_2\text{SO}_4$ . After evaporation the crude product was dissolved in a little bit volume of DCM (3 mL) and the solution was dropwise added to a lot of  $\text{Et}_2\text{O}$  (100 mL) to make most of quaternary amine precipitate. (three equivalents of ethyl chloromethylenepyridylcarboxylate **20a** was introduced on one equivalent of *N*-methyl TACN). The mixture was filtered and the filtration was concentrated to give some crude product which was purified subsequently by alumina chromatography (EA : EtOH = 100 : 5) to give 0.52 g yellow oil as the target product **12c** in overall yield 53.1% for two steps.  $^1\text{H}$  NMR (300 MHz,  $\text{CDCl}_3$ )  $\delta$  9.12 (2H, d,  $J = 1.6$  Hz), 8.22 (2H, dd,  $J = 8.1, 2.2$  Hz), 7.42 (2H, d,  $J = 8.0$  Hz), 4.39 (4H, q,  $J = 7.1$  Hz), 3.98 (4H, s), 3.72 (4H, s), 3.20 (4H, s), 2.91 (3H, s), 2.71 (4H, s), 1.41 (6H, t,  $J = 7.1$  Hz);  $^{13}\text{C}$  NMR (75 MHz,  $\text{CDCl}_3$ )  $\delta$  165.01, 162.57, 150.51, 137.67, 125.25, 122.98, 62.64, 61.54, 54.16, 50.97, 43.30, 14.28; ESI-MS: calcd. for  $\text{C}_{25}\text{H}_{36}\text{N}_5\text{O}_4$  [ $\text{M} + \text{H}$ ] 470.2762; found 470.2755.

#### Compound **15c**

The product **12c** (0.32 g, 0.68 mmol) was added 15 mL HCl (2 N), then heated to 70 °C and LCMS monitored the reaction. 37 h later heating was stopped and the reaction was cooled down to RT. Then all the volatiles were removed by evaporator and some toluene was used for complete removal of water to give 0.34 g brown powder as product **15c** in yield 40.6%.  $^1\text{H}$  NMR (300 MHz,  $\text{D}_2\text{O}$ )  $\delta$  9.01 (2H, d,  $J = 1.6$  Hz), 8.69 (2H, dd,  $J = 8.2, 1.6$  Hz), 7.87 (2H, d,  $J = 8.3$  Hz), 4.33 (4H, s), 3.44 (4H, s), 3.23 (4H, s), 2.98 (3H, s), 2.85 (4H, s);  $^{13}\text{C}$  NMR (75 MHz,  $\text{D}_2\text{O}$ )  $\delta$  165.61, 155.97, 145.40, 144.75, 128.55, 126.54, 57.22, 53.44, 50.17, 48.14, 44.12; ESI-MS: calcd. for  $\text{C}_{21}\text{H}_{28}\text{N}_5\text{O}_4$  [ $\text{M} + \text{H}$ ] 414.2136; found 414.2134.

#### Compound **13a**

It was synthesized directly from the TACN.3HCl.

Compound **11a** (0.2 g, 0.60 mmol) was dissolved in the mixture of 5 mL  $\text{CH}_3\text{CN}$  and

1 mL H<sub>2</sub>O, to the solution benzyl chloromethylenepyridylcarboxylate **20b** (0.32 g, 1.20 mmol) and K<sub>2</sub>CO<sub>3</sub> (0.17 g, 1.20 mmol) was added. The mixture was heated to 50 °C overnight. Afterwards it was added 10 mL H<sub>2</sub>O and extracted with DCM (20 mL×3). The obtained DCM solution was washed with brine and dried with anhydrous Na<sub>2</sub>SO<sub>4</sub>. Another batch in the same scale was carried out and treated in the same method. The extraction solutions of two batches were combined and after evaporation the crude product was purified by alumina chromatography (EA : MeOH = 30 : 1) to give 0.43 g yellow oil as the target product **13a** in yield 52.6%. <sup>1</sup>H NMR (300 MHz, CDCl<sub>3</sub>) δ 9.12 (2H, d, *J* = 1.7 Hz), 8.45 (1H, d, *J* = 4.1 Hz), 8.22 (2H, dd, *J* = 8.1, 2.1 Hz), 7.62-7.57 (3H, m), 7.46-7.24 (11H, m), 7.10-7.06 (1H, m), 5.34 (4H, s), 3.86 (4H, s), 3.80 (2H, s), 2.85 (12H, s); <sup>13</sup>C NMR (75 MHz, CDCl<sub>3</sub>) δ 165.26, 165.13, 160.16, 150.31, 148.86, 137.41, 136.29, 135.63, 128.62, 128.39, 128.22, 124.29, 123.21, 122.64, 121.88, 66.88, 64.72, 64.47, 55.90, 55.82. ESI-MS: calcd. for C<sub>40</sub>H<sub>43</sub>N<sub>6</sub>O<sub>4</sub> [M + H] 671.3340; found 671.3337.

#### Compound **13b**

Compound **11c** reacted with the synthon **20b** in the mixture of CH<sub>3</sub>CN and water in the presence of K<sub>2</sub>CO<sub>3</sub> produce the quaternary amine. So the corresponding ligand was synthesized under the condition of NaH/THF.

Compound **11c** (0.5 g, 1.99 mmol) was dissolved in 6 mL NaOH (1 M), then it was extracted with DCM three times and the organic phase was washed with saturated NaCl solution and dried with anhydrous Na<sub>2</sub>SO<sub>4</sub>, subsequently it was concentrated and dried under vacuum to give 0.18 g colorless powder which was directly used for alkylation.

The obtained oil (0.18 g, 1.26 mmol) was mixed with 10 mL THF, to the solution NaH (0.06 g, 2.52 mmol) was added under argon. Then the mixture was heated to 50 °C. The solution of benzyl chloromethylenepyridylcarboxylate **20b** (0.66 g, 2.52 mmol) in 4 mL THF was added. The reaction was kept at 50 °C overnight. Afterwards it was added 10 mL H<sub>2</sub>O and extracted with DCM (20 mL×3). The obtained DCM

solution was washed with brine and dried with anhydrous  $\text{Na}_2\text{SO}_4$ . After evaporation the crude product was purified subsequently by twice alumina chromatography (EA : DCM : MeOH = 50 : 50 : 2) to give 0.24 g yellow oil as the target product **13b** in overall yield 32% for two steps.  $^1\text{H}$  NMR (300 MHz,  $\text{CDCl}_3$ )  $\delta$  9.13 (2H, d,  $J = 1.6$  Hz), 8.21 (2H, dd,  $J = 8.1, 2.1$  Hz), 7.46-7.36 (12H, m), 5.38 (4H, s), 5.30 (2H, s), 3.94 (6H, s), 3.17 (4H, s), 2.86 (3H, s), 2.65 (4H, s);  $^{13}\text{C}$  NMR (75 MHz,  $\text{CDCl}_3$ )  $\delta$  164.87, 162.85, 150.64, 137.80, 135.44, 128.72, 128.58, 128.42, 124.95, 123.05, 67.20, 62.81, 54.19, 53.44, 51.35, 43.37. ESI-MS: calcd. for  $\text{C}_{35}\text{H}_{40}\text{N}_5\text{O}_4$  [ $\text{M} + \text{H}$ ] 594.3075; found 594.3049.

### Synthesis of the complexes

#### Complex **16a**

The compound **13a** (0.75 g, 1.12 mmol) was dissolved in 2.5 mL degassed anhydrous EtOH, then the solution of  $\text{Fe}(\text{BF}_4)_2 \cdot 6\text{H}_2\text{O}$  (0.38 g, 1.12 mmol) in 1.5 mL degassed anhydrous EtOH was dropwise added. The solution became brown from yellow and the reaction was monitored by LCMS. 10 min later there was a lot of precipitate which was subsequently filtered and washed with anhydrous EtOH and diethyl ether to give 0.9 g crude product. Then 0.5 g red powder was crystallized in acetonitrile by gas diffusion of THF to give 0.4 g dark crystals as the complex **16a**, but I did not succeed in obtaining monocrystals thus I do not have its X-Ray Diffraction analysis.  $^1\text{H}$  NMR (500 MHz,  $\text{D}_2\text{O}$ )  $\delta$  8.41 (1H, d,  $J = 7.9$  Hz), 8.28 (1H, d,  $J = 7.9$  Hz), 7.83 (1H, t,  $J = 7.5$  Hz), 7.79 (1H, d,  $J = 7.9$  Hz), 7.68 (2H, d,  $J = 6.7$  Hz), 7.63 (2H, s), 7.44 (3H, s), 7.38 (3H, s), 7.31 (3H, s), 7.26 (3H, s), 5.28-5.18 (4H, m), 4.75 (3H, s), 4.22-4.13 (3H, s), 3.58 (2H, s), 3.40 (4H, s), 3.19-3.16 (3H, m), 3.29 (3H, s); ESI-MS: calcd. for  $\text{C}_{40}\text{H}_{42}\text{FeN}_6\text{O}_4$  [ $\text{M} + 2\text{H}$ ]/2 363.1303; found 363.1297.

#### Complex **16b**

The compound **13b** (0.36 g, 0.61 mmol) was dissolved in 1.5 mL degassed anhydrous MeOH, then the solution of  $\text{Fe}(\text{BF}_4)_2 \cdot 6\text{H}_2\text{O}$  (0.21 g, 0.61 mmol) in 0.5 mL degassed anhydrous MeOH was dropwise added. There was some sticky product was produced. The reaction was stirred under argon and monitored by LCMS. 12 h later there was

some precipitate which was subsequently filtered and washed with iPrOH and diethyl ether to give 0.2 g yellow powder as the crude product **16b**. When I tried to purified it by  $C_{18}$ , the most of the product was absorbed and the obtained a little of powder was not very pure which was shown by LCMS. Thus there was no further characterization.

### Complex **16c**

It was synthesized by two ways:

1) Hydrochloride of ligand **15a** (0.3 g) was dissolved in 2.0 mL degassed anhydrous MeOH under argon, then the solution of  $Fe(BF_4)_2 \cdot 6H_2O$  (0.143 g) in 1.0 mL MeOH was dropwise added. The mixture became dark red from a little pink. After that 0.7 mL solution of  $Et_3N$  in MeOH (which was prepared with 0.35 mL  $Et_3N$  dissolved in 1.0 mL MeOH ) was dropwise added and it was monitored by LCMS. In an hour it showed that there was no ligand any more in the solution, 6.0 mL  $Et_2O$  was added to produce some precipitate which was subsequently filtered and washed with iPrOH and anhydrous  $Et_2O$  to give 0.24 g red powder as low-spin complex.  $^1H$  NMR (500 MHz,  $D_2O$ )  $\delta$  8.30 (2H, t,  $J = 7.5$  Hz), 7.85 (1H, t,  $J = 7.6$  Hz), 7.74-7.70 (4H, m), 7.62 (1H, d,  $J = 7.8$  Hz), 7.32 (1H, d,  $J = 4.9$  Hz), 7.23 (1H, t,  $J = 6.4$ Hz), 4.22 (4H, d,  $J = 15.5$  Hz), 3.57 (3H, s), 3.37 (4H, s), 3.08 (4H, d,  $J = 12.8$  Hz), 2.29 (3H, s); ESI-MS: calcd. for  $C_{26}H_{30}FeN_6O_4 [M + 2H]/2$  273.0833; found 273.0841.

Or it was prepared in degassed anhydrous EtOH. Compound **15a** (0.38 g) was dissolved in 3.0 mL degassed anhydrous EtOH under argon, then the solution of  $Fe(BF_4)_2 \cdot 6H_2O$  (0.18 g) in 1.0 mL EtOH was dropwise added. With increasing of its addition, Some white precipitate was produced and became red but when addition of the solution of  $Fe(BF_4)_2 \cdot 6H_2O$  was finished, the precipitate completely disappeared. Afterwards  $Et_3N$  (0.45 mL) was dropwise added and a lot of precipitate was produced again but LCMS monitored the solution which did not give any signal, neither that of the ligand nor the complex. 30 min later, the precipitate was filtered and washed with iPrOH and anhydrous  $Et_2O$  to give 0.20 g dark red powder as the complex **16c** which was used for other analysis.  $^1H$  NMR (500 MHz,  $D_2O$ )  $\delta$  8.30 (2H, s), 7.85 (1H, s),

7.71 (4H, s), 7.62 (1H, s), 7.31 (1H, s), 7.24 (1H, s), 4.23 (4H, s), 3.58 (3H, s), 3.35 (4H, s), 3.08 (4H, s), 2.28 (3H, s); ESI-MS: calcd. for  $C_{26}H_{30}FeN_6O_4$   $[M + 2H]/2$  273.0833; found 273.0839.

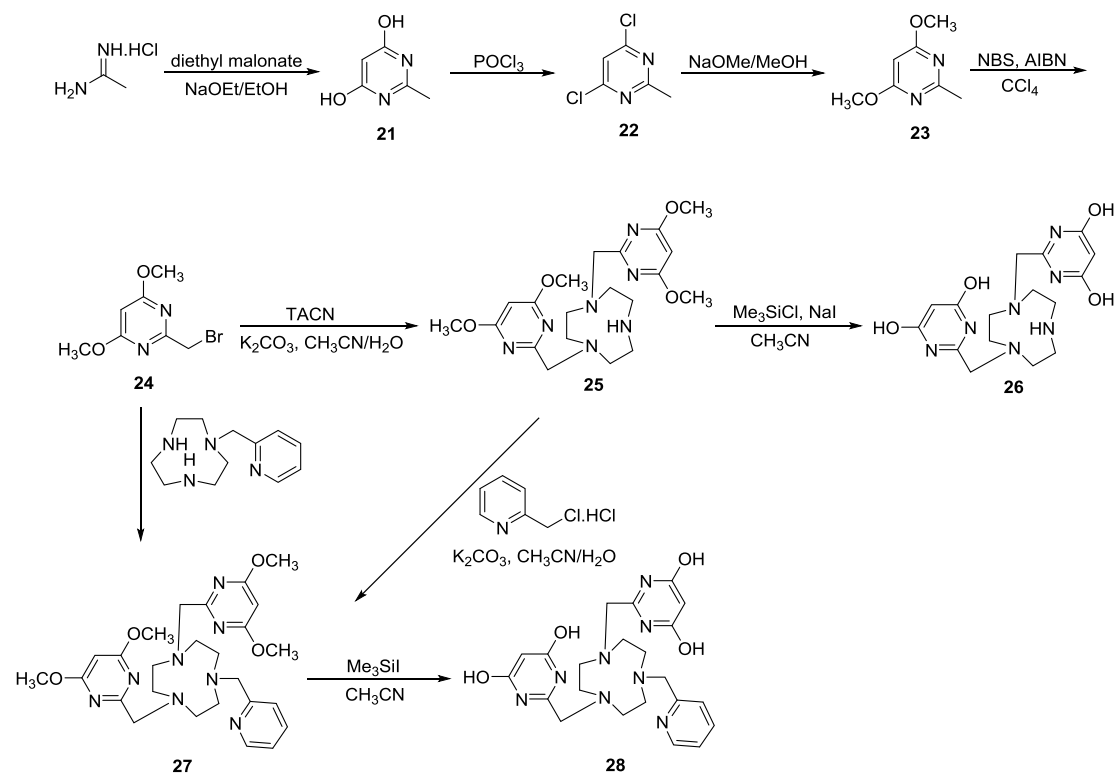
2) The complex with benzyl ester groups **16a** (0.3 g) was dissolved in 10 mL  $CH_3CN$  and 10 mL  $H_2O$ , then 30 mg Pd/C (5%) was added and  $H_2$  bubbled in the flask. The reaction was kept stirred at rt for 4 h and LCMS showed that the reaction had finished. Then the mixture was filtered on celite and the filtrate was evaporated and made the product dry by oil pump to give 0.2 g red powder.  $^1H$  NMR (500 MHz,  $D_2O$ )  $\delta$  8.22 (2H, t,  $J = 9.2$  Hz), 7.83 (1H, t,  $J = 7.2$  Hz), 7.71-7.65 (4H, m), 7.60 (1H, d,  $J = 7.9$  Hz), 7.32 (1H, s), 7.23 (1H, s), 4.23 (4H, s), 3.56 (3H, s), 3.35 (4H, s), 3.07 (4H, s), 2.28 (3H, s); ESI-MS: calcd. for  $C_{26}H_{30}FeN_6O_4$   $[M + 2H]/2$  273.0833; found 273.0837.

#### Complex **16d**

The hydrochloride of the ligand **15b** (0.25 g) was dissolved in degassed solvent mixture of 1.0 mL MeOH and 2.0 mL  $CH_3CN$  under argon, subsequently  $Et_3N$  (0.36 mL) was dropwise added to neutralize HCl completely. The solution was light brown. Then solution of  $Fe(BF_4)_2$  (0.125 g) in 1.0 mL MeOH was dropwise added, but also the rinse solution (1.0 mL MeOH) of iron (II) salt. The mixture became dark. The reaction was kept at RT overnight, but there was still no precipitate. After 15 mL  $Et_2O$  was added, it produced some oil stuff which looked like resin. Then decanted all the upper solution and the rest was added with  $Et_2O$  again to make it powder which was subsequently purified by  $C_{18}$  ( $H_2O : CH_3CN = 100 : 10$ ) to give 110 mg dark yellow or brown powder. 30 mg powder was dissolved in 3.0 mL MeOH and 5% water, then it was crystallized by gas diffusion with  $Et_2O$ . Two days later there was precipitate which was afterwards filtered and the filtrate was concentrated by evaporator. During evaporation there were crystals produced in the flask then they were filtered to give 20 mg needle dark yellow crystals as the complex **16d**. Both the powder and the crystals were used for the further analysis. ESI-MS: calcd. for  $C_{27}H_{31}FeN_5O_4$   $[M + 2H]/2$  272.5857; found 272.5867.

## Synthesis II

The following scheme is showing the synthetic route of the ligands and the complexes based on the 4, 6-pyrimidinediol.



### Compound **21**

To the solution of EtONa in anhydrous EtOH, which was prepared with sodium (7.59 g, 0.33 mol) in 190 mL EtOH, acetamidine hydrochloride (10.00 g, 0.11 mol) was added under argon and the mixture was stirred for 10 min. Diethyl malonate (14.0 mL, 0.09 mol) was injected. The resulting mixture was heated to 85 °C and kept for 2 h. Then it came back to the ambient temperature, and 215 mL distilled water was added to make the suspension clear. After that 20 mL concentrated HCl was dropwise added to it and 10.57 g white precipitate as the product **21** was obtained by filtering and washing with anhydrous EtOH and Et<sub>2</sub>O in yield 91%. <sup>1</sup>H NMR (200 MHz, DMSO-d<sub>6</sub>) δ 11.69 (2H, s), 4.97 (1H, s), 2.22 (3H, s).

### Compound **22**

Compound **21** (2.5 g, 0.02 mol) was dissolved in 15 mL POCl<sub>3</sub> and heated to 140°C. 3 h later the excessive POCl<sub>3</sub> was distilled and the residue was poured onto crushed ice. The mixture was extracted with dichloromethane and the organic phase was washed with saturated brine, dried with anhydrous Na<sub>2</sub>SO<sub>4</sub> and concentrated under pressure. The crude product was purified by silica gel column chromatography (PE : EA = 100 : 1) to afford 2.1 g white solid as the product **22** in yield 65%.

#### Compound **23**

Compound **22** (8.00 g, 0.05 mol) was added into the solution of MeONa in MeOH which was prepared with sodium (2.25 g, 0.1 mol) in 100 mL MeOH. The suspension was refluxed for 3 h, and poured to 200 mL distilled water. The mixture was extracted with dichloromethane and the organic phase was dried with anhydrous Na<sub>2</sub>SO<sub>4</sub> and concentrated under pressure. The crude product was purified by silica gel column chromatography (PE : EA = 100 : 1) and gave 6.51 g white solid as the compound **23** in yield 86.0%. <sup>1</sup>H NMR (300 MHz, CDCl<sub>3</sub>) δ 5.84 (1H, s), 3.91 (6H, s), 2.52 (3H, s); <sup>13</sup>C NMR (75 MHz, CDCl<sub>3</sub>) δ 171.39, 167.55, 86.40, 53.90, 25.86.

#### Compound **24**

To the solution of compound **23** (2.78 g, 0.02 mol) in 60 mL anhydrous CCl<sub>4</sub>, N-bromosuccinimide (3.56 g, 0.02 mol) and azodiisobutyronitrile (AIBN) (0.49 g, 0.003 mol) were added. The suspension was heated to 70 °C and kept for 20 h. After that the mixture was filtered and the filtrate was concentrated under pressure. The resulting residue was purified by silica gel column chromatography (PE : EA = 100 : 1) to give 0.9 g colorless solid as the product **24** in yield 21.4%. <sup>1</sup>H NMR (200 MHz, CDCl<sub>3</sub>) δ 5.92 (1H, s), 4.39 (2H, s), 3.95 (6H, s); <sup>13</sup>C NMR (50 MHz, CDCl<sub>3</sub>) δ 171.56, 164.85, 88.49, 54.09, 33.68.

#### Compound **25**

2-bromomethyl-4,6-dimethoxypyrimidine **24** (0.98 g, 4.2 mmol) and 1,4,7-Triazacyclononane. 3HCl (Compound **5**) (0.5 g, 2.1 mmol) were dissolved in 40

mL mixture of acetonitrile and distilled water (V/V = 2 : 1), then 20 mL CH<sub>3</sub>CN was added to it. To the resulting solution, K<sub>2</sub>CO<sub>3</sub> (1.45 g, 10.5 mmol) was dissolved in 10 mL distilled water and added using syringe pump. LCMS monitored the reaction. 7 h later the target product is major and there was no trisubstituted product. We stopped the reaction and 6.5 mL solution of K<sub>2</sub>CO<sub>3</sub> in water was left. Acetonitrile was removed by rotary evaporator, the residue was extracted with dichloromethane and the organic phase was washed with saturated brine and dried with anhydrous Na<sub>2</sub>SO<sub>4</sub>. then it was concentrated under pressure and purified by aluminium oxide column chromatography (PE : EA : MeOH = 10 : 1 : 0.5) to afford 0.28 g white solid as the product **25** in yield 30.7%. <sup>1</sup>H NMR (200 MHz, CDCl<sub>3</sub>) δ 5.81 (1H, s), 3.83 (6H, s), 3.77 (2H, s), 3.17 (2H, d, *J* = 4.80 Hz), 3.08 (2H, d, *J* = 4.60 Hz), 2.75 (2H, s); <sup>13</sup>C NMR (50 MHz, CDCl<sub>3</sub>) δ 171.35, 167.26, 87.32, 59.87, 54.10, 51.63, 48.78, 44.55; HRMS: calcd. for C<sub>24</sub>H<sub>34</sub>N<sub>5</sub>O<sub>4</sub> [M + H] 456.2605; found 456.2600.

#### Compound **26**

To the suspension of compound **25** (0.05 g, 0.12 mmol) and NaI (0.35 g, 2.3 mmol) in 8 mL anhydrous CH<sub>3</sub>CN, Me<sub>3</sub>SiCl (0.3 mL, 2.3 mmol) was dropwise added. The mixture was refluxed for 24 h at 80 °C. After that acetonitrile was removed using rotatory evaporator and the residue was added with 5 mL distilled water. Some dark precipitate was filtered and washed with saturated Na<sub>2</sub>S<sub>2</sub>O<sub>4</sub>, anhydrous EtOH and Et<sub>2</sub>O to give 10 mg white solid as the product **26** in yield 23.0%. <sup>1</sup>H NMR (500 MHz, D<sub>2</sub>O) δ 4.79 (1H, s), 3.95 (2H, s), 3.25 (2H, s), 3.04 (2H, s), 2.82 (2H, s); <sup>13</sup>C NMR (125 MHz, D<sub>2</sub>O) δ 167.55, 161.11, 95.15, 56.00, 50.27, 47.33, 43.65; HRMS: calcd. for C<sub>16</sub>H<sub>24</sub>N<sub>7</sub>O<sub>4</sub> [M + H] 378.1884; found 378.1881.

#### Compound **27**

Compound **11a** (0.3 g, 0.91 mmol) was dissolved in 10 mL NaOH (1 M), then it was extracted with DCM three times and the organic phase was washed with saturated NaCl solution and dried with anhydrous Na<sub>2</sub>SO<sub>4</sub>, subsequently it was concentrated

and dried under vacuum to give 0.20 g light yellow oil which was directly used for alkylation.

The obtained oil (0.20 g, 0.91 mmol) was dissolved in 8 mL CH<sub>3</sub>CN and 2 mL H<sub>2</sub>O, to the solution 2-bromomethyl-4,6-dimethoxypyrimidine **24** (0.32 g, 1.37 mmol) and K<sub>2</sub>CO<sub>3</sub> (0.25 g, 1.82 mmol) was added. The mixture was heated to 50 °C and kept it for 2 h. Afterwards it was added 10 mL H<sub>2</sub>O and extracted with DCM (20 mL×3). The obtained DCM solution was washed with brine and dried with anhydrous Na<sub>2</sub>SO<sub>4</sub>. After evaporation the crude product was purified by alumina chromatography (EA : MeOH = 100 : 5) to give 0.20 g yellow oil as the target product **27** in overall yield 55.6% for two steps. <sup>1</sup>H NMR (300 MHz, CDCl<sub>3</sub>) δ 8.58 (1H, d, *J* = 4.6 Hz), 7.75-7.7.66 (2H, m), 7.25 (1H, d, *J* = 5.5 Hz), 5.91 (2H, s), 4.45 (2H, s), 3.94 (4H, s), 3.90 (12H, s), 3.45 (4H, s), 3.24 (4H, s), 3.08 (4H, s); <sup>13</sup>C NMR (75 MHz, CDCl<sub>3</sub>) δ 171.48, 166.84, 149.44, 137.10, 124.49, 123.26, 87.71, 60.71, 54.22, 52.53, 21.05, 14.19; HRMS: calcd. for C<sub>26</sub>H<sub>37</sub>N<sub>8</sub>O<sub>4</sub> [M + H] 525.2932; found 525.2910.

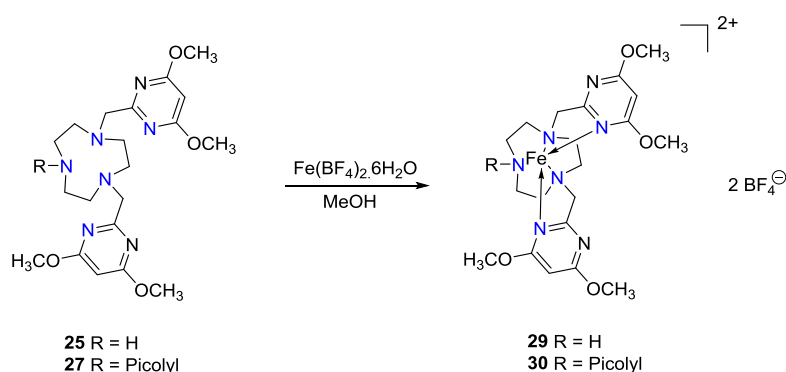
The compound **27** was also synthesized from **25**. The compound **25** (0.2 g, 0.46 mmol) was dissolved in the mixture of 7.5 mL CH<sub>3</sub>CN and 7.5 mL H<sub>2</sub>O, to the solution the picolyl chloride hydrochloride (0.08 g, 0.46 mmol) and K<sub>2</sub>CO<sub>3</sub> (0.10 g, 0.72 mmol) was added then the mixture was heated to 60 °C and kept it for 3 h. Afterwards 10 mL water was added and the product was extracted with DCM three times and the combined organic phase was washed with brine and dried with anhydrous Na<sub>2</sub>SO<sub>4</sub>. After evaporation the crude product was purified by alumina chromatography (DCM : MeOH = 100 : 1), 0.19 g yellow oil was obtained in yield 79.2%.

#### Compound **28**

The compound **27** (0.12 g, 0.23 mmol) was dissolved in 10 mL anhydrous CH<sub>3</sub>CN, Me<sub>3</sub>SiI (0.65 mL, 4.58 mmol) was dropwise added under argon. The mixture was refluxed for 24 h at 80 °C. After that acetonitrile was removed using rotatory evaporator and the residue was added with 5 mL EtOH. The mixture was stirred at RT

for 15 min then EtOH was removed and Et<sub>2</sub>O was added to make it be yellow precipitate (89 mg, the product **28**, yield 83.2%) which was characterized by NMR and HRMS. <sup>1</sup>H NMR (300 MHz, DMSO-d<sub>6</sub>) δ 8.81 (1H, d, *J* = 4.4 Hz), 8.08 (1H, t, *J* = 7.7 Hz), 7.79 (1H, d, *J* = 7.8 Hz), 7.65 (1H, t, *J* = 6.4 Hz), 5.27 (2H, s), 4.55 (2H, s), 3.83 (4H, s), 3.23 (4H, s), 3.01 (4H, s), 2.94 (4H, s); <sup>13</sup>C NMR (75 MHz, DMSO-d<sub>6</sub>) δ 167.21, 159.77, 152.09, 148.04, 140.80, 125.89, 125.18, 89.08, 58.13, 56.26, 55.41, 50.86, 50.24, 48.65; HRMS: calcd. for C<sub>22</sub>H<sub>29</sub>N<sub>8</sub>O<sub>4</sub> [M + H] 469.2306; found 469.2293.

### Synthesis of the complexes



#### Compound **29**

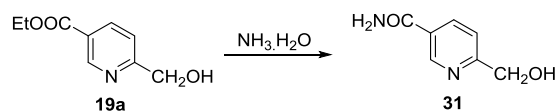
The ligand **25** (0.2 g, 0.46 mmol) was dissolved in 0.6 mL degassed anhydrous MeOH, then the solution of Fe(BF<sub>4</sub>)<sub>6</sub>·6H<sub>2</sub>O (0.31 g, 0.92 mmol) in 0.5 mL degassed anhydrous MeOH was dropwise added. The solution was stirred and kept at RT overnight. LCMS monitored the reaction to make sure it was completely finished. The precipitate was filtered and washed with MeOH, iPrOH and Et<sub>2</sub>O to give 0.15 g yellow powder which was subsequently crystallized in acetonitrile by gas diffusion of Et<sub>2</sub>O. Some crystals grew up like small needles but their quality was not good enough to do XRD characterization.

#### Compound **30**

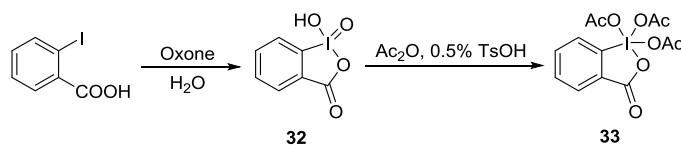
The ligand **27** (0.18 g, 0.30 mmol) was dissolved in 0.5 mL degassed anhydrous MeOH, then the solution of Fe(BF<sub>4</sub>)<sub>6</sub>·6H<sub>2</sub>O (0.10 g, 0.30 mmol) in 0.4 mL degassed anhydrous MeOH was dropwise added. The solution became green and it was stirred at RT overnight. LCMS monitored the reaction until the ligand was totally consumed. 2.5 mL Et<sub>2</sub>O was added to make the complex precipitate which was filtered and washed with iPrOH and Et<sub>2</sub>O to give 168 mg green powder. It was crystallized in acetonitrile by gas diffusion of Et<sub>2</sub>O to give prismatic green crystals for XRD.

### Synthesis III

Some other successful synthesis relative to my project, maybe it is useful for further research.



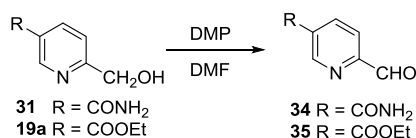
Compound **19a** (0.5 g, 2.76 mmol) was mixed with 5 mL ammonia water (37%), and it was stirred at RT overnight. **19a** was gradually dissolved then some precipitate was produced which was filtered and washed with a little of EtOH to give 0.41 g white compound **31** in yield 98% after the starting material was completely consumed. <sup>1</sup>H NMR (300 MHz, D<sub>2</sub>O) δ 8.71 (1H, d, *J* = 1.7 Hz), 8.07 (1H, dd, *J* = 8.2, 2.1 Hz), 7.47 (1H, d, *J* = 8.2 Hz), 4.65 (2H, s); <sup>13</sup>C NMR (75 MHz, D<sub>2</sub>O) δ 163.02, 147.40, 138.85, 137.16, 127.84, 120.94, 63.71; ESI-MS: calcd. for C<sub>7</sub>H<sub>8</sub>N<sub>2</sub>NaO<sub>2</sub> [M + Na] 175.0478; found 175.0473.



Oxone (90.5 g, 0.15 mol) was put in 325 mL water, then 2-Iodobenzoic acid (25 g, 0.1

mol) was added. The suspension was stirred in the opened system which was heated slowly to 70 °C and kept it for 3 h. Then the mixture was cooled down to 5 °C in an ice bath and stirred for 1.5 h at this temperature. Subsequently the precipitate was filtered and washed with water (50 mL ×6) then acetone (50 mL×2) to give 23.5 g white powder as the product **32** in yield 83.3%. <sup>1</sup>H NMR (300 MHz, DMSO-d<sub>6</sub>) δ 8.14 (1H, d, *J* = 7.8 Hz), 8.05-8.01 (2H, m), 7.83 (1H, t, *J* = 7.2 Hz).

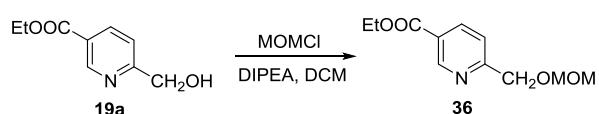
Compound **32** (20 g, 0.07 mol) was dissolved in 80 mL Ac<sub>2</sub>O in the presence of TsOH.H<sub>2</sub>O (0.1 g, 0.5 mmol). The mixture was heated to 80 °C and kept it for 2 h. The system was cooled down and put in an ice bath to make the product precipitate which was filtered and washed with anhydrous Et<sub>2</sub>O to give 21.45 g white powder as the product **33** in yield 70.8%. <sup>1</sup>H NMR (300 MHz, CDCl<sub>3</sub>,) δ 8.29 (2H, td, *J* = 7.7, 1.5 Hz), 8.06 (1H, td, *J* = 7.8, 1.5 Hz), 7.90 (1H, td, *J* = 7.4, 0.8 Hz), 2.35 (3H, s), 2.02 (6H, s)



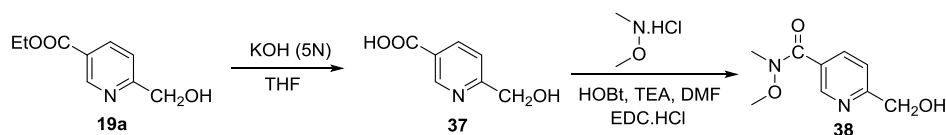
Compound **31** (0.2 g, 1.30 mmol) was dissolved in 10 mL DMF, to the solution DMP **33** (0.84 g, 1.97 mmol) was added. There was some precipitate was produced. The mixture was stirred at RT overnight. Then the precipitate was filtered and the filtrate was concentrated and purified by silica gel chromatography (DCM : MeOH = 30 : 1) to give the compound **34** in yield 60%. <sup>1</sup>H NMR (300 MHz, D<sub>2</sub>O) δ 9.90 (1H, s), 8.95 (1H, s), 8.77 (3H, s), 8.28 (1H, d, *J* = 8.1 Hz), 8.13 (3H, dd, *J* = 8.2, 1.9 Hz), 7.99 (1H, d, *J* = 8.1 Hz), 7.61 (3H, d, *J* = 8.2 Hz), 5.94 (3H, s). Seen from its H NMR, 25% of product was converted to its acetal form in D<sub>2</sub>O. ESI-MS: calcd. for C<sub>7</sub>H<sub>6</sub>N<sub>2</sub>NaO<sub>2</sub> [M + Na] 173.0321; found 173.0315.

Compound **31** (2.0 g, 0.01 mol) was dissolved in 30 mL DCM, to the solution DMP **33** (7.02 g, 0.02 mmol) was added. The mixture was stirred at RT overnight. Then 20

mL saturated NaHCO<sub>3</sub> was added to neutralize it and extracted with DCM. The combined organic phase was washed with brine and dried with anhydrous Na<sub>2</sub>SO<sub>4</sub>, then concentrated and purified by silica gel chromatography (PE : EA = 10 : 1) to give the compound **35** in yield 65.8%. <sup>1</sup>H NMR (300 MHz, CDCl<sub>3</sub>) δ 10.15 (1H, d, *J* = 0.8 Hz), 9.37 (1H, dd, *J* = 2.0, 0.8 Hz), 8.47 (1H, d, *J* = 1.2 Hz), 8.02 (1H, dd, *J* = 8.0, 0.8 Hz), 4.43 (2H, q, *J* = 7.1 Hz), 1.42 (3H, t, *J* = 7.1 Hz); <sup>13</sup>C NMR (75 MHz, CDCl<sub>3</sub>) δ 192.66, 164.34, 154.84, 151.19, 138.29, 129.55, 121.07, 62.04, 14.23

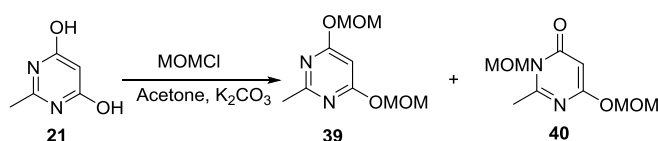


To the solution of compound **19a** (0.2 g, 1.10 mmol) in 10 mL DCM, DIPEA (0.21 g, 1.66 mmol) and MOMCl (0.13 g, 1.66 mmol) was added. The mixture was stirred at RT overnight, then the solvent was removed by evaporator to give the crude product which was purified by silica gel chromatography. 44 mg product was obtained as the compound **36** in yield 17.6%. <sup>1</sup>H NMR (CDCl<sub>3</sub>, 300 MHz) δ 9.15 (1H, s), 8.28 (1H, d, *J* = 8.2, 2.1 Hz), 7.53 (1H, d, *J* = 8.2 Hz), 4.79 (2H, s), 4.77 (2H, s), 4.37 (2H, q, *J* = 7.1 Hz), 3.42 (3H, s), 1.38 (3H, t, *J* = 7.1 Hz); <sup>13</sup>C NMR (CDCl<sub>3</sub>, 75 MHz) δ 165.23, 162.65, 150.35, 137.71, 125.01, 120.54, 96.48, 69.90, 61.35, 55.58, 14.26.

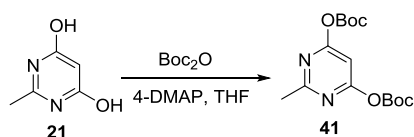


Compound **19a** (0.2 g, 1.10 mol) was dissolved in 5 mL THF, then 0.43 mL KOH (5N) was added and the mixture was stirred at for 3 h. Afterwards the solvent was removed by rotary evaporator to give some white powder which consisted of excess KOH and potassium salt of compound **37**. This mixture was directly used for its condensation with *N*-methoxymethylamine hydrochloride (0.13 g, 1.33 mmol) in 10 mL DMF. At the same time, Et<sub>3</sub>N (1.5 mL), HOBt (0.18 g, 1.33 mmol) and EDC.HCl (0.32 g, 1.65

mmol) were added. The mixture was stirred at RT overnight then 10 mL water was added and extracted with DCM. The crude product obtained after evaporation was purified by silica gel chromatography to give 83 mg product as the compound **38** in overall yield 38.2%.  $^1\text{H}$  NMR (300 MHz,  $\text{CDCl}_3$ )  $\delta$  8.92 (1H, d,  $J = 2.0$  Hz), 8.04 (1H, dd,  $J = 8.1, 1.5$  Hz), 7.34 (1H, d,  $J = 8.1$  Hz), 4.83 (2H, s), 3.57 (3H, t,  $J = 1.4$  Hz), 3.40 (3H, t,  $J = 1.6$  Hz);  $^{13}\text{C}$  NMR (75 MHz,  $\text{CDCl}_3$ )  $\delta$  167.21, 161.38, 148.42, 137.01, 128.49, 119.65, 64.22, 61.29, 33.20.



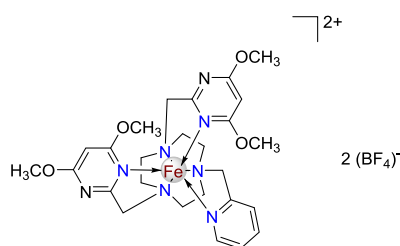
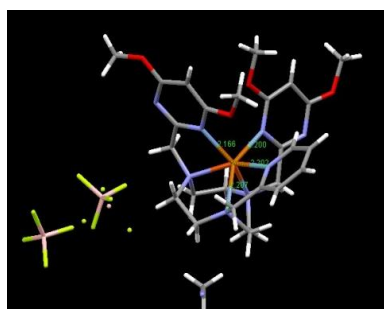
To the suspension of compound **21** (0.5 g, 3.97 mmol) in 15 mL acetone,  $\text{K}_2\text{CO}_3$  (1.10 g, 7.90 mmol) and MOMCl (0.64 g, 7.90 mmol) were added. The mixture was stirred at RT for 12 h, then it was filtered and the filtrate was made dry by evaporator, followed by purification by silica gel chromatography. The product **39** (0.18 g) was obtained when the eluent PE : EA = 20 : 1 was used  $^1\text{H}$  NMR (200 MHz,  $\text{CDCl}_3$ )  $\delta$  5.78 (1H, s), 5.24 (4H, s), 3.27 (6H, s), 2.26 (3H, s);  $^{13}\text{C}$  NMR (50 MHz,  $\text{CDCl}_3$ )  $\delta$  210.48, 207.80, 132.35, 128.67, 97.40, 66.01; While compound **40** (0.30 g) was obtained when the eluent DCM : MeOH = 100 : 1 was used.  $^1\text{H}$  NMR (200 MHz,  $\text{CDCl}_3$ )  $\delta$  5.44 (1H, s), 5.15 (2H, d,  $J = 1.4$  Hz), 5.05 (2H, d,  $J = 1.5$  Hz), 3.21 (3H, d,  $J = 1.6$  Hz), 3.12 (3H, d,  $J = 1.7$  Hz), 2.30 (3H, d,  $J = 1.2$  Hz);  $^{13}\text{C}$  NMR (50 MHz,  $\text{CDCl}_3$ )  $\delta$  207.23, 204.63, 201.08, 132.89, 130.76, 113.47, 97.36, 97.21, 62.19.



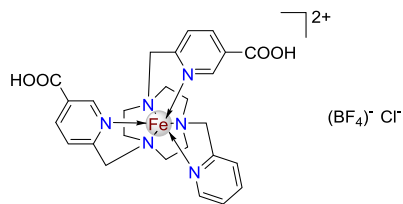
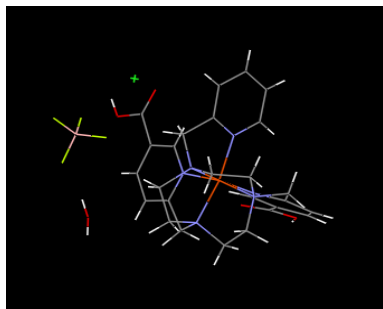
To the suspension of compound **21** (0.5 g, 3.96 mmol) and 4-DMAP (0.02 g, 0.12 mmol) in 10 mL THF,  $\text{Boc}_2\text{O}$  (1.73 g, 7.93 mmol) was added. It was stirred at RT overnight then THF was removed by evaporator to give the crude product which was

subsequently purified by silica gel chromatography. 0.86 g colorless oil was obtained in yield 66.7%.  $^1\text{H}$  NMR (300 MHz,  $\text{CDCl}_3$ )  $\delta$  6.97 (1H, s), 2.68 (3H, s), 1.58 (18H, s);  $^{13}\text{C}$  NMR (75 MHz,  $\text{CDCl}_3$ )  $\delta$  169.28, 166.57, 149.03, 99.48, 85.26, 27.58, 25.65.

## The structures of the complexes



empirical formula	$\text{C}_{26}\text{H}_{36}\text{FeN}_8\text{O}_4 \cdot 2(\text{BF}_4) \cdot \text{C}_2\text{H}_3\text{N}$
M / g.mol	795.13
Crystal system	Monoclinic
Space group	$P2_1/a$
a / Å	16.659 (1)
b / Å	13.1305 (7)
c / Å	17.421 (1)
$\beta$ / deg	115.906 (8) $^\circ$
V / Å <sup>3</sup>	3427.8 (4)
Z	4
T / K	100
$\lambda$ / Å	0.7107
$D_{\text{cal}}$ / mg. cm <sup>3</sup>	1.541
M (Mo Ka) / mm <sup>-1</sup>	0.53
No. of data measured	8335
Unique data ( $R_{\text{int}}$ )	(0.047)
Observed data [ $I > 2\sigma(I)$ ]	6685
$R[F^2 > 2\sigma(F^2)]^a$	0.046
$wR(F^2)^b$	0.1
$\Delta\rho_{\text{min}}, \Delta\rho_{\text{max}}$ / e. Å <sup>3</sup>	-0.86, 0.71



empirical formula	$C_{26}H_{30}FeN_6O_4 \cdot BF_4 \cdot Cl \cdot H_2O$
M / g.mol	686.68
Crystal system	Monoclinic
Space group	$P2_1/n$
a / Å	13.014 (1)
b / Å	12.449 (1)
c / Å	17.724 (2)
$\beta$ / deg	96.55 (1) <sup>o</sup>
V / Å <sup>3</sup>	2852.7 (5)
Z	4
T / K	160
$\lambda$ / Å	0.7107
D <sub>cal</sub> / mg. cm <sup>3</sup>	1.599
M (Mo Ka) / mm <sup>-1</sup>	0.70
No. of data measured	26543
Unique data (R <sub>int</sub> )	(0.072)
Observed data [I > 2(σ)I]	4994
R[F <sup>2</sup> > 2σ(F <sup>2</sup> )] <sup>a</sup>	0.064
wR(F <sup>2</sup> ) <sup>b</sup>	0.168
$\Delta\rho_{\min}, \Delta\rho_{\max}$ / e. Å <sup>3</sup>	-1.56, 1.05

## Acknowledgements

I would like to give my great thankness to Jens Hasserodt, my supervisor, who recruited me and gave me the opportunity to work on this project. I appreciated so much his tremendous respect, special understanding, unusual trust and forever support in those four years. From him I learnt a lot of professional knowledge, but also I improved my english and french level. He instructed me on the thesis with his brilliant mind and set a positive example with his excellant personality in daily life.

I also would like to express my gratitude to Fan Yang, my Chinese supervisor, who always take care of me since 2008 both on chemistry and in life. It was her unconditional help and warm encouragement that always raised my spirits to overcome any difficuty in the past seven years. I am so grateful that she gave me a chance to know and join the program between ECNU and ENS-LYON, and that she devoted her precious time and intellectual advices to correcting my thesis.

I am very grateful to Philippe Maurin. It was my hornor to know him on the course given by him during my master. His selfless help and kindly smile on his face always moved me. I want to thank him for every discussion about my project in the first year of my PhD. His compliments and encouragements highly motivated me to conquer any problem. At the same time, I am deeply grateful to the professor Jie Tang. Any word can not express this gratitude from my heart for many things that I have received in those years. He always take me as a child to protect and encourage.

I want to thank ....for their valuable comments as the referees of my manuscript. I also would like to give my sincere thankness to Pierre Audebert, Wanbin Zhang and Xiaobing Zhang for agreeing on joining the examination committee.

I would like to thank the collaborators, Erwann Jeanneau for the X-ray experiments, Olivier Beuf and Laurence Canaple for the MRI experiments, Christophe Bucher for measurement of Cyclic Voltammogram.

I sincerely want to thank the “international” office members, Jacek Lukasz KOLANOWSKI, Oliver Thorn-Seshold, and Guillaume Gros, who consist of a warm “family” to me. Their humorous and friendly talk, intellectual insights into research left me an unforgettable memory. I also want to thank Maxime Prost for warm care and communication with his great wisdom, Fayçal Touti for his inspiring discussion, Corentin Gondrand for cytotoxicity tests, Benjamin Bourdon for preparing all kinds of solutions for us in the lab, Pauline Renoud for friendly help and translation. I would like to thank Delphine Pitrat and Anne-Gaelle for ordering chemicals, Christian Melkonian for taking care of my computer. Thank all of people in the “laboratoire de chimie”, because of whom I had a really happy time.

I also would like to express my great gratitude to the Chinese friends, Yuting Zheng, Yuemei Sun, Xiangjian Shen, Nannan Wu, Zheng Zheng, Dawei Zhang, Wenyue Guan, Xiaopeng Fu, Xinnan Lu with whom I spent three years in Lyon. I deeply thank them for company at those both good and bad moments. It was my honor to know some professors, Wei Dong, Gang Fu, Kun Zhang, Shuangliang Zhao, Xiaobing Zhang and Shuhua Yang, who treated me as good friends regardless of our status. I am very grateful to the members of the group in East China Normal University, Yifan Shan, Yantao Qi, Libo Ruan, Shiwei Mao, Jiefeng Zhang and so on, who helped me a lot on administration work when I was in Lyon.

I really do not know how to express my deep gratitude to my family for their invaluable mental support. And I can not find any suitable word to thank my husband, Wen Yang, who did countless things for me to give his maximum support since we knew each other, no matter what I did and no matter how far I was away from him.

## Compound table

Compound	<sup>1</sup> H NMR	<sup>13</sup> C NMR	MS
<b>1</b>	√	√	
<b>3</b>	√	√	
<b>4</b>	√	√	
<b>5</b>	√	√	
<b>6</b>	√		
<b>7</b>	√		
<b>8a-c</b>			
<b>9a-c</b>			
<b>10a-c</b>			
<b>11a</b>	√	√	√
<b>11b</b>	√	√	√
<b>11c</b>	√	√	√
<b>12a</b>	√	√	√
<b>12b</b>	√	√	√
<b>12c</b>	√	√	√
<b>13a</b>	√	√	√
<b>13b</b>	√	√	√
<b>14a</b>	√	√	√
<b>14b</b>	√	√	√
<b>15a</b>	√	√	√
<b>15b</b>	√	√	√
<b>15c</b>	√	√	√
<b>16a</b>	√		√
<b>16b</b>			
<b>16c</b>	√		√
<b>16d</b>			√
<b>17</b>			
<b>18a</b>	√	√	
<b>18b</b>	√	√	√
<b>19a</b>	√	√	
<b>19b</b>	√	√	√
<b>20a</b>	√	√	
<b>20b</b>	√	√	√
<b>21</b>	√		
<b>22</b>			
<b>23</b>	√	√	
<b>24</b>	√	√	

<b>25</b>	√	√	√
<b>26</b>	√	√	√
<b>27</b>	√	√	√
<b>28</b>	√	√	√
<b>29</b>			
<b>30</b>			
<b>31</b>	√	√	√
<b>32</b>	√		
<b>33</b>	√		
<b>34</b>	√		√
<b>35</b>	√	√	
<b>36</b>	√	√	
<b>37</b>			
<b>38</b>	√	√	

The compounds from **8a-c** to **10a-c** and were intermediate ones, they were not characterized and directly used for the next steps. Compound **17** was available which was bought from the supplier. Compounds **1-7** and **18a-20a**, **21**, **23-24** were known in the publications, thus they were characterized only with two methods, even only one. Compounds **16a-d** and **29-30** were complexes. Compounds from **31** to **38** are some intermediates during the unsuccessful synthetic methods for the target compounds presented in the thesis.